Australian Government
Geoscience Australia

Seismic velocity models of the sediments and upper crust of the Capel & Faust Basins, Lord Howe Rise

Peter Petkovic

Record
2010/03

GeoCat # 69470

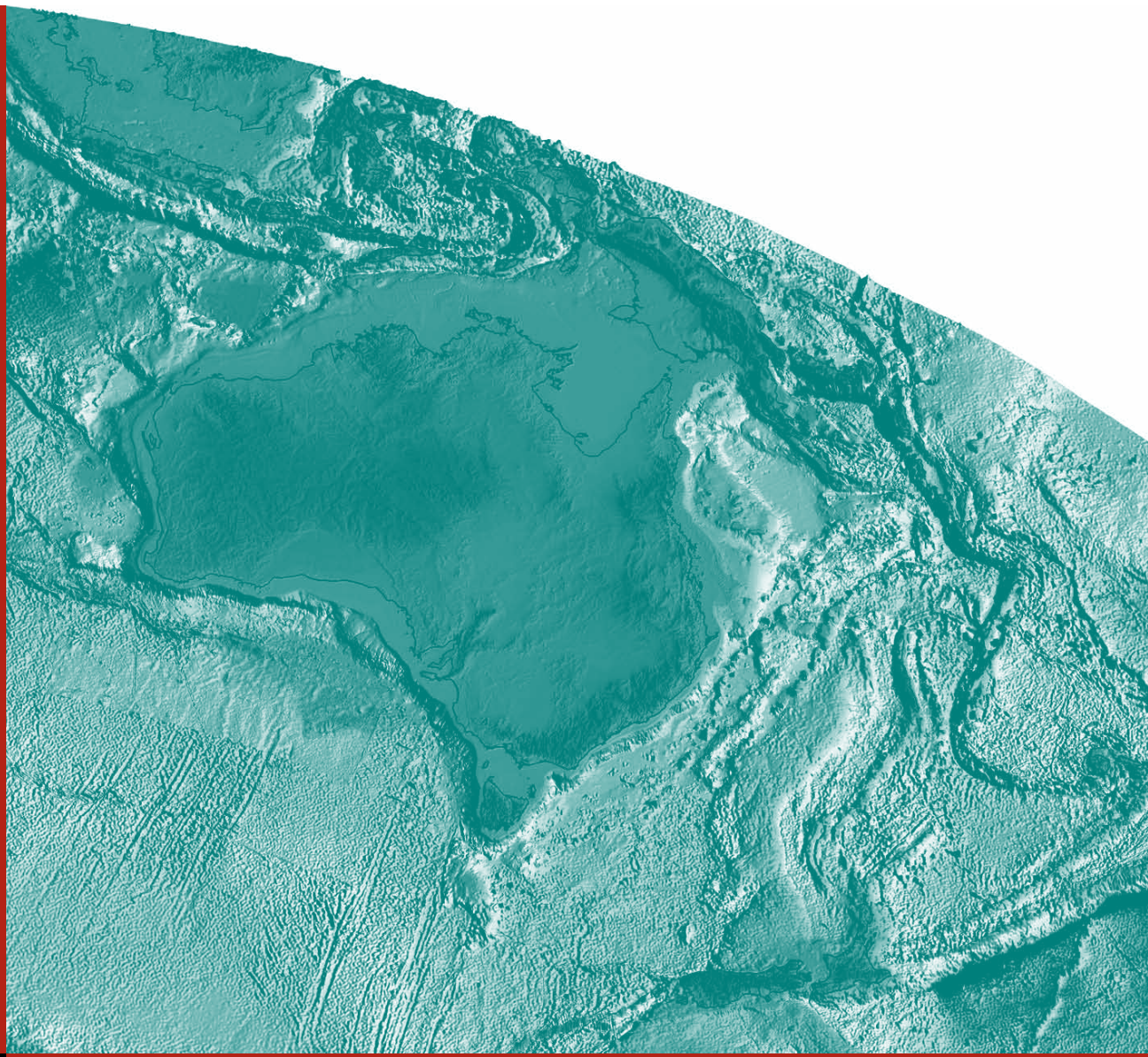

Seismic velocity models of the sediments and upper crust of the Capel & Faust Basins, Lord Howe Rise

GEOSCIENCE AUSTRALIA
RECORD 2010/03

by

Peter Petkovic

Petroleum & Marine Division, Geoscience Australia
GPO Box 378, Canberra, ACT, 2601

CANBERRA 2010

Department of Resources, Energy and Tourism
Minister for Resources and Energy: The Hon. Martin Ferguson, AM MP
Secretary: Mr John Pierce

Geoscience Australia
Acting Chief Executive Officer: Dr Chris Pigram

ISSN 1448-2177
ISBN 978-1-921672-56-9

GeoCat No. 69470

Bibliographic reference: Petkovic, P. 2010. *Seismic velocity models of the sediment and upper crust of the Capel and Faust Basins, Lord Howe Rise. Record 2010/03.* [CD-ROM] Geoscience Australia: Canberra.

Contents

Executive Summary

During the summer of 2006/07, Geoscience Australia acquired 5920 km of deep 2D seismic reflection data using an 8 km solid streamer, sonobuoy refraction and potential field data over the Capel and Faust Basins, Lord Howe Rise, in Australia's remote eastern frontier 800 km to the east of Brisbane.

This survey, GA-302, was the final phase of the Australian Government's New Petroleum Program. The program commenced in 2003 to provide pre-competitive data and knowledge in frontier basins to support acreage release. Previous data coverage over the region is sparse, and the present survey provides explorers with high quality data acquired and processed to modern standards.

This report documents the modelling of the sonobuoy refraction data and interval velocities from seismic stacking velocity data. The objectives of this work were to improve estimates of sediment thickness, a critical parameter in evaluating the petroleum potential of the province.

From mapping of the reflection seismic interpreted horizon travel times and applying a conversion to depth using the velocity functions derived from velocity models, the maximum thickness of sediment is estimated to exceed 6000 m in some depocentres.

Introduction

The Lord Howe Rise is believed to be underlain by continental crust which was part of eastern Gondwana before its breakup and initiation of the Tasman Sea spreading during the Late Cretaceous (Van de Beuque *et al.* 2003). The Capel and Faust basins lie within the northern Lord Howe Rise region, some 800 km due east of Brisbane in water depths of 1100-2700 m. Previous seismic surveys by Geoscience Australia (GA) over the area were reconnaissance seismic lines shot on the *R/V Rig Seismic* survey GA-177[1] in 1996 (Ramsay *et al.* 1997) and survey GA-206 in 1998 (Bernardel *et al.* 1999) as part of the Australian government's programme to define Australia's legal continental shelf margin for the United Nations Convention on the Law of the Sea. These data allowed approximate boundaries for the Capel and Faust basins to be defined by Stagg *et al.* (1999).

As a result of this reconnaissance work, which suggested the existence of sedimentary depocentres, the region gained interest as a possible frontier petroleum province. Geoscience Australia then completed a regional marine seismic survey over the basins during the summer of 2006/07, to commence an appraisal of their hydrocarbon potential. The survey (GA-302[2]) was the final phase of the Australian Government's New Petroleum Program (2003-2007) to promote exploration interest in these remote frontier basins. The survey was conducted on behalf of Geoscience Australia by Compagnie Générale de Géophysique (now CGG Veritas) on the platform *Pacific Titan*. The survey collected 5920 km of high-quality 106 fold 2D seismic reflection data using an 8 km streamer to 12 s two-way time (TWT) at 37.5 m shot interval. Gravity and magnetic data were acquired continuously along the reflection seismic lines, and over 90 sonobuoys were deployed. Following this in late 2007, the survey GA-2436[3] on the *R/V Tangaroa* (Heap *et al.* 2009) collected potential field, multi-beam bathymetry data at a 4 km line spacing and geological sample data over the northwest part of the area, where GA-302 results indicated that sediment thickness was greatest (Colwell *et al.* 2010). The location of these two recent Geoscience Australia surveys is shown in Figure 1.

The key geological question posed during the early stages of interpretation of the GA-302 seismic reflection profiles was the likely thickness of the sedimentary sequence. Although the seismic energy was sufficient to image events well into the lower crust, the picking of a base of sediments in the data

[1] Geoscience Australia internal databases omit the "GA-" prefix for marine survey identifiers. The prefix is used in this report to signify that the survey was acquired for Geoscience Australia (GA).

[2] GA-302 will also be referred to as '302' in unambiguous context, such as where individual lines in figures and text are labelled like '302-19' for Line 19 of survey GA-302.

[3] GA-2436 is also referred in various documents as TAN713, or "the Tangaroa survey" after the name of the platform, New Zealand government's R/V Tangaroa.

was problematic due to the variability of basement character including the occurrence of reflectors within what was interpreted as basement. The geological team inferred that basement consists of older, pre-rift basin sequences, whose physical properties are not always of sufficient contrast to distinguish it from overlying sediment (Colwell *et al.* 2010).

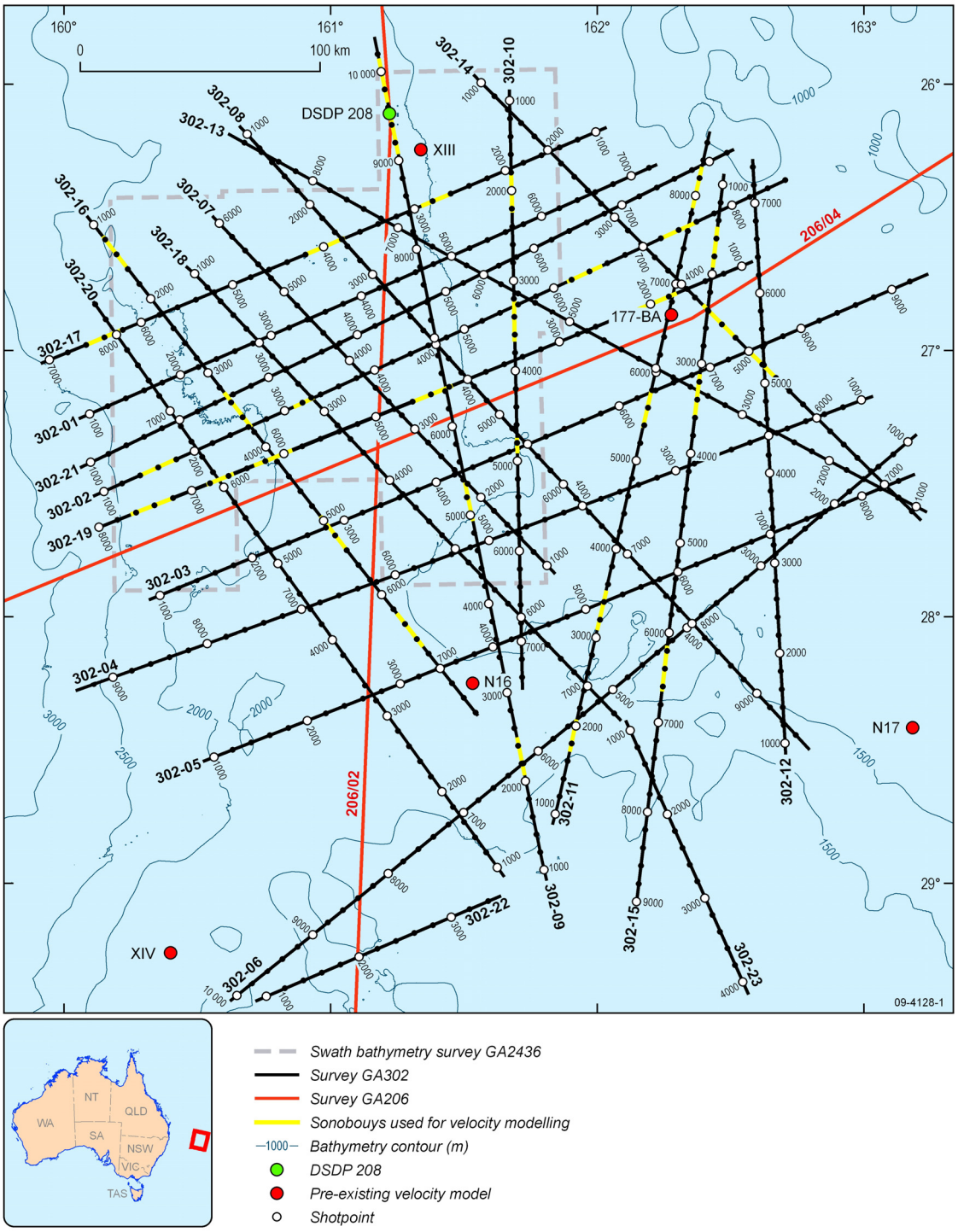

Figure 1. *Location of seismic lines from surveys GA-302 and GA-206 [lines with labels] and swath bathymetry survey GA-2436 [green closely spaced lines]; sonobuoys used for velocity modelling in this study from survey GA-302 [thick red segments]; the location of DSDP 208 [●]; pre-existing velocity models [●]. Water depth contours from levelled ship track and swath bathymetry data are given in 200m intervals in the background.*

Picking top of basement was further complicated as overlying reflector sequences contained dipping, intruded and possibly altered strata. This is illustrated in Figure 2 to Figure 4 showing portions of the reflection seismic section from line GA-302-19 with a version of the basement interpretation. For the reasoning behind the preferred seismic stratigraphy developed by the seismic reflection interpretation team, see Colwell *et al.* (2010).

It was anticipated that gravity modelling using densities inferred from the refraction velocity data could provide additional information on the depth to interpreted basement horizon. This document records the velocity modelling performed on the sonobuoy refraction data and interval velocities from stacking velocity data to provide input parameters for depth conversion and gravity modelling.

Previous Work

VELOCITY MEASUREMENTS

Velocity data over the Capel and Faust basins are scarce. Two-ship sesimic refraction work in the region using explosive sources was reported by Shor et al (1971) from the Scripps Institution of Oceanography. Moho depth was determined at 18 km at one end of a reversed E-W profile (station N16 in Figure 1, near the southern ends of lines 302-10 & 302-16) and 29 km at the other (N17, ~170 km to the east, Figure 1). Their model assumed the uppermost ~350 m of sediment to have P-wave velocity of 2150 m/s, and calculated the lower 900-1700 m thick sedimentary pile to have 3900 m/s P-wave velocity. For an upper crust 8-13 km thick the P-wave velocity was computed at 5950-6190 m/s while the lower crust velocity given at 6820 m/s. Shor *et al.* (1971) noted that the velocity of the upper crust was comparable to that of crustal velocity data from eastern Australia, and concluded that the Lord Howe Rise is likely to be a continental fragment.

The Deep Sea Drilling Project completed hole DSDP-208 on leg 21 during 1971-72 (Burns *et al.* 1973a), and as part of the site survey collected sonobuoy data near the 594 m hole at 26.110217°S, 161.221167°E. The velocities interpreted from these data were: 1500 m/s (0-0.23 s TWT); 1586 m/s (0.23-0.35 s TWT); 1898 m/s (0.35-0.65 s TWT); 2345 m/s (0.65 s TWT to below bottom of hole). An Eocene-Oligocene regional unconformity was recorded as a reflector at 0.575 s TWT (~488 m) (Andrews, 1973), which was identified as the bottom of the uppermost sediment layer[4] and used in subsequent gravity modelling by Petkovic *et al.* (in prep). The DSDP-208 sonobuoy data indicate an average velocity of this upper unit to be ~1650 m/s, consistent with the sampling of deep-ocean

[4] The term “layer” is used to denote an interval or body of sediment, as represented in the reflection seismic data and in velocity models, whose upper and lower bounding surfaces are “horizons”.

unconsolidated sediments at this site (Burns *et al.* 1973b), and similar to other sampling of shallow Pacific Ocean marine sediments (Wilkens and Handyside, 1985). The upper unit is characterised by mostly transparent seismic facies, marked at its base by a negative polarity reflector (the Eocene–Oligocene unconformity), overlying a high amplitude stratified seismic unit (Colwell *et al.* 2010).

Willcox *et al.* (1981), reporting on a co-operative 1978 survey (Sonne 7) between the Bureau of Mineral Resources (precursor of Geoscience Australia) and Bundesanstalt für Geowissenschaften und Rohstoffe (BGR), lists sonobuoy XIV (Figure 1) with upper sediment velocity of 2270 m/s and below this layers of 2940 m/s, 3920 m/s and 4950 m/s down to a total depth below sea floor of 3270 m. Sonobuoy XIII (Figure 1) only recorded an upper sediment velocity of 2800 m/s. From the collated refraction results Willcox et al (1981) proposed a velocity model of upper sediments as 2000-2400 m/s, lower sediments (assumed lower Paleogene or Cretaceous rift-fill) as 2800-2600 m/s, and basement as 4000-5000 m/s for metasediments and >5000 m/s for magmatic rocks.

Velocity data over the present study area were recorded during the GA-177 survey from a sonobuoy launched at 26.8664°S, 162.2781°E on line LHRNR-BA (Ramsay et al, 1997). This sonobuoy (labelled 177-BA in Figure 1), near sonobuoy GA-302-19-66[5] on the present survey, recorded a distinct first arrival with apparent velocity of 5900 m/s from a shallow event 0.9 s TWT below sea floor, and a strong later arrival of ~4600 m/s from a variable depth refractor. The sonobuoy is located over the eastern part of the study area where shallow basement is mapped in the seismic reflection data, supported by these refraction results.

Although not in the study area, it is worth noting that Klingelhoefer *et al.* (2007) modelled data from a wide-angle ocean-bottom seismometer and reflection experiment (Zoneco-11) west of New Caledonia, along two transects of the Lord Howe Rise, the New Caledonia and Fairway basins. Sediment thickness was observed up to 5 km for the northern line with three sediment layers of velocity ranges: 2.15-2.7 (Mid-Miocene to present), 2.8-3.15 (post-Upper Eocene to Lower Miocene), and 3.2-4.6 (Cretaceous to Paleocene). Up to 3km of sediment was modelled for the southern line with two layers of sediment with velocity ranges: 2.16-3.2 (Miocene to present), and 3.2-4.3 (Cretaceous to Miocene) km/s. Basement was modelled with velocities ranging 4.0-5.8 km/s and thought to be volcanic or sedimentary rocks based on the variability of velocities and character of the seismic reflection data.

[5] Nomenclature for identifying sonobuoys appends a sequence number to the line name, thus GA-302-19-66 is the 66th sonobuoy deployed on the survey, and was deployed on seismic line GA-302-19.

SYNTHESIS OF PREVIOUS STUDIES

The complete list of surveys that have crossed the area is documented in Table 1. The results from these surveys were synthesised by Van de Beuque *et al.* (2003) who concluded, on the basis of the compiled data and pre-existing models (summarised by Gaina *et al.* 1998), that the Lord Howe Rise is underlain by continental crust, possibly corresponding to Palaeozoic New England Fold Belt (Norvick *et al.* 2008; Mortimer *et al.* 2008) detached from the Australian mainland during Tasman Sea rifting from the Late Cretaceous. Their subdivision of the Lord Howe Rise places the Faust Basin in a "central rift province" characterised by irregularly block-faulted basement, and the neighbouring Capel Basin in a "western rift province" where basement is also faulted but sediments are considerably thicker. In addition, to the east lies a "planated basement province" where the sedimentary section is thin. Interpretation of seismic data and dredge samples of rocks (Burns *et al.* 1973c; Colwell *et al.* 2006; Heap *et al.* 2009) indicate that volcanic processes have been extensive in time and space across the Lord Howe Rise and that volcanism continued well into post-breakup phases. However the quality of seismic data acquired prior to 2006 was too poor to define any structure internal to the basement, and knowledge of basement terranes remains poor.

Table 1. *List of surveys which cross the area of the present study. GA=Geoscience Australia; SIO=Scripps Institution of Oceanography; LDGO=Lamont-Doherty Geological Observatory; BGR= Bundesanstalt für Geowissenschaften und Rohstoffe; SOEST = School of Earth Science and Technology, University of Hawaii; IPEV = Institut Polaire Français Paul Emile Victor. Grav/Mag indicates whether (G)ravity and (M)agnetic data were acquired.*

Survey id	Year	Platform	Institution	Grav/ Mag	Reference
NOVA05AR	1967	Argo	SIO	M	Shor *et al.* 1971
NOVA1AHO	1967	Horizon	SIO	M	Shor *et al.* 1971
ELT-29	1967	Eltanin	LDGO	G,M	Hayes *et al.* 1972
71042604	1971	Kana Keoki	SOEST	M	Andrews & Foreman, 1971
DSDP21GC	1972	Glomar Challenger	SIO	M	Burns *et al.* 1973
SONNE7	1978	Sonne	BGR/GA	M	Willcox *et al.* 1981
DSDP90GC	1983	Glomar Challenger	SIO	M	Kennett *et al.* 1986
WEST06MV	1994	Melville	SIO	G,M	Hill, P.J., 1995
GA-177	1996	Rig Seismic	GA	G,M	Ramsay *et al.* 1997
GA-206	1998	Rig Seismic	GA	G,M	Bernardel *et al.* 1999
MD-153	2006	Marion Dufresne	IPEV	G,M	Colwell *et al.* 2006
GA-302	2007	Pacific Titan	GA	G,M	Fugro Robertson Inc., 2007
GA-2436	2007	Tangaroa	GA	G,M	Heap *et al.* 2009

Seismic Reflection Data

Basic metadata for each seismic reflection line of the GA-302 survey is given in Table 2. An interpretation of these lines, supplemented by lines from an earlier survey GA-206, is given by Colwell *et al.* (2010).

Table 2. *Seismic line statistics for Capel/Faust survey GA-302. The table gives position (Lat, Lon) and shot (spn) at start and end of line, the line length (L) and heading (H). Shot spacing is 37.5 m.*

Line	spn1	Lat1 (°)	Lon1 (°)	spn2	Lat2 (°)	Lon2 (°)	L (km)	H (°)
302-01	1002	-27.23825	160.09707	7273	-26.30311	162.21972	235.1	64.3
302-02	1001	-27.52976	160.15063	8609	-26.35884	162.70949	285.2	63.5
302-03	1001	-27.91975	160.36075	9387	-26.71408	163.23722	314.4	65.5
302-04	1001	-27.18687	162.99059	9380	-28.27542	160.04804	314.1	246.7
302-05	1001	-28.52658	160.56339	8564	-27.46663	163.18784	283.5	66.2
302-06	1001	-27.34423	163.16451	10077	-29.44037	160.62608	340.2	226.4
302-07	1001	-27.80759	161.81099	6092	-26.49798	160.55939	190.8	319.2
302-08	1001	-26.18832	160.68756	9794	-28.49503	162.79296	329.6	141.3
302-09	1001	-28.94939	161.80004	10378	-25.82699	161.16513	351.5	349.6
302-10	981	-26.05580	161.67128	7521	-28.26872	161.71979	245.2	178.9
302-11	1001	-28.74013	161.84358	8712	-26.18208	162.42150	289.0	11.5
302-12	1001	-28.47379	162.70424	7473	-26.28618	162.58308	242.6	357.1
302-13	1001	-27.58667	163.19572	8979	-26.18827	160.61971	299.1	300.6
302-14	1001	-25.99526	161.56579	7521	-27.63499	163.21172	244.4	138.4
302-15	1001	-26.37866	162.47070	9033	-29.08136	162.14609	301.1	186.0
302-16	1001	-26.52880	160.11196	7624	-28.36709	161.54936	248.3	145.4
302-17	1001	-26.18024	161.99351	7081	-27.04726	159.91716	227.9	244.6
302-18	1001	-26.71276	160.49067	7489	-28.38566	162.08616	243.2	140.0
302-19	1001	-26.68389	162.54159	8011	-27.66604	160.12691	262.8	245.0
302-20	1001	-28.94098	161.62500	8423	-26.81939	160.11193	278.2	327.3
302-21	1001	-27.41994	160.10086	8264	-26.24666	162.50874	272.3	62.0
302-22	1001	-29.42448	160.76033	3525	-29.04899	161.63478	94.6	64.1
302-23	1001	-28.42761	162.12409	4134	-29.41413	162.56500	117.5	158.6

Examples of the sedimentary and basement character recorded by seismic reflection are given in the figures below. The horizons shown, interpreted by Colwell *et al.* (2010) are boundaries of layers used in subsequent gravity modelling by Petkovic *et al.* (in prep.), and for which starting estimates of density are inferred from the velocity models developed here. The lower boundary of the shallowest layer, 'SedUpper', is the Eocene/Oligocene unconformity encountered in DSDP 208 and mapped by Colwell *et al.* (2010) as 'Olig'. The highly stratified 'SedMiddle', also interpreted to contain post-rift sediments, is bounded at its base by an unconformity denoted by 'Sr2B'. Syn-rift sediments of 'SedLower' are interpreted to occur below this horizon. The base of the syn-rift sedimentary sequence is a horizon mapped as 'CretRift', below which is basement. The figures illustrate the problems picking the top of basement, and the presence of layering within it indicating existence of pre-rift sediments, possibly altered and intruded.

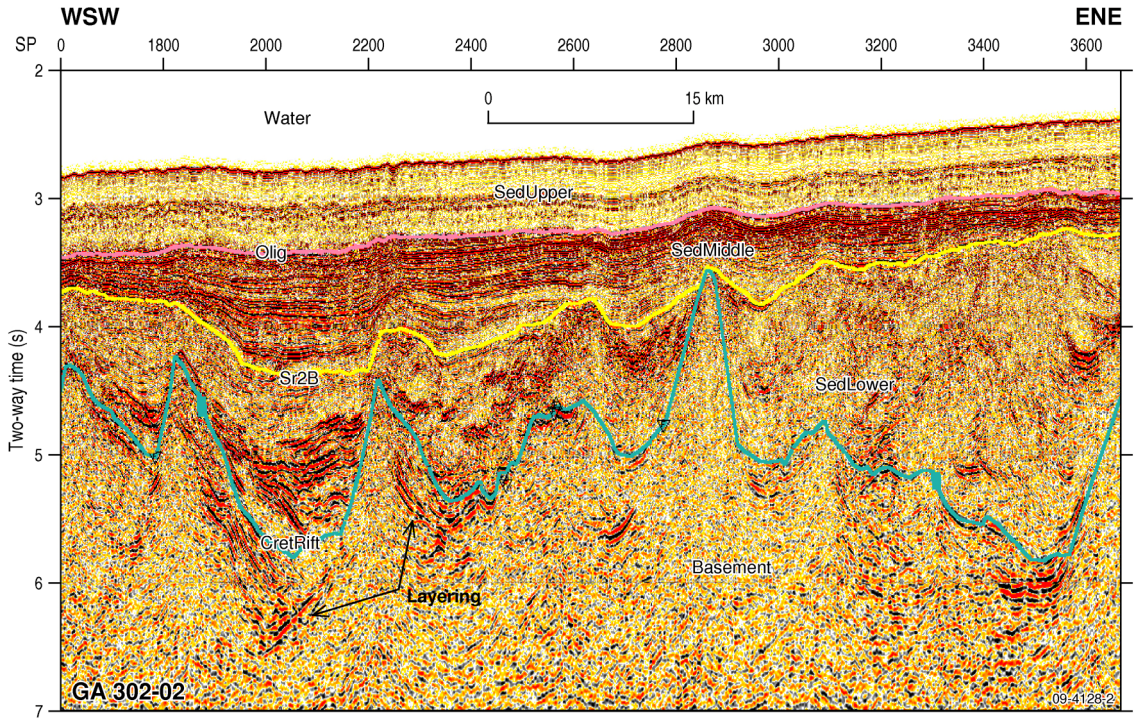

Figure 2. *Portion of reflection seismic line GA-302-02 (shotpoint 1601 to 3650, 76.8 km) showing layers used for modelling and horizon boundaries. Note layering in some parts of Basement (after Colwell et al. 2010).*

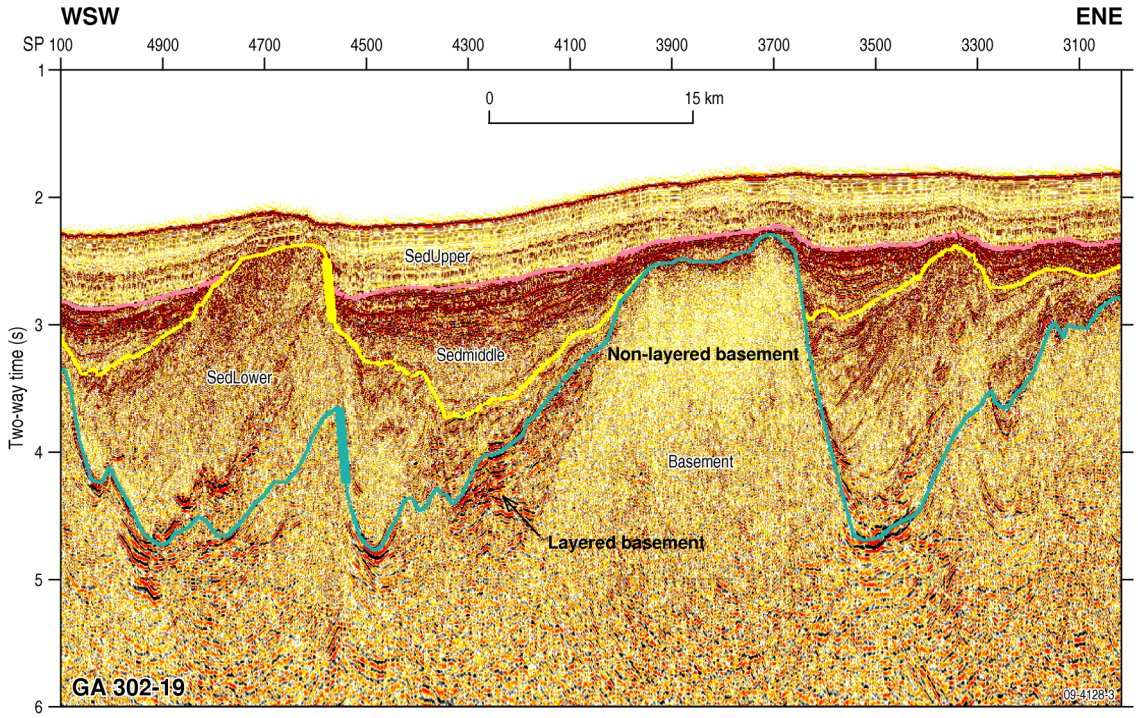

Figure 3. *Portion of reflection seismic line GA-302-19 (shotpoint 5091 to 3005, 78.2 km) showing variability of basement character from layered to non-layered (opaque or transparent). The non-layered Basement (named 'bland' by Colwell et al. 2010) is most common in the eastern and central part of the study area.*

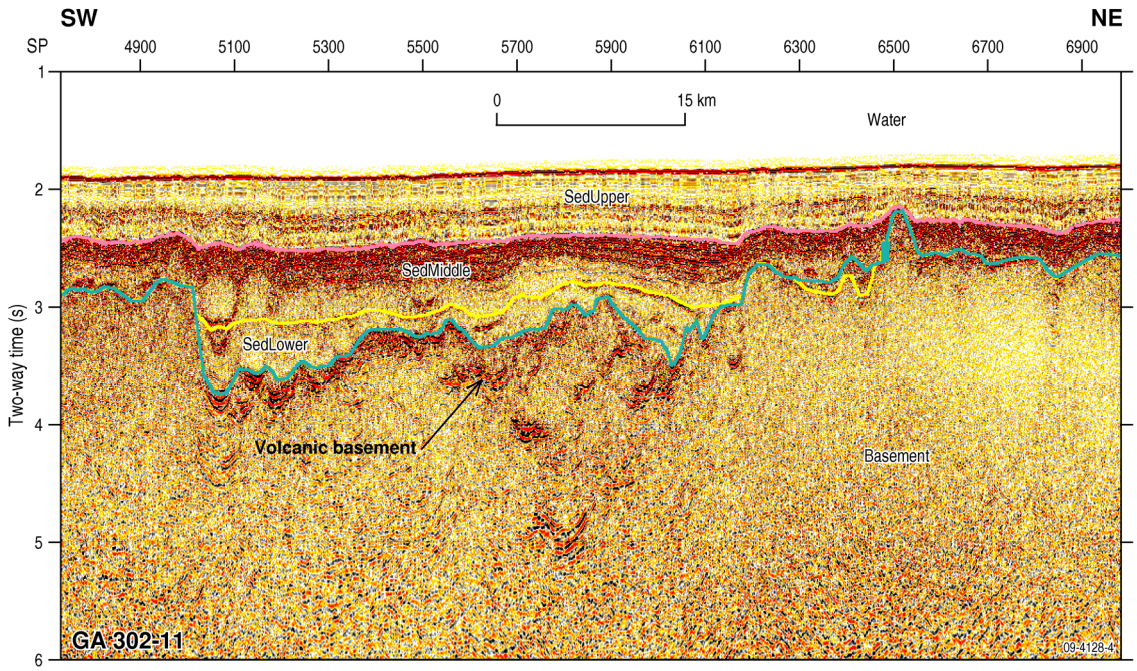

Figure 4. *Portion of reflection seismic line GA-302-11 (shotpoint 4704 to 7083, 88.5 km) showing characteristic of layered volcanic Basement. This type of basement occurs most commonly in the eastern and southern part of the study area (after Colwell et al. 2010)*

The present work attempts to estimate interval velocities for these layers to facilitate determination of total sediment thickness and isopach mapping, and allow inference of densities for gravity modelling.

Velocity Models

SONOBUOY DATA

As noted in the introduction, sediment thickness is a key question in an assessment of this remote frontier area for petroleum potential. In light of this, sonobuoys were deployed during survey GA-302 to obtain P-wave velocities to supplement stacking velocities, which are typically used for depth conversion in the absence of refraction velocity measurements.

Ninety six sonobuoys were deployed during the survey, however half failed due to technical problems, principally due to truncation by the seismic cable. The sonobuoys for which some useful refracted energy was recorded are listed in Table 3. The sonobuoy SEG-Y files delivered post-survey were filtered using Disco/Focus®[6] with a band-pass filter of 6-30 Hz over 51 traces with low side ramp of 12 db/cycle and high side ramp of 72 db/cycle, then displayed for interpretation and event identification in Geoframe®[7]. The refraction seismic events were hand picked via the Geoframe graphical user interface and classified according to their apparent velocities.

Apparent velocities

The refraction arrival travel time picks were exported from Geoframe and reformatted using program *gf2sigma.pl*[8], developed by the author, for input to the ray-tracing stage of interpretation. The deviation of the velocity of the water wave from 1500 m/s was taken to represent in-line drift of the sonobuoy relative to the ship, while the cross-line drift could not be determined. The scaling of the distance from energy source to the sonobuoy, due to in-line sonobuoy drift, was applied using:

$$D = d_0 * 1500 / V_a$$

where,

D is actual distance of source to sonobuoy (m),

d_0 is the nominal distance calculated from the shotpoint interval, 37.5 m, and

V_a is apparent velocity (m/s)

[6] Paradigm software for processing seismic data; new name is Echos™ (http://www.pdgm.com/products/seismic-processing-imaging/echos.aspx)

[7] Schlumberger software for workstation seismic display and interpretation (http://www.slb.com/content/services/software/geo/geoframe/index.asp)

[8] this and other open source programs cited in the text were developed by the author and written in Perl

A supplementary program used to compute apparent velocities in order to classify the events is *linear.pl* which computes the line of best fit for a set of points, and used for the picks exported from Geoframe.

Ray-tracing software – Sigma

The refraction picks adjusted for in-line sonobuoy drift were imported to Sigma ray-tracing software developed by Seismic Image Software Ltd (Seismic Image Software, 1995). Sigma is a graphical front-end to the ray-tracing algorithm of Zelt & Smith (1992) for forward and inverse 2-dimensional velocity modelling of vertical sections. Sigma models consist of a set of continuous layers from beginning to end of line. Referring to Figure 5 for clarification, the geometry of a layer boundary is determined by depth-control points (black circles in the diagram).

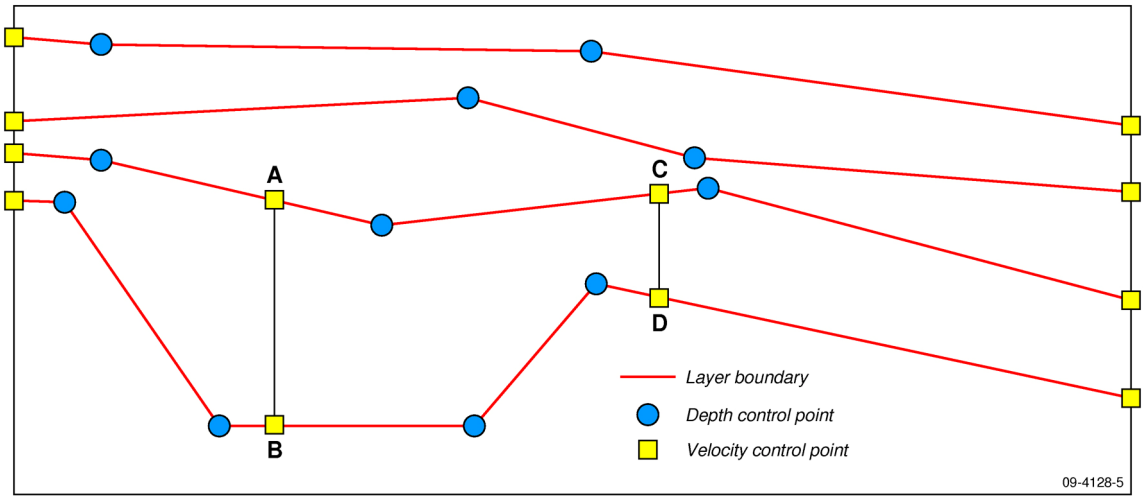

Figure 5. *Geometry of a Sigma model: diagram illustrates the subdivision of a vertical section in a Sigma model by depth control points (•) which define the layer geometry, and velocity control points (▪) which define the velocity distribution. Velocities are specified at points A, B, C, D and all other velocity control points. Within each polygon like ABDC the program performs a linear interpolation between the velocity control points to obtain a velocity at each point within the model.*

Each layer may be subdivided by vertical boundaries whose ends are velocity control points (red squares in the figure) forming a set of polygonal bodies with vertical sides (eg AB and CD in the diagram). P-wave velocities are specified at the velocity control points (eg A, B, C, D) defining the vertical boundaries, and the program applies linear interpolation to determine the velocity at any point within each body. The diagram in Figure 6 is a set of raypaths through the model with increasing velocity with depth and velocity discontinuities at layer boundaries, showing two sets of turning rays from source S1 and a set of headwaves used to model the source S2.

When employing heuristic forward modelling the parameters defining the model (depth and velocity control points) are adjusted to achieve a match between the travel times computed by the program and

the observed travel times picked from the sonobuoy records. When a reasonable match is achieved, the program allows a further refinement of model parameters by inversion.

Many iterations of model development are typically needed to achieve a good match between computed and observed travel times, adjusting velocity profile and layer thickness independently, and this may include reclassification of events and repeating the export from Geoframe and subsequent processes.

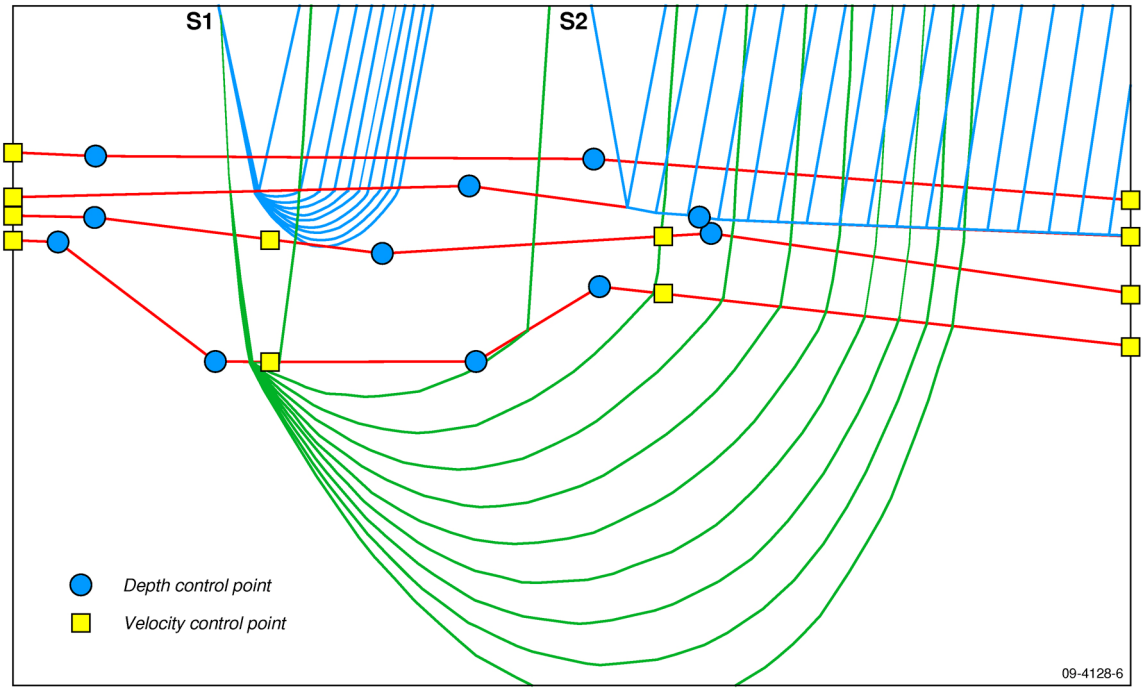

Figure 6. *Geometry of a Sigma model: diagram illustrates computed ray paths through a vertical section of a layered velocity model in which velocity increases with depth in each layer and with velocity discontinuities at layer boundaries. S1 and S2 are sources and the illustration shows both turning rays (for S1) and head waves (for S2) travelling to the right.*

Starting model classification of apparent velocities

The starting model classification of apparent velocities, adjusted for sonobuoy drift, is given in Table 3. This table lists the apparent velocities in four categories (columns A-D) which comprise four nominal layers prior to commencement of ray-tracing. Two additional layers are part of the starting model:

a) a water layer of sound velocity of 1500 m/s. This velocity is nominal for conversion of echo sounder arrival times to water depth. It is supported by CDT (Conductivity, Temperature, Depth) data acquired on survey GA-2436 in the same area approximately 11 months after survey GA-302. Figure 7 shows the speed of sound computed from the primary observations for the seven CTD casts made during this survey (Heap *et al.* 2009). Computed speed of sound varies from ~1525 m/s at the surface, 1480 m/s at 1200 m depth, to 1490 m/s at 2200 m.

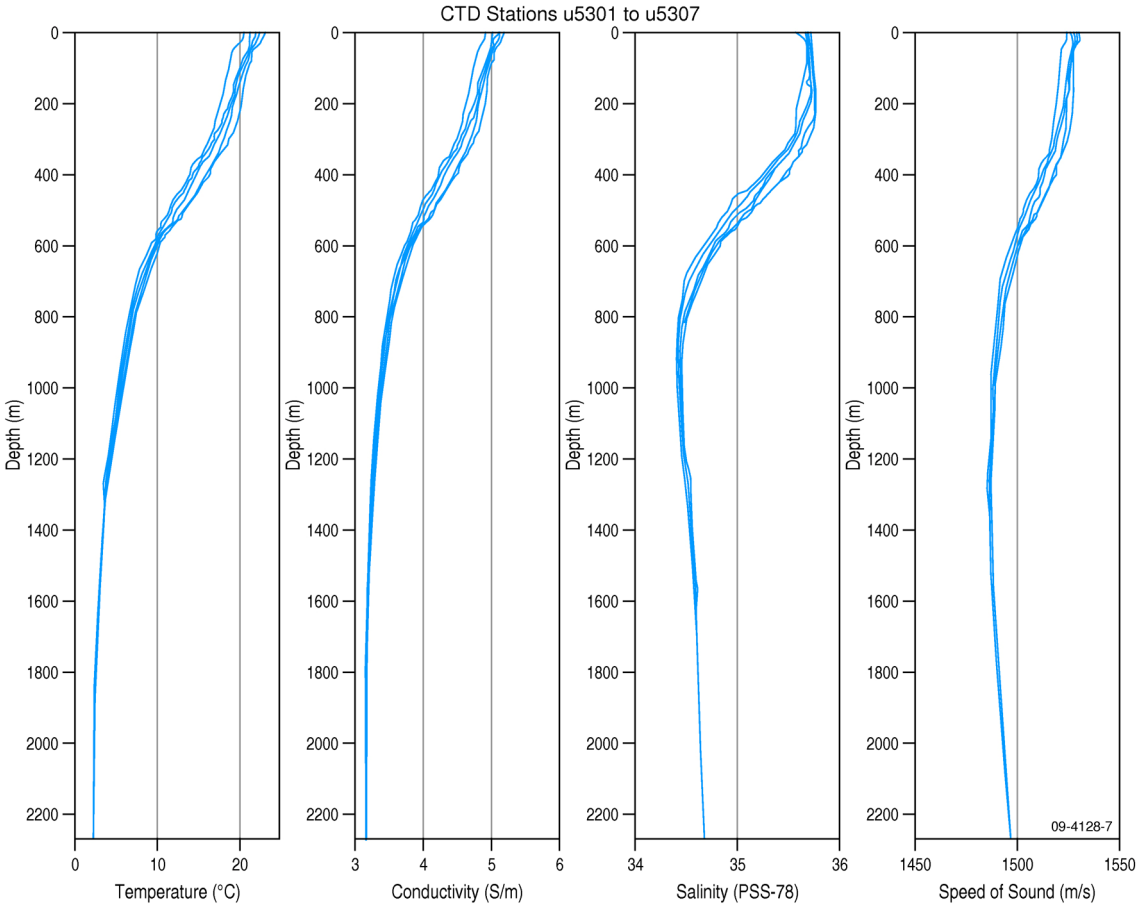

Figure 7. *Profile of speed of sound in water from temperature-conductivity-salinity measurements on survey GA-2436 in the same area in November 2007. These data support use of 1500 m/s as a nominal speed of sound to be used for the water layer in modelling the refraction results.*

b) A shallowest sediment layer undetected by refraction arrivals but sampled in DSDP 208 in the shallowest 500m of sediment with average velocity of ~1650 m/s (refer to section on previous work in the area).

The refraction picks for lines with two or more sonobuoys in close proximity, and those with good quality data, were then entered into velocity modelling software Sigma to arrive at velocity models for those parts of the seismic lines where sonobuoy data gave sufficient coverage. The models derived by this process are shown in Appendix 2.

Table 3. *Summary of observations for sonobuoys that did not fail, with left-most column (id) as sonobuoy identifier (first 2 characters are line number). 'M' marks sonobuoys used in ray-trace forward modelling. 'SPN' is deployment shotpoint; 'LatS' and 'LonE' are sonobuoy deployment coordinates; 'WD' is water depth; 'WW' column contains apparent speed of sound for water wave measured on refraction records; 'Drift' is rate of drift of sonobuoy in the direction of ship motion due to ocean currents, assuming that speed of sound in water is 1500 m/s; 'R' is the range to signal fade-out (km). Columns A-E give apparent velocities of refracted arrivals (km/s), adjusted for sonobuoy drift, classified in five layers for the starting model.*

id	M	SPN	LatS	LonE	WD (m)	WW (m/s)	Drift (kn)	R km	A km/s	B km/s	C km/s	D km/s
01-03		2206	27.0607	160.5090	2004	1480	-0.07	7	2.3			
01-05		6348	26.4428	161.9108	1322	1587	0.27	11	2.5		4.5	
02-42	✓	1373	27.4737	160.2770	2250	1375	-0.45	14	2.0	3.0		5.5
02-43	✓	3087	27.2134	160.8575	1939	1505	0.02	8		3.0	4.0	
02-46	✓	6139	26.7442	161.8846	1405	1497	-0.01	11	2.5		5.5	6.5
02-47	✓	7221	26.5759	162.2466	1374	1504	0.01	9	2.5			5.0
03-79		3561	27.5580	161.2455	1773	1580	0.25	12	2.5	3.0		6.0
04-83		5457	27.7736	161.4330	1570	1387	-0.41	7			4.5	
04-84		8243	28.1315	160.4508	2004	1337	-0.61	12	2.5		4.0	
05-85		1576	28.4478	160.7647	2041	1438	-0.22	8				5.5
06-88		3905	28.0202	162.3631	1525	1562	0.20	9				5.0
07-11		1960	27.5605	161.5718	1566	1651	0.46	11			4.0	
08-58		4581	27.1313	161.5344	1486	1558	0.19	4				5.5
09-34	✓	2074	28.5923	161.7256	1622	1492	-0.03	10	2.0	3.5	4.0	
09-36	✓	4957	27.6327	161.5275	1538	1494	-0.02	10	2.5	3.0	4.0	
09-39	✓	9137	26.2428	161.2476	1610	1556	0.18	14		3.0	4.0	5.0
09-40	✓	9733	26.0429	161.2079	1597	1564	0.20	16	2.0	3.5		5.5
10-06	✓	1809	26.3378	161.6774	1331	1528	0.09	9	2.0			5.0
10-09	✓	3254	26.8250	161.6881	1430	1598	0.31	12	2.5	3.0	4.0	6.5
10-10	✓	4748	27.3323	161.6990	1532	1463	-0.13	5			4.0	
11-20	✓	1713	28.5041	161.8982	1594	1342	-0.59	7	2.5		4.0	
11-22	✓	3109	28.0412	162.0044	1482	1446	-0.19	11	2.0		4.0	
11-25	✓	5370	27.2912	162.1743	1466	1461	-0.13	12	2.0	2.5	4.5	
11-26	✓	7876	26.4596	162.3601	1378	1559	0.19	14	2.5	3.0	4.5	
13-53	✓	3381	27.1745	162.4206	1435	1533	0.11	13	2.5	3.0	4.0	
13-54	✓	4482	26.9813	162.0623	1374	1453	-0.16	4		3.5		
13-56	✓	7674	26.4202	161.0367	1652	1559	0.19	17	2.2	4.0	5.0	5.5
14-49	✓	4345	26.8387	162.4040	1413	1489	-0.04	11	2.0	2.5	5.0	
14-51	✓	5031	27.0112	162.5774	1379	1442	-0.20	10	2.5	3.0		5.5
15-27	✓	1514	26.5514	162.4506	1375	1577	0.24	13	2.0	3.5	4.5	
15-29	✓	3170	27.1087	162.3846	1425	1536	0.12	12	2.5	3.5	4.5	
15-32	✓	6199	28.1279	162.2624	1485	1596	0.30	7			4.5	7.5
16-14	✓	1154	26.5714	160.1447	1931	1533	0.11	14			5.0	5.5
16-15	✓	2266	26.8826	160.3839	2083	1603	0.32	16	2.5			5.0
16-17	✓	3300	27.1701	160.6067	1991	1491	-0.04	7		3.4		
16-18	✓	4973	27.6330	160.9684	1961	1509	0.03	12	3.0	3.5	4.5	
17-60	✓	2611	26.4128	161.4467	1474	1501	0.00	10	2.5	3.0	4.0	

17-61	✓	3780	26.5803	161.0484	1617	1570	0.22	11		3.0	4.5	
17-62	✓	6233	26.9283	160.2087	2197	1593	0.29	11				5.0
18-94		2641	27.1373	160.8895	1876	1557	0.18	17		3.5	4.0	
18-95		5448	27.8614	161.5790	1419	1509	0.03	5				5.5
19-66	✓	1731	26.7879	162.2920	1398	1599	0.31	10	2.5		4.5	
19-67	✓	2122	26.8436	162.1582	1384	1575	0.24	7	2.5		4.5	
19-72	✓	4187	27.1354	161.4494	1647	1529	0.09	12	3.0	3.5	4.5	
19-76	✓	5931	27.3789	160.8478	1987	1548	0.16	12		3.0	4.0	
19-77	✓	6559	27.4661	160.6305	2183	1469	-0.11	10	2.5		4.0	
19-78	✓	7220	27.5573	160.4014	2174	1480	-0.07	13	2.0		4.0	
20-92		2216	28.5948	161.3732	1578	1513	0.04	13		2.5		6.0
20-93		5445	27.6728	160.7119	2113	1451	-0.17	10		3.0		5.0
23-96		3430	29.1926	162.4652	1266	1653	0.46	12	2.5	3.5		5.5

Results of ray-tracing

A summary of ray-tracing statistics is given in Table 4, and the results of the modelling are presented in Appendix 3 as one-dimensional velocity-depth functions extracted from the Sigma model files. This style of presentation was chosen because sparse sampling (few successful sonobuoys) inhibited model continuity along the seismic lines. Line GA-302-19 was sampled by six sonobuoys (66, 67, 72, 76, 77, 78) although the along-line distribution was irregular. The 1D 'slices' shown in Appendix 3 were extracted at locations in the model at which the ray coverage was considered to be the greatest, and hence not necessarily at the sonobuoy deployment locations.

Table 4. *Statistics for the seismic lines and sonobuoys modelled by forward raytracing as described in the text. The statistics do not include the water bottom reflector. N is the number of picks. The normalised χ2 is an indicator of relative goodness of fit for each of the phases, and is the rms misfit normalised to the uncertainty of the pick. The remaining lines were not modelled due to insufficient sonobuoys or sonobuoys too far apart to realise a reliable model.*

Line	Sonobuoys	N	RMS (s)	Norm χ^2
302-02	42, 43, 46, 47	621	0.034	1.80
302-09	34, 36, 39, 40	471	0.028	1.22
302-10	06, 09, 10	413	0.033	1.75
302-11	20, 22, 25, 26	644	0.039	2.48
302-13	53, 54, 56	574	0.018	0.52
302-14	49, 51	204	0.007	0.09
302-15	27, 29, 32	397	0.021	0.69
302-16	14, 15, 17, 18	616	0.019	0.59
302-17	60, 61, 62	456	0.017	0.46
302-19	66, 67, 72, 76, 77, 78	855	0.029	1.35

Time-depth functions

The results given in Appendix 3 can be used for depth conversion of reflection seismic horizon travel-time picks. The chosen method combined the refraction results over the whole area by least-squares fit of a function to depth-time coordinate pairs computed from the 1D velocity models in Appendix 3. Deep parts of models with velocity greater than 6 km/s were excluded so that the function is characteristic for the sediments only across the whole area:

$$Z = 250\, t^{2} + 869\, t \qquad ①$$

and the instantaneous velocity function by differentiation[9]:

$$V_t = 1000\, t + 1738 \qquad ②$$

where,

Z = depth below sea floor (m)

t = two-way travel time below sea floor (s)

V_t = instantaneous sonic velocity at travel time t (s) below sea floor (m/s)

These symbols are used in all functions given below.

As discussed by Robein (2003, pp71-76) the linear velocity-time function is often used for depth conversion for its mathematical simplicity and realistic approximation to the velocity profile of basin geology where the layers are not too lithologically distinct. As the refraction results have shown, this is not strictly the case in the study area, and several distinct layers have been identified. When contemplating conversion of travel-time picks to depth, the geophysicists needs to assess the merits of applying a single function derived from refraction modelling across the whole area versus a scheme which interpolates between sonobuoy locations and extrapolates into regions of lines not modelled.

The graph of the time-depth function ① is presented in Figure 8, across the travel times spanning the total sediment thickness which reaches a maximum of 3.5 s as mapped in the reflection seismic data by Colwell *et al.* (2010). By extrapolation, the maximum sediment thickness at 3.5 s travel time is 6104 m and the slope of the function at this time is a velocity of 5238 m/s in the sediments.

It may be of interest to compare these results with those of the two deep crustal transects to the north, of Klingelhoefer *et al.* (2007), if they are given the same treatment (i.e. extraction of 1D velocity profiles above basement at 50km intervals). Figure 9 is a reproduction of Figure 8 with the addition of points extracted from models of Klingelhoefer *et al.* (2007). Although many of the points are from

[9] Note use of one-way travel time before applying differentiation.

parts of the models over the New Caledonia and Fairway basins, the same general trend is observed for the sedimentary section.

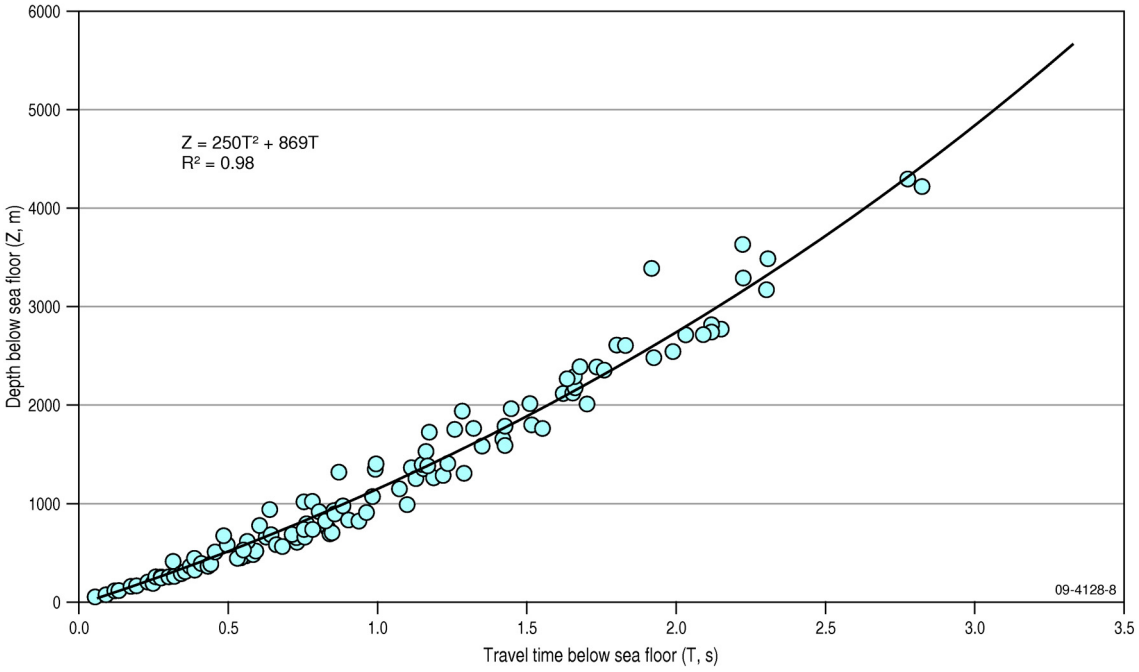

Figure 8. *Modelled sonobuoy data with best fit function which can be used for depth conversion.*

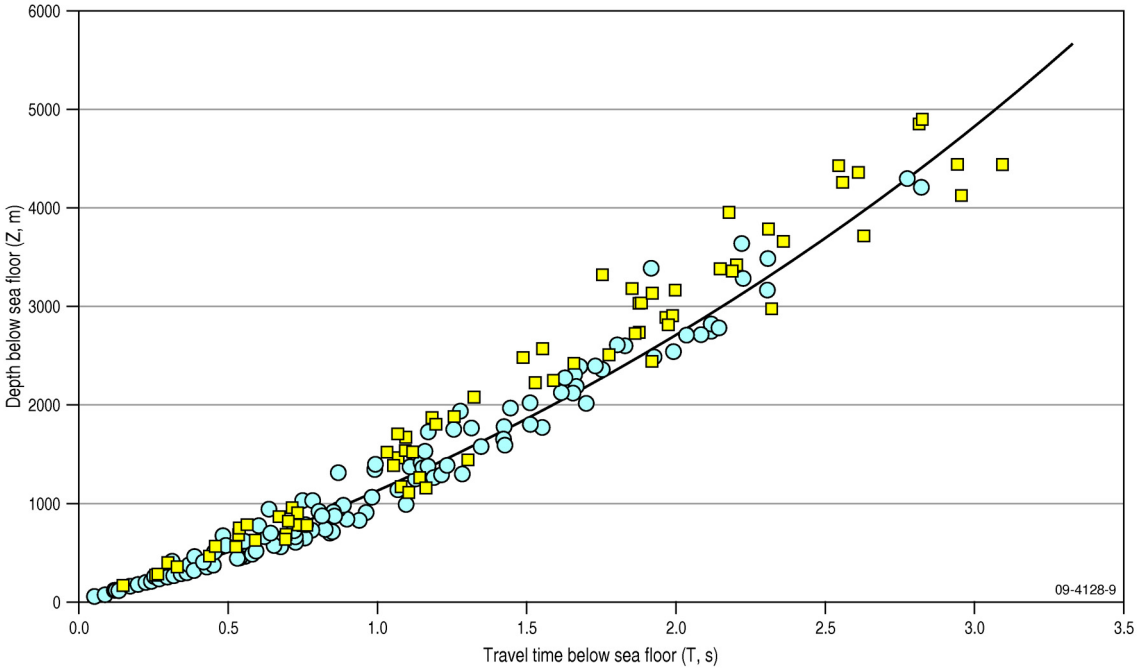

Figure 9. *Same as Figure 6 with the addition of points (■)abstracted from the models of Klingelhoefer et al. (2007), for comparison.*

STACKING VELOCITIES

Stacking velocities were obtained from the processing of the reflection seismic data for all lines, and later new set of velocities were obtained after depth-migration of line GA-302-19. The velocities were smoothed using an 11 point averaging filter and then interval velocities calculated using the Dix equation coded in program *deptime.pl* written by the author. For subsequent analysis the interval velocities were resturicted to <5500 m/s as a way of obtaining a result relevant for the sedimentary part of the section. At a maximum depth of burial of 5-6 km, the sediment velocity is not expected to exceed 5000 m/s. Several sources support this expectation:

- Collins *et al.* (1992) mapped P-wave velocities up to 4000 m/s in the Gippsland Basin at 10 km depth from a refraction experiment.
- Brocher (2008) examined velocity data from a variety of sources including well logs for sedimentary rocks in California, and reports P-wave velocities not exceeding 5500 m/s at 6 km sediment thickness.
- An extrapolation of the Nafe and Drake (1963) deep-water function applicable to marine sediments to 2 km depth below sea floor yields a P-wave velocity of 4400 m/s at 6 km depth of burial.
- Averbukh & Nikolayev (1990) published velocity-depth functions for Cenozoic terrigenous sediments to 4 km depth in several U.S.S.R. wells which extrapolate to 4200 m/s and Mesozoic sediments which extrapolate to 4600 m/s at 6 km depth.
- Acheson (1981), in a comparative study of velocity data in wells to 3000 m from sedimentary basins of the Arctic Islands and Western Canada, proposes a set of generally applicable power law relations for sandstones and shales which extrapolate to $\leq$ 4700 m/s at 6 km depth.
- Storvoll *et al.* (2005) compiled previously published velocity log data to depths of 4700 m on mostly marine shales from the North Sea region. A linear velocity-depth trend of $Z = 1.76\ V_p - 2600$ metres below sea floor[10] was estimated from these data (where V_p is in metres per second). Extrapolated to Z=6000m, this trend gives a velocity of 4890 m/s, although the spread in velocities at all depths is considerable.

Also excluded from the stacking velocity analysis were travel times > 3.5 s, the maximum sediment thickness observed in the reflection seismic data, and intervals shorter than 0.1 s, the denominator of the Dix (1957) relation, which may produce erratic interval velocities.

[10] This is approximately $Z = 250t^2 + 445t$ where t is two-way travel time in seconds.

Time-depth functions

The depths to each point in the 1D stacking velocity function were computed from the interval velocities and travel times. The result is graphed in Figure 10, and the quadratic function of best fit is:

$$Z = 368\,t^{2} + 799t \qquad (\text{m}) \qquad ③$$

giving a sediment thickness of 7305 m at 3.5 s TWT maximum mapped thickness. The derived instantaneous velocity function by differentiation is:

$$V_t = 1472\,t + 1598 \qquad (\text{m/s}) \qquad ④$$

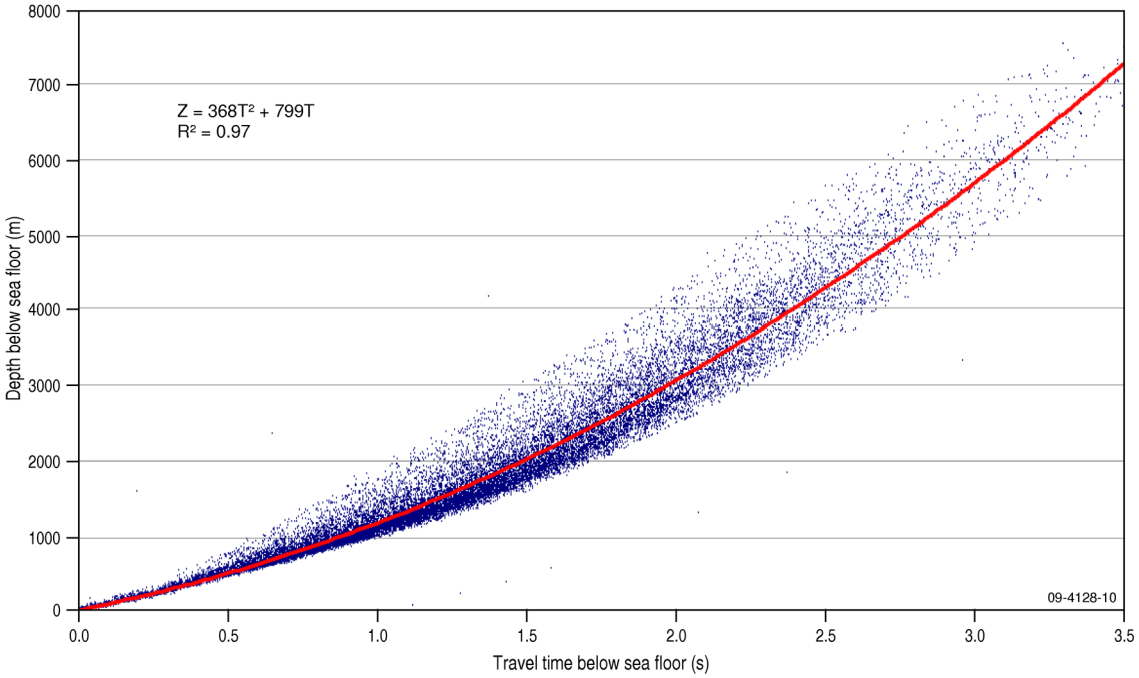

Figure 10. *Time to depth function as best fit to data points calculated from interval velocities derived from stacking velocities for all lines for survey GA-302.*

The time to depth function from the velocities used to depth migrate GA-302-19 is:

$$Z = 342\,t^{2} + 782\,t \qquad (\text{m}) \qquad ⑤$$

Figure 11 shows this function as the best fit to data points calculated from interval velocities.

The derived instantaneous velocity function by differentiation is:

$$V_t = 1368\,t + 1564 \qquad (\text{m/s}) \qquad ⑥$$

An alternative approach is to use a set of horizons picked on the time section as reference, and then by inspection pick the same events on the depth migrated section. Using shot-point number as the key,

merge the two sets of picks to obtain a relationship between depth and time. The result is shown in Figure 12 and the time to depth which best fits the data points is:

$$Z = 345\,t^{2} + 705\,t \quad (\text{m}) \qquad ⑦$$

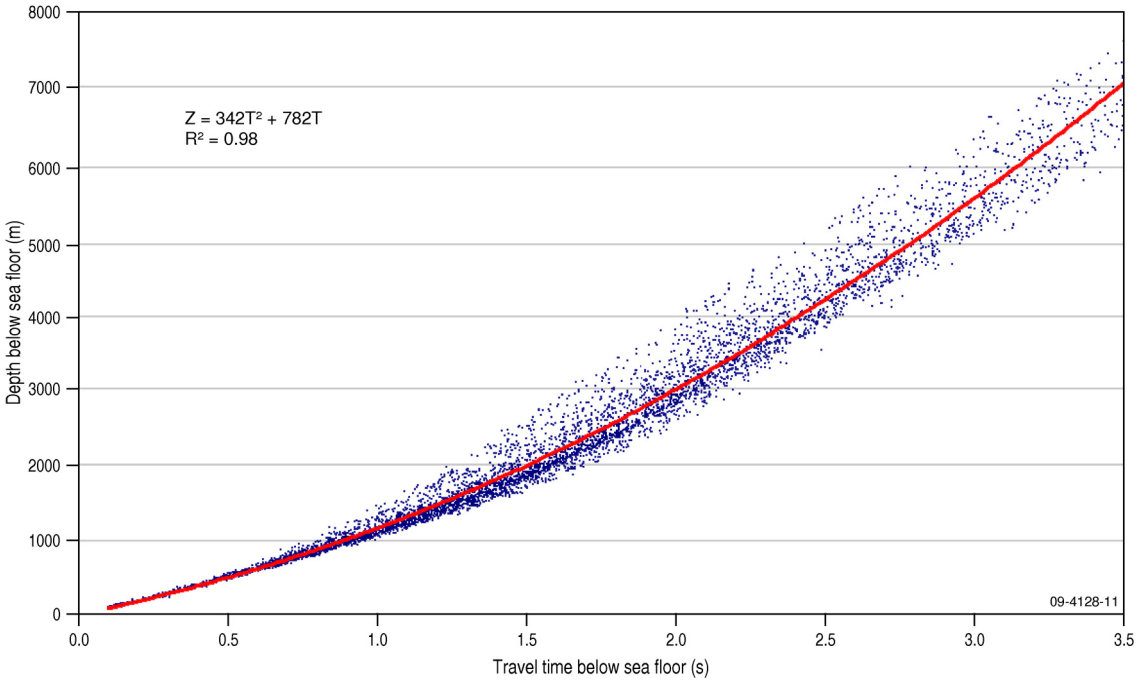

Figure 11. *Time to Depth function from velocities used to depth migrate GA-302-19.*

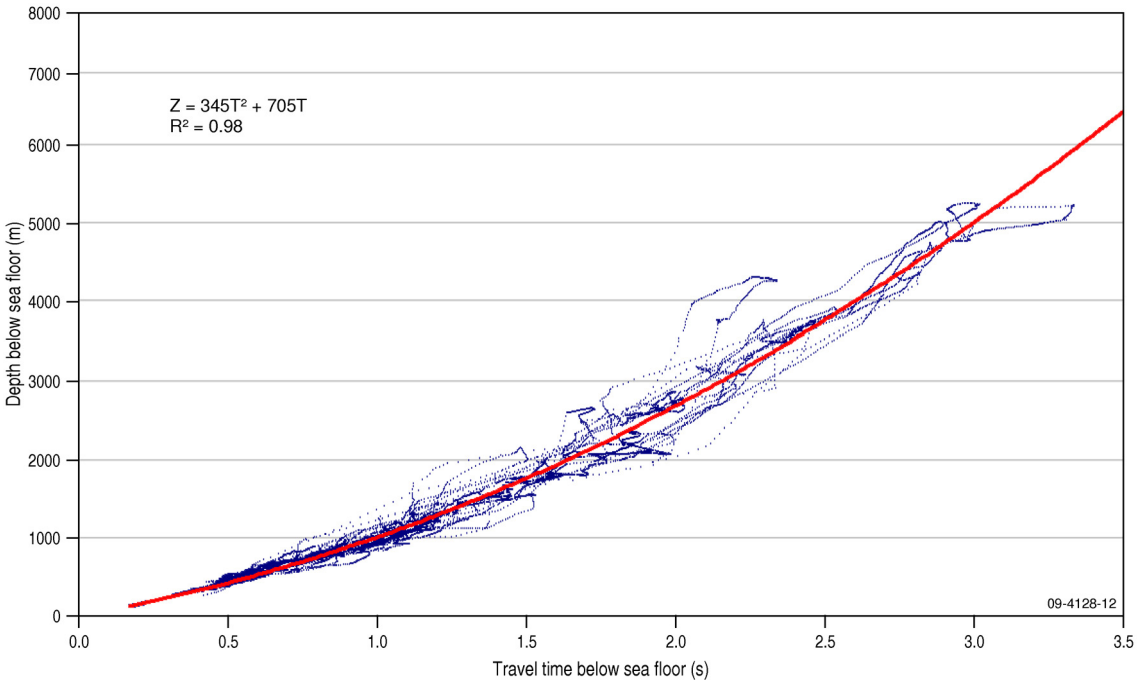

Figure 12. *Time to depth best fit function to data points from matching horizons in time and depth sections.*

The derived instantaneous velocity function by differentiation is:

$$V_t = 1380\ t + 1410 \qquad (\text{m/s}) \qquad ⑧$$

The maximum difference between equations 5 and 7, based on fundamentally the same data, is less than 240 metres in the range of sediment thickness.

Summary – all functions

The depth-time functions for refraction models and interval velocities from seismic processing velocities are summarised in Table 5 and graphed in Figure 13 for comparison.

Table 5. *Summary of time-depth functions derived from various sources. 'F' is function identifier corresponding to text; Z is depth below sea floor (m); t is two-way travel time below sea floor (s); Vt is velocity (m/s) derived from the corresponding depth-time function as noted in 'Source'; 'Range' is the range of the function over 0-3.5 s TWT; 'Vav' is the average velocity for this range.*

F	Function	Source	Range over 0-3.5 s TWT	V_{av} m/s
①	$Z = 250\ t^2 + 869\ t$	Sonobuoys	0 - 6104 m	3488
②	$V_t = 1000\ t + 1738$	from ① by differentiation	1738 - 5238 m/s	
③	$Z = 368\ t^2 + 799\ t$	Stacking velocities	0 - 7305 m	4174
④	$V_t = 1472\ t + 1598$	from ③ by differentiation	1598 - 6750 m/s	
⑤	$Z = 342\ t^2 + 782\ t$	Depth migration velocities, GA-302-19	0 - 6927 m	3958
⑥	$V_t = 1368\ t + 1564$	from ⑤ by differentiation	1564 – 6352 m/s	
⑦	$Z = 345\ t^2 + 705t$	Correspondence between Time & Depth migrated, GA-302-19	0 - 6694 m	3825
⑧	$V_t = 1380\ t + 1410$	from ⑦ by differentiation	1410 – 6240 m/s	

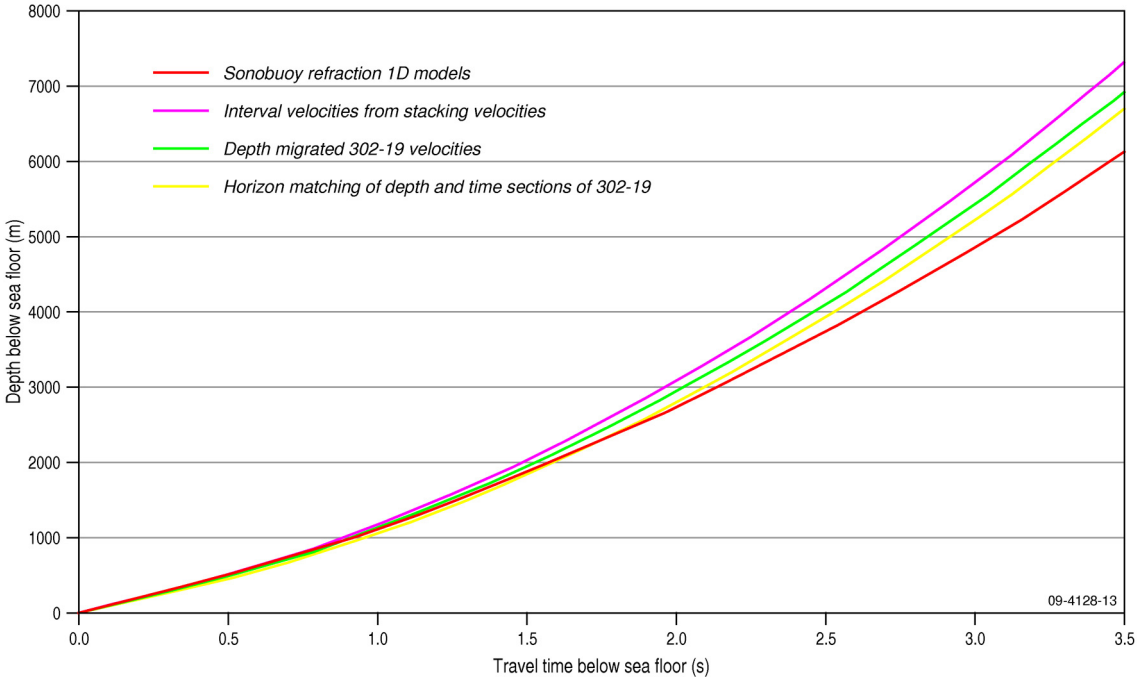

Figure 13. *Comparison of time to depth functions presented in the text for sonobuoy models and stacking velocity sources.*

APPLICATION OF THE VELOCITY MODELS

Depth conversion and sediment thickness

The 'best' time-depth function will optimise ties with independent measurements such as wells. In this area the only well, DSDP 208, penetrated the top 594 m of the sedimentary section in the very northern part of the study area[11]. Higgins (in prep.) found that the best tie for the Oligocene-Eocene boundary at DSDP 208 was achieved using the stacking velocity function (③).

However, this gives an unreasonably high instantaneous velocity in the sediments of 6750 m/s at the maximum depth to basement of 3.5 s TWT, and for this reason the sonobuoy function is preferred for the deeper sediments. A hybrid approach might be justified in this instance, in which the stacking velocity function is used in the shallow section, crossing over to the sonobuoy function for the deeper section.

This signals a caution to the common practice of depth conversion by applying interval velocities derived from stacking velocity functions. Although convenient to do so, the interval velocities derived in this way are observed to be too high at depth (Petkovic 2004a, 2004b), and hence maximum sediment thicknesses will be over-estimated by an unknown amount. Al Chalabi (1994) warns that 'stacking velocity' is a misleading term, being merely a suitably dimensioned by-product of seismic processing, and depth conversion using unadjusted stacking velocities can lead to considerable errors. Fortunately, interval velocities derived from stacking velocities are observed to be close to measured P-wave velocities for typical drilling depths in basin contexts in shallow water where layering is close to horizontal (Petkovic, 2004a), and depth conversion using individual stacking velocity functions every kilometre or so along the line is an acceptable practice in regional studies under those circumstances.

In the present study, the depths obtained from the stacking velocity-derived function are less than 5% greater than corresponding depths from the refraction function up to 1 s TWT, but this difference increases to ~20% at 3.5 s TWT. The difference between the three seismic processing velocity functions is up to 10%. The figures indicate the uncertainty in sediment thickness and horizon depth estimates based on these methods.

The sediment isopach is given in Figure 14, which shows the compartmentalised nature of the study area, with the thickest pockets of sediment in the northwest. The gravity trends (Petkovic *et al.* in prep.) support and emphasise the N-W trends evident in the sediment thickness map in the northwest

[11] For DSDP 208 correlation with the seismic data, see report prepared by S. McGiveron in Appendix 1 of Colwell et al. (in prep.)

of the study area. In the remainder of the study area the basement is relatively shallow and the sediment cover generally thin (Colwell *et al.* 2010).

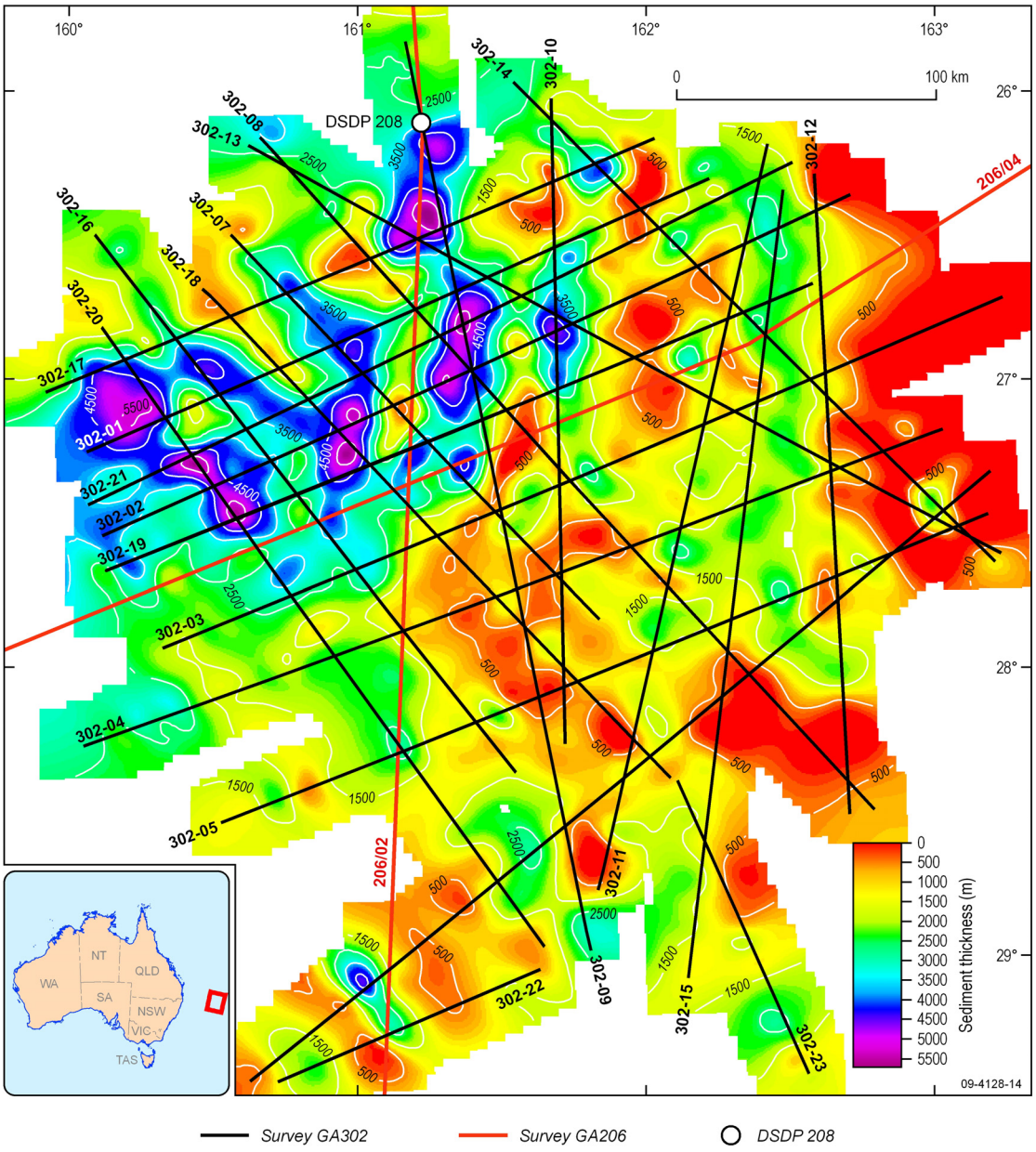

Figure 14. *Sediment thickness for the study area. The image was computed from a basement horizon interpreted from the reflection seismic data by Colwell et al. (2010) along the survey GA-302 and GA-206 ship tracks shown. The travel times were converted to depth using the sonobuoy refraction function discussed in the text then gridded using a minmum curvature algorithm with 3 km grid cell size and 12km clipping away from data points.*

Density estimation for gravity modelling

The velocity model can also be used for estimating a density for gravity modelling. The Nafe-Drake relationship (Ludwig *et al.* 1970) as digitised by Brocher (2005) can be used to infer density from velocity for sedimentary rocks. For the deeper parts of a gravity model, Christensen & Mooney (1995)

provide a compilation that may be used to infer density for basement and crustal model layers. Two approaches are possible:

- using one of the velocity-time functions to give a continuous density function of time, or
- using 1D velocity models to estimate average layer densities.

Either approach is reproducible from the data presented in this report. The former is achieved by simple substitution into the density-velocity relationship. The latter is achieved by the method described below.

Interpreted refraction and reflection layer boundaries in general don't coincide, as was observed by Petkovic *et al.* (2000) and Goncharov (2004) after ocean-bottom seismometer experiments on the North-West Shelf, and the same is true in the present study. In order to apply the 1D velocity models of Appendix 3 to determine average reflection seismic layer interval velocities, program '*vprofile.pl*' was written by the author. Input to this program is a file of depth-converted reflection seismic horizon interpreted picks, and the 1D velocity models listed in Appendix 3. From these, the program computes the instantaneous velocity at small increments of depth, say 100m, for each shotpoint at which there is a 1D velocity model. The set of instantaneous velocities that fall within a layer are averaged to provide an interval velocity for the layer at that shotpoint. These are then averaged across the whole area at all locations where 1D velocity models exist. The density-velocity function of Brocher (2005) can then be used to estimate density for the sedimentary layers.

For example, Petkovic *et al.* (in prep.) carried out gravity modelling of the Capel and Faust basins using a 3-layer sediment sub-division as recommended by the reflection seismic interpretation team Colwell *et al.* (2010). Gravity model sediment layers SedUpper, SedMiddle, SedLower and the Basement are separated by interpreted reflection seismic horizons CF_Olig, CF_Sr2B and CF_CretRift respectively, as defined by Colwell *et al.* (2010). An output from program '*vprofile.pl*', applied to these depth converted horizons is given in Table 6.

Table 6. *Average densities for 3 sediment intervals mapped in the reflection seismic data by Colwell et al. (2010) using the method described in the text. 'N' is the number of sonobuoy-derived 1D velocity models from Appendix 3 used to compute statistics; 'Mean' is the average velocity (m/s) for each interval having a standard deviation of 'std'. Median (m/s) of the N values is also given. 'Density' (t/m3) is derived from 'Mean' using the 'Nafe-Drake' velocity-density function of Brocher (2005). In the same way, 'Range' is the density range corresponding to the standard deviation of the mean velocities.*

Layer	N	mean	std	median	Density	Range
Water	36	1505	0.1	1505	1.01	1.01-1.01
SedUpper	36	1880	209.6	1814	1.85	1.01-1.94
SedMiddle	35	2624	483.5	2786	2.13	1.97-2.25
SedLower	32	3442	629.6	2879	2.31	2.18-2.40
Basement	21	5063	730.0	4700	2.54	2.44-2.67

In this case basement density was also computed using the velocity-density function of Brocher (2005), as it is proposed by Colwell *et al.* (2010) to consist, in large part, of older basin material with areas of featureless non-stratified lithology and volcanic facies. However, the compilation of global crustal averages for velocity and density by Christensen & Mooney (1995) may be used for those areas where a crystalline basement hypothesis is proposed and P-wave velocities therein exceed 5.5 km/s. Modelled velocities mapped below the SedLower layer were in the range 3700-6500 m/s with a mean of 5063 m/s, indicating highly variable composition within the nominal basement, and indicating a sedimentary, metasedimentary and partly igneous composition.

Summary & Conclusions

Refraction data acquired from 36 sonobuoys during survey GA-302 over the Capel and Faust basins, Lord Howe Rise, were modelled by forward ray-tracing giving a velocity profile through the sedimentary sequence. Reflection seimsic data interpretation indicated a maximum sediment thickness of 3.5 s TWT in the northwest part of the study area within the Capel Basin (Colwell *et al.* 2010). The refracted raypaths did not achieve this penetration, but extrapolation of a quadratic time-depth function derived from the velocity models suggests that a twt-way travel time of 3.5 s corresponds to a sediment thickness of a little in excess of 6000 m, an average interval velocity for the sedimentary pile of ~3490 m/s. The quadratic time-depth function has a slope at this maximum depth of ~5240 m/s.

For comparison, interval velocities from smoothed stacking velocities were treated globally with suitable constraints to yield a quadratic time-depth function. This characteristic curve yields a total sediment thickness of ~7300 m and an average sediment velocity of ~4170 m/s. However, at the maximum depth of 3.5 s TWT, the function has a slope of ~6750 m/s, which is unlikely for sediments, and the use of stacking velocity data for estimating total thickness is not recommended in this area.

In the shallow section stacking velocities from long cable data and in a horizontally layered environment should yield adequate results for regional studies. The present study affords a simplistic estimate of the accuracy of stacking velocity data used in this way, by comparisons with velocities from the depth-migrated reflection seismic line GA-302-19. Such comparison suggests that average velocities derived from seismic processing can vary by 10% but be in error by 20% in comparison to measured refraction velocities, and the error increases with depth.

Such results suggest it is advantageous to routinely acquire refraction data on regional surveys to allow an independent check on depth conversion by the common practice of applying interval velocities derived from stacking velocities. These are processing parameters selected by inspection to optimise

the reflection seismic image and only approximate true propagation velocities under limited conditions.

Velocity models can also be used to estimate layer densities for gravity modelling, by application of published velocity-density relations. The basement velocities (and hence densities) are highly variable with an average of 5063 m/s (2.54 t/m^3), supporting a sedimentary or metasedimentary origin of rocks below the basement horizon interpreted in reflection data.

Acknowledgements

The author thanks Richard Lane and Riko Hashimoto for commentary, criticism and encouragement, Tanya Fomin, Alexey Goncharov and Goutam Nayak who reviewed the manuscript, Anne Fleming and Andrea Cortese for assistance with data and application software, and Veronika Galinec for draughting of the figures. The author publishes with the permission of the Chief Executive Officer, Geoscience Australia.

References

Acheson, C.H. 1981. 'Time-depth and velocity-depth relations in sedimentary basins – a study based on current investigation in the Arctic Islands and an interpretation of experience elsewhere'. *Geophysics*, 46(5): 707-716.

Al-Chalabi, M. 1994. 'Seismic velocities – a critique'. *First Break*, 12(12): 589-596.

Andrews, J.E. 1973. 'Correlation of seismic reflectors', in Burns, R.E., Andrews, J.E., *et al.*, *Initial reports of the Deep Sea Drilling Project. Volume 21*, U.S. Government Printing Office: Washington, D.C., pp. 459-479.

Andrews, J.E. & Foreman, J.A. 1971. *Sediment core descriptions: R/V Kana Keoki 1971 cruise, eastern and western Pacific Ocean. Report ADA015676*. Hawaii Institute of Geophysics: Honolulu.

Averbukh, A.G. & Nikolayev, A.V. 1990. 'Seismic properties of rocks and geological strata' in Nomokonov, V.P. (ed), *Seismic prospecting - geophysicist's reference book. Volume 1*. (in Russian). Nedra Publishers: Moscow, pp. 91-114.

Bernardel, G., Lafoy, Y., Van de Beuque, S., Missegue, F & Nercessian, A. 1999. *Preliminary results from AGSO Law of the Sea Cruise 206: an Australia/French collaborative deep-seismic marine survey in the Lord Howe Rise/New Caledonia region. Record 1999/14.* Australian Geological Survey Organisation: Canberra.

Brocher, T.M. 2005. 'Empirical relations between elastic wavespeeds and density in the Earth's crust'. *Bulletin of the Seismological Society of America*, 95(6): 2081-2092.

Brocher, T.M. 2008. 'Compressional and shear-wave velocity versus depth relations for common rock types in Northern California'. *Bulletin of the Seismological Society of America*, 98(2): 950-968.

Burns, R.E., Andrews, J.E., *et al.* 1973a. *Initial reports of the Deep Sea Drilling Project. Volume 21*. U.S. Government Printing Office: Washington, D.C.

Burns, R.E., Andrews, J.E., van der Lingen, G.J., Churkin Jr., M., Galehouse, J.S., Packham, G.H., Davies, T.A., Kennett, J.P., Dumitrica, P., Edwards, A.R. & Von Herzen, R.P. 1973b. 'Site 208' in Burns, R.E., Andrews, J.E., *et al.*, *Initial reports of the Deep Sea Drilling Project. Volume 21*. U.S. Government Printing Office: Washington, D.C., pp. 271-331.

Burns, D., Watters, W.A. & Webb, P.N. 1973c. 'Site 207' in Burns, R.E., Andrews, J.E., *et al.*, *Initial reports of the Deep Sea Drilling Project. Volume 21*. U.S. Government Printing Office: Washington, D.C., pp. 197-269.

Christensen, N.I. & Mooney, W.D. 1995. 'Seismic velocity structure and composition of the continental crust: a global view'. *Journal of Geophysical Research*, 100(B6): 9761-9788.

Collins, C.D.N., Cull, J.P., Colwell, J.B. & Willcox, J.B. 1992. 'The deep velocity structure beneath the Gippsland Basin from long-offset seismic data'. *Exploration Geophysics*, 23: 69-74.

Colwell, J.B., Foucher, J-P., Logan, G. and Balut, Y. 2006. 'Partie 2, Programme AUSFAIR (Australia–Fairway basin bathymetry and sampling survey) Cruise Report' in *Les rapports de campagnes à la mer, MD 153/AUSFAIR–ZoNéCo 12 and VT 82/GAB on board R/V*

Marion Dufresne. Réf : OCE/2006/05. Institut Polaire Français Paul Emile Victor: Plouzané, France.

Colwell, J.B., Hashimoto, T., Rollet, N., Higgins, K.L., Bernardel, G. & McGiveron, S. 2010. *Interpretation of seismic data, Capel and Faust Basins, Australia's Remote Offshore Eastern Frontier. Record 2010/06*.[CD-ROM] Geoscience Australia : Canberra.

Dix, C.H. 1955. 'Seismic velocities from surface measurements'. *Geophysics*, 20: 68-86.

Fugro Robertson Inc. 2007. *Geoscience Australia marine survey 302: final survey report*. [CD-ROM]. Geoscience Australia: Canberra.

Gaina, C., Müller, R.D., Royer, J-Y., Stock, J., Hardebeck, J. & Symonds, P. 1998. 'The tectonic history of the Tasman Sea: a puzzle with 13 pieces'. *Journal of Geophysical Research*, 103(B6): 12413-12433.

Goncharov, A. 2004. 'Basement and crustal structure of the Bonaparte and Browse basins, Australian northwest margin' in Ellis, G.K., Baillie, P.W. & Munson, T.J. (eds) 2004. *Timor Sea Petroleum Geoscience. Proceedings of the Timor Sea Symposium, Darwin, Northern Territory, 19-20 June, 2003. Special Publication 1*. Northern Territory Geological Survey: Darwin, pp. 551-566.

Hayes, D.E., Talwani, M., Houtz, R. & Walter, C.P. 1972. *U.S.N.S. Eltanin cruises 28-32, March 1967-March 1968. Technical Report CU-1-72*. Lamont Doherty Geological Observatory of Columbia University: New York.

Heap, A.D., Hughes, M., Anderson, T., Nichol, S., Hashimoto, T., Daniell, J., Przeslawski, R., Payne, D., Radke, L. & Shipboard Party. 2009. *Seabed environments and subsurface geology of the Capel and Faust basins and Gifford Guyot, Eastern Australia. Record 2009/22*. Geoscience Australia: Canberra.

Higgins, K.L. in prep. *Building a 3D GOCAD Model in Offshore Frontier Basins for Prospectivity Assessment: Capel/Faust Basins, Lord Howe Rise. Record*. Geoscience Australia: Canberra.

Kennett, J.P., Von der Borch, C.C., *et al.* 1986. *Initial reports of the Deep Sea Drilling Project*. U.S. Government Printing Office: Washington.

Klingelhoefer, F., Lafoy, Y., Collot, J., Cosquer, E., Géli, L., Nouzé, H. & Vially, R. 2007. 'Crustal structure of the basin and ridge system west of New Caledonia (southwest Pacific) from wide-angle and reflection seismic data'. *Journal of Geophysical Research*, 112, B11102, doi:10.1029/2007JB005093.

Ludwig, W.J., Nafe, J.E. & Drake, C.L. 1970. 'Seismic refraction' in Maxwell, A.E. (ed), *The Sea, Volume 4*. Wiley-Interscience: New York, pp. 53-84.

Mortimer, N., Hauff, F. & Calvert, A.T. 2008. 'Continuation of the New England Orogen, Australia, beneath the Queensland Plateau and Lord Howe Rise'. *Australian Journal of Earth Science*, 55: 195-209.

Nafe, J.E. & Drake, C.L. 1963. 'Physical properties of marine sediments' in Hill, M.N. (ed), *The Sea. Volume 3*. Interscience Publishers: New York, pp. 794-815.

Norvick, M.S., Langford, R.P., Rollet, N., Hashimoto, T., Earl, K.L. and Morse, M.P. 2008. 'New insights into the evolution of the Lord Howe Rise (Capel and Faust basins), offshore eastern Australia, from terrane and geophysical data analysis' in: Blevin, J.E., Bradshaw,

B.E. and Uruski, C. (eds), *Eastern Australasian Basins Symposium III: Energy security for the 21st century*. Petroleum Exploration Society of Australia: Perth, pp. 291–310.

Petkovic, P., Lane, R., Rollet, N. & Nayak, G. (in prep.). *3D mapping and gravity modelling of Capel and Faust basins, Lord Howe Rise. Record.* Geoscience Australia: Canberra.

Petkovic, P. 2004a. *Time-depth functions for the Great Australian Bight. Record 2004/01*. Geoscience Australia: Canberra.

Petkovic, P. 2004b. *Time-depth functions for the Otway Basin. Record 2004/02*. Geoscience Australia: Canberra.

Petkovic, P., Collins, C.D.N. and Finlayson, D.M. 2000a. *A crustal transect between Precambrian Australia and the Timor Trough across the Vulcan Sub-basin*. Tectonophysics, 329, 23-38.

Ramsay, D.C., Herzer, R.H. & Barnes, P.M. 1997. *Continental shelf definition in the Lord Howe Rise and Norfolk Ridge regions: Law of the Sea survey 177, Part 1 – preliminary results. Record 1997/54.* Australian Geological Survey Organisation: Canberra.

Robein, E. 2003. *Velocities, time-imaging and depth-imaging in reflection seismics: principles and methods*. EAGE Publications: Netherlands.

Seismic Image Software Ltd. 1995. *Seismic interpretation and geological modelling application (SIGMA)*. Geological Survey of Canada: Ottawa.

Shor, G.G., Kirk, H.K. & Menard, H.W. 1971. 'Crustal structure of the Melanesian area'. *Journal of Geophysical Research*, 76(11): 2562-2586.

Stagg, H.M.J., Borissova, I., Alcock, M. & Moore, A.M.G. 1999. 'Tectonic provinces of the Lord Howe Rise; Law of the Sea study has implications for frontier hydrocarbons'. *Australian Geological Survey Organisation Research Newletter*, 31: 31-32.

Storvoll, V., Bjørlykke, K. & Mondol, N.H. 2005. 'Velocity-depth trends in Mesozoic and Cenozoic sediments from the Norwegian Shelf'. *American Association of Petroleum Geologists Bulletin*, 89(3): 359-381.

Wilkens, R.H. & Handyside, T. 1985. 'Initial Report 28: Physical properties of equatorial Pacific sediments' in Mayer, L., Theyer, E, *et al., Initial Reports of the Deep Sea Drilling Project. Volume 85*. U.S. Government Printing Office: Washington, D.C., pp. 839-847.

Willcox, J.B., Symonds, P.A., Bennett, D. & Hinz, K. 1981. *Lord Howe Rise area, offshore Australia: preliminary results of a co-operative Federal Republic of Germany/Australia geophysical survey. Report 228.* Bureau of Mineral Resources, Geology & Geophysics: Canberra.

Van De Beuque, S., Stagg, H.M.J., Sayers, J., Willcox, J.B. & Symonds, P.A. 2003. *Geological framework of the northern Lord Howe Rise and adjacent areas. Record 2003/01*. Geoscience Australia: Canberra.

Zelt, C.A. & Smith, R.B. 1992. 'Seismic traveltime inversion for 2D crustal velocity structure'. *Geophysics Journal International*, 108: 16-34.

Appendix 1 – Sonobuoy and coincident reflection data

The sonobuoy data are shown (right half of each figure) with the equivalent portion of seismic reflection record (left half of each figure) and interpreted reflection seismic horizons 'Olig' (shallowest), 'Sr2B' (middle) and 'CretRift' (deepest) after Colwell *et al.* (2010). The apparent velocities are shown as labels on the refraction record and arrows are omitted where the event referred to is unambiguous. The sonobuoy identifier is given as 302-LL-SS, where LL is line number and SS is a sequential sonobuoy identifier. The vertical axis is two-way travel time in seconds and the horizontal axis is shot number, where the shot spacing is 37.5 m.

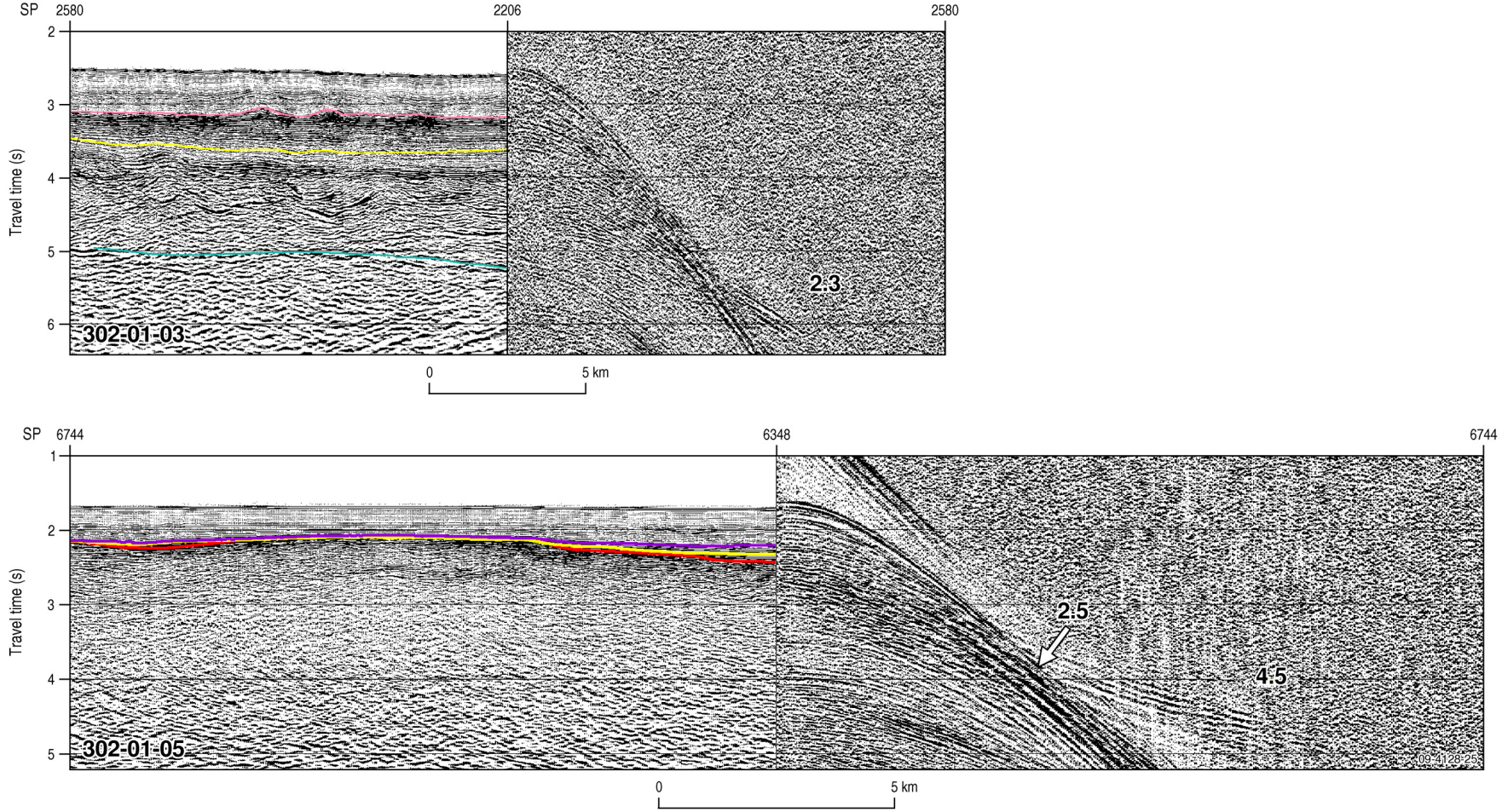

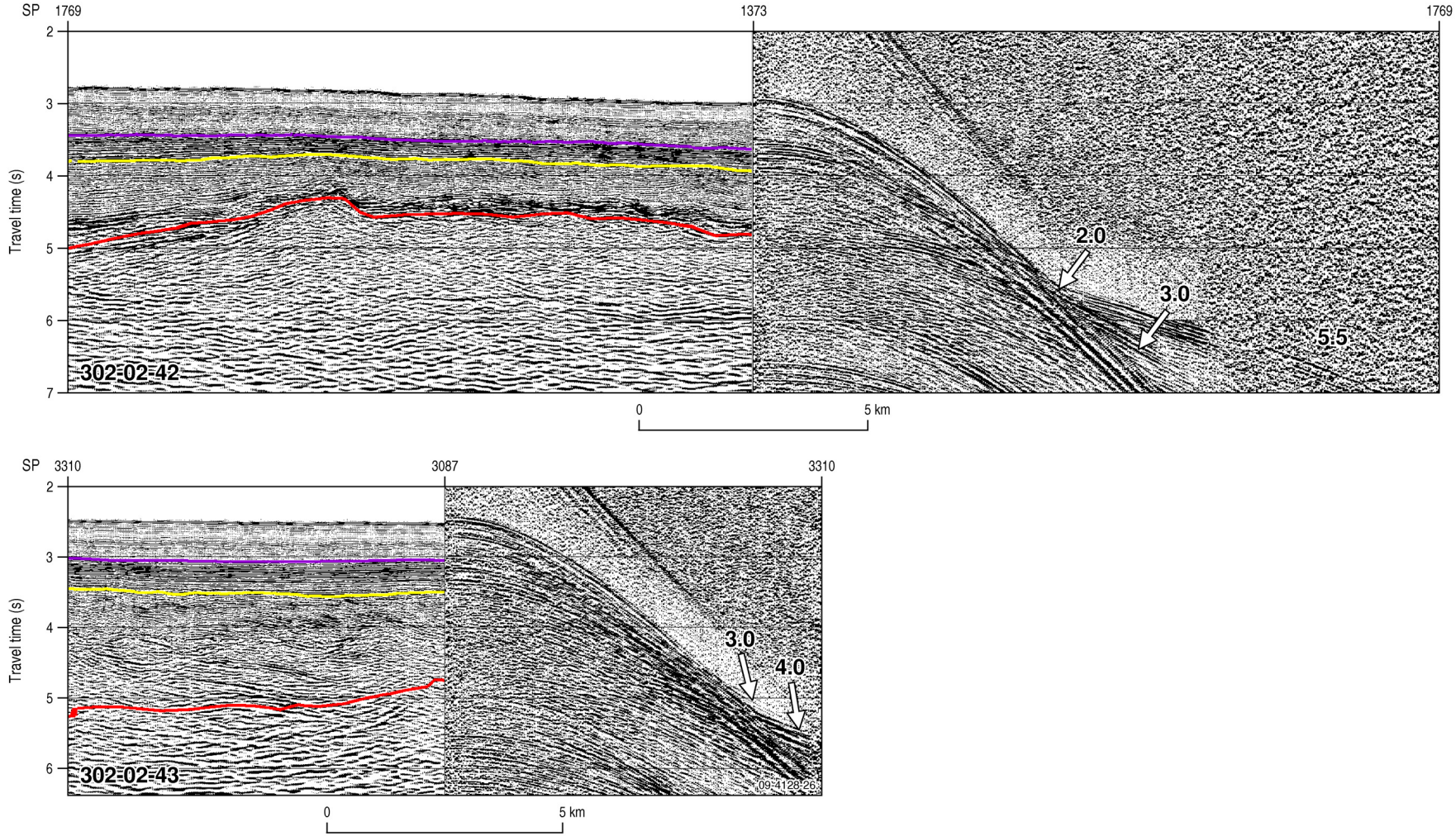
SP 1769
1373
1769
Travel time (s)
2
3
4
5
6
7
2.0
3.0
5.5
302-02-42
0
5 km
SP 3310
3087
3310
3.0
4.0
302-02-43
09-4128-26
0
5 km

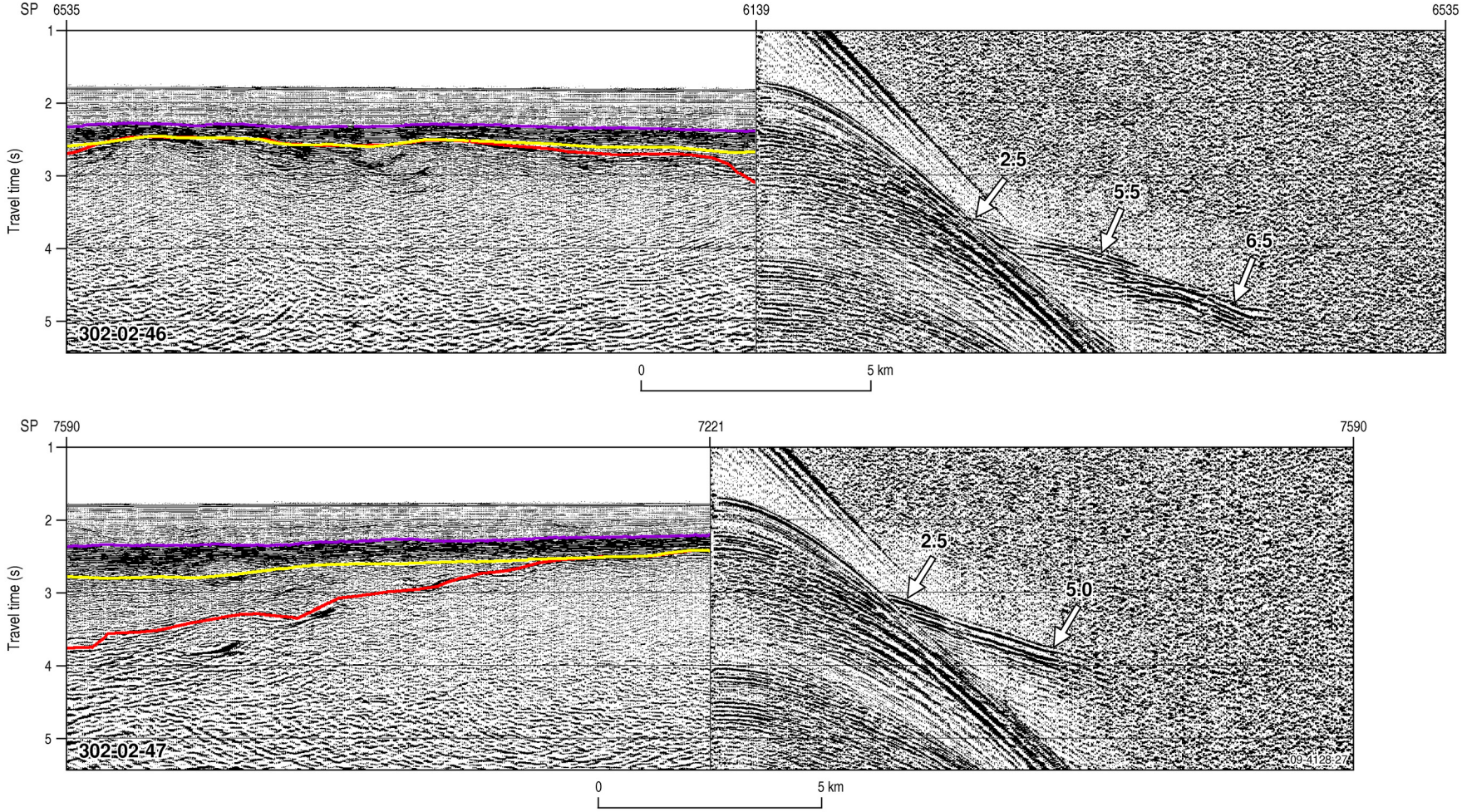
SP 6535
6139
6535
1
2
3
4
5
Travel time (s)
2.5
5.5
6.5
302-02-46
0
5 km
SP 7590
7221
7590
1
2
3
4
5
Travel time (s)
2.5
5.0
302-02-47
09-4128-27d
0
5 km

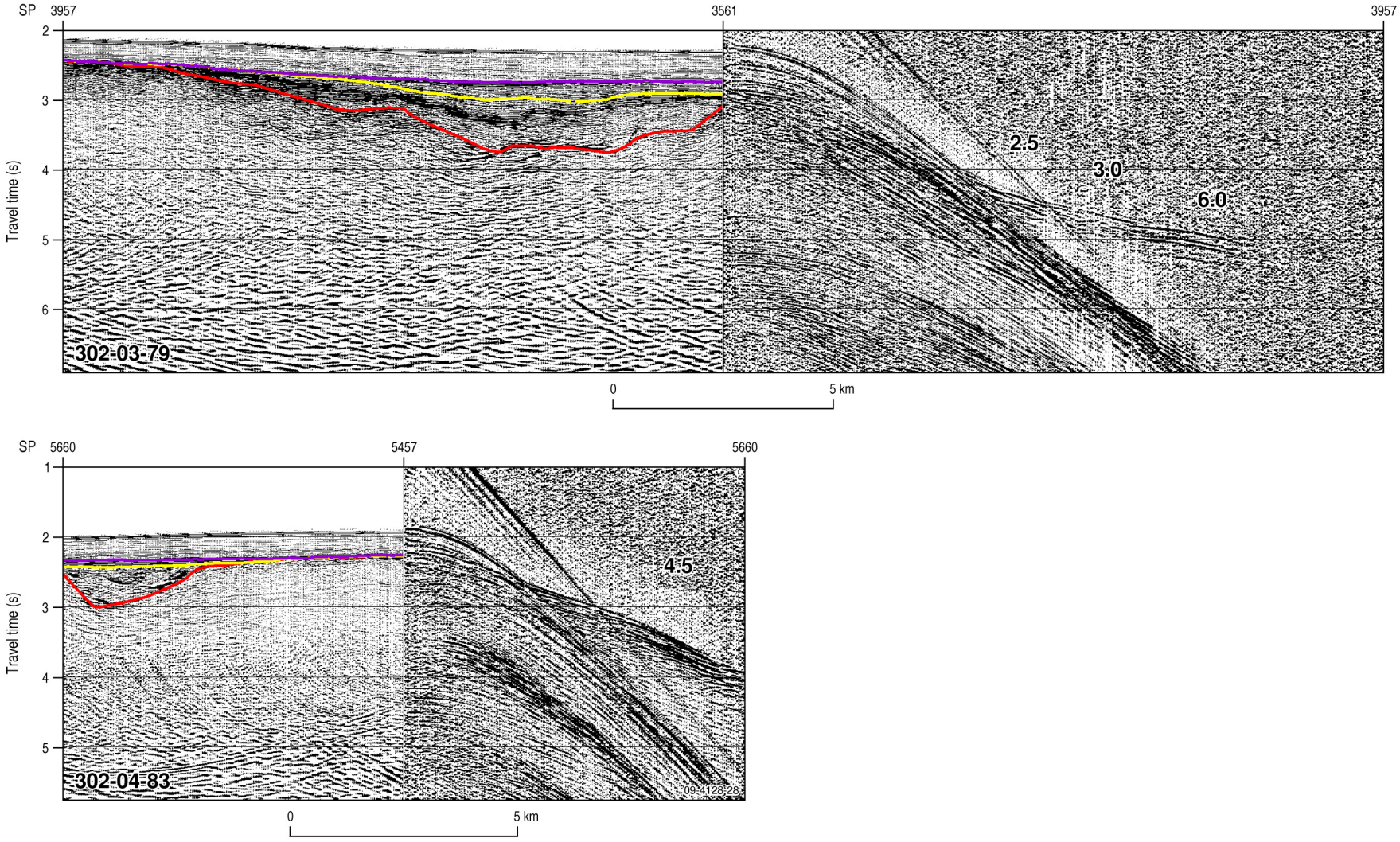
SP
3957
3561
3957
2
3
4
5
6
Travel time (s)
2.5
3.0
6.0
302-03-79
0
5 km
SP
5660
5457
5660
1
2
3
4
5
Travel time (s)
4.5
302-04-83
09-4128-28
0
5 km

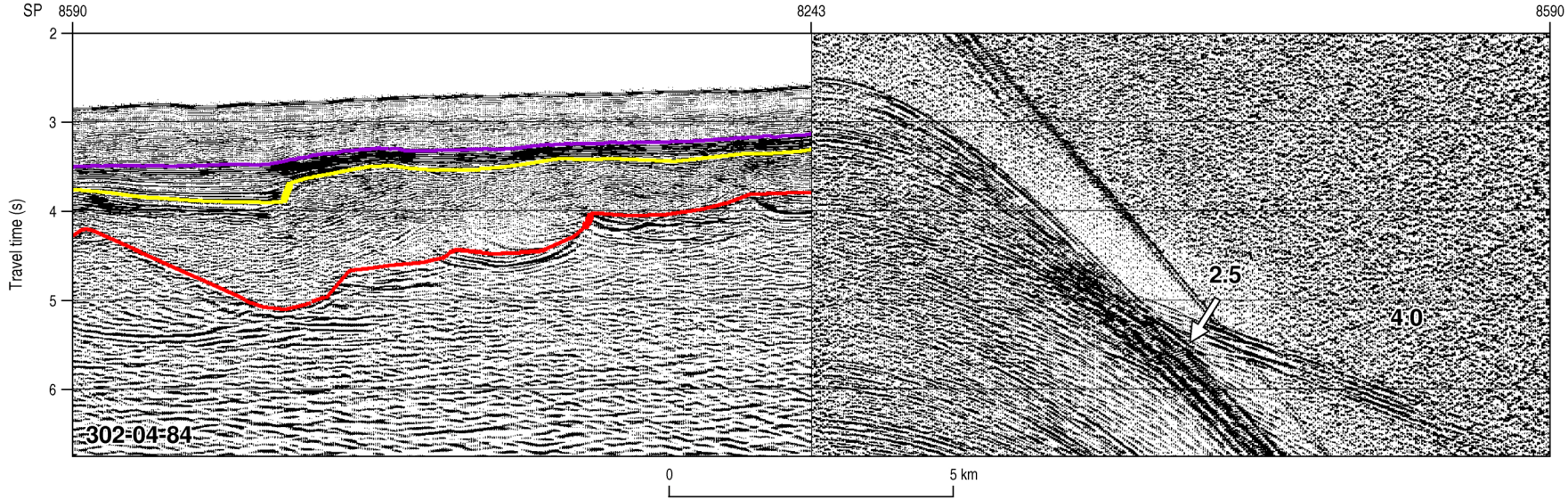
SP
8590
8243
8590
2
3
4
5
6
Travel time (s)
2.5
4.0
302-04-84
0
5 km

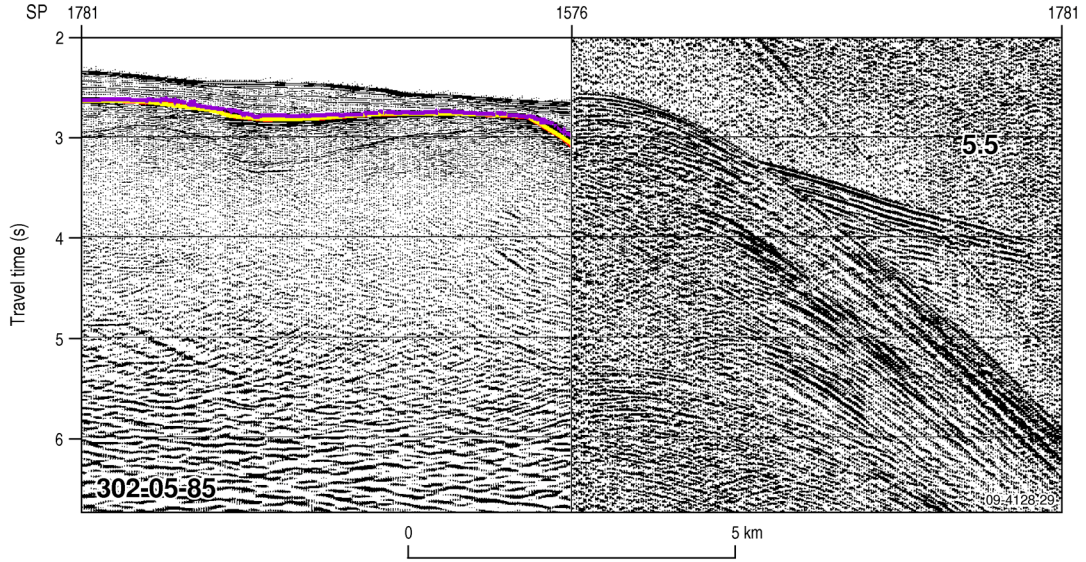
SP
1781
1576
1781
2
3
4
5
6
Travel time (s)
5.5
302-05-85
09-4128-29
0
5 km

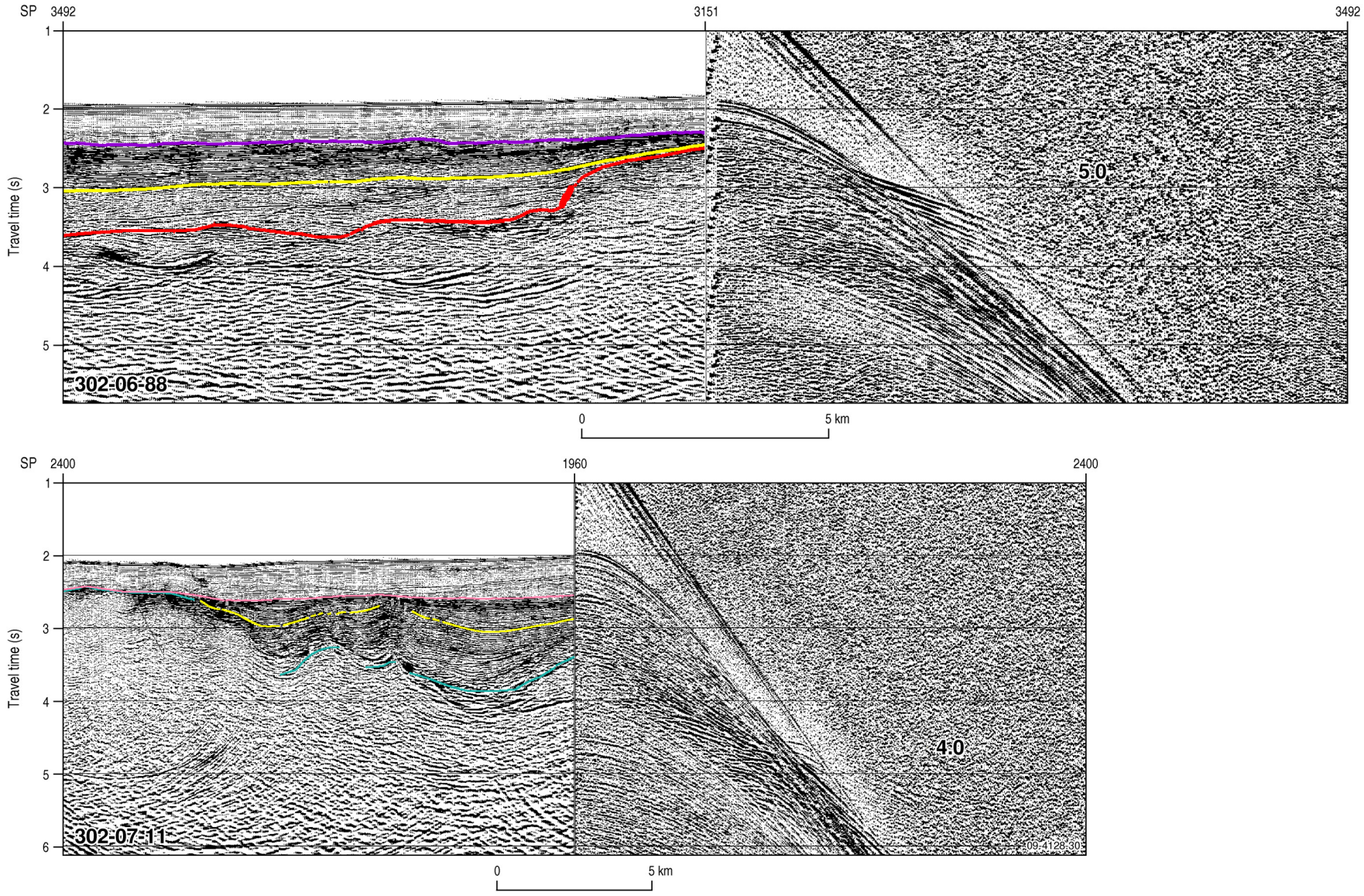
SP 3492
3151
3492
1
2
3
4
5
Travel time (s)
5.0
302-06-88
0
5 km
SP 2400
1960
2400
1
2
3
4
5
6
Travel time (s)
4.0
302-07-11
09-4128-30
0
5 km

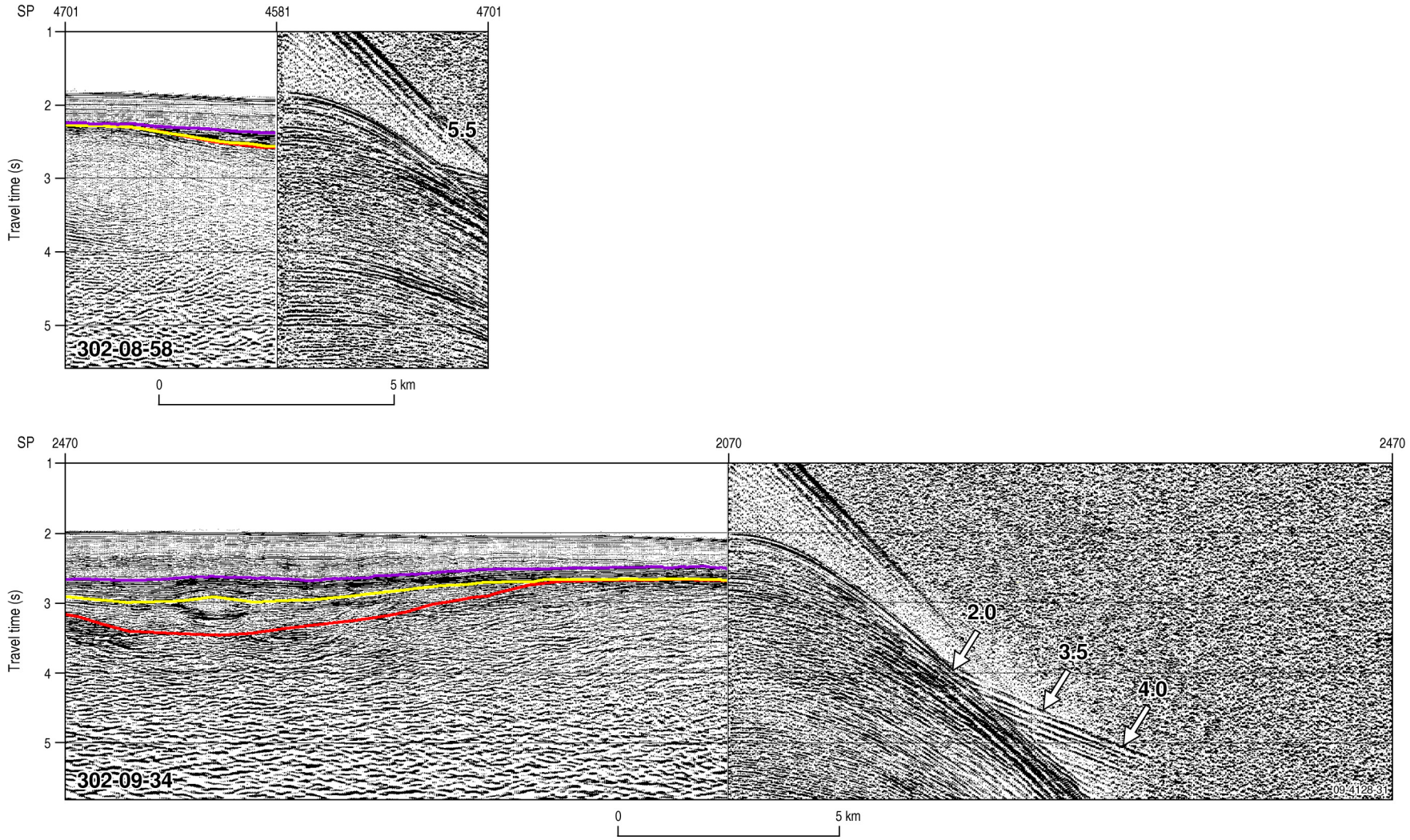
SP
4701
4581
4701
1
2
3
4
5
Travel time (s)
5.5
302-08-58
0
5 km
SP
2470
2070
2470
1
2
3
4
5
Travel time (s)
2.0
3.5
4.0
302-09-34
09_4128_31
0
5 km

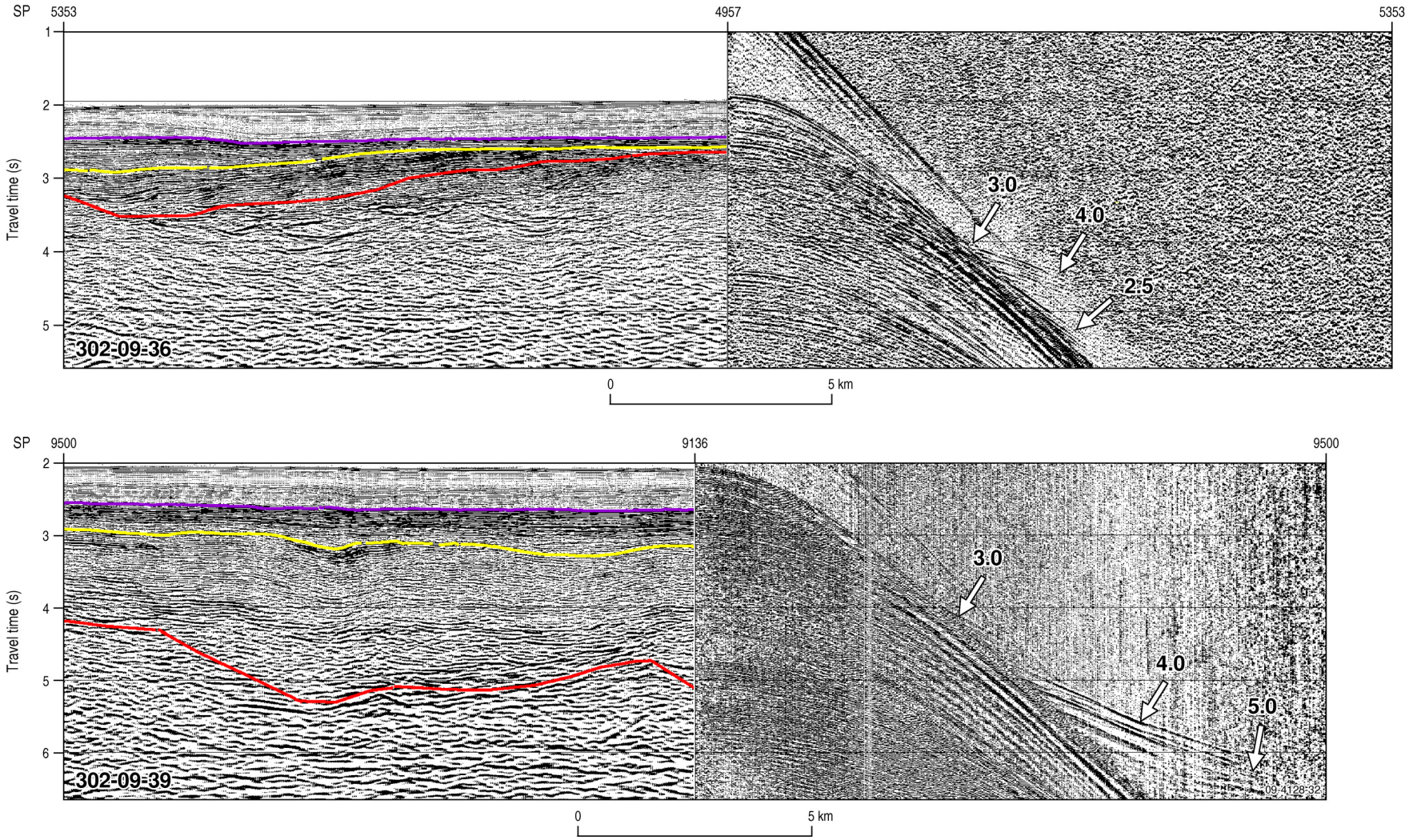
SP
5353
4957
5353
1
2
3
4
5
Travel time (s)
3.0
4.0
2.5
302-09-36
0
5 km
SP
9500
9136
9500
2
3
4
5
6
Travel time (s)
3.0
4.0
5.0
302-09-39
09-4128:32
0
5 km

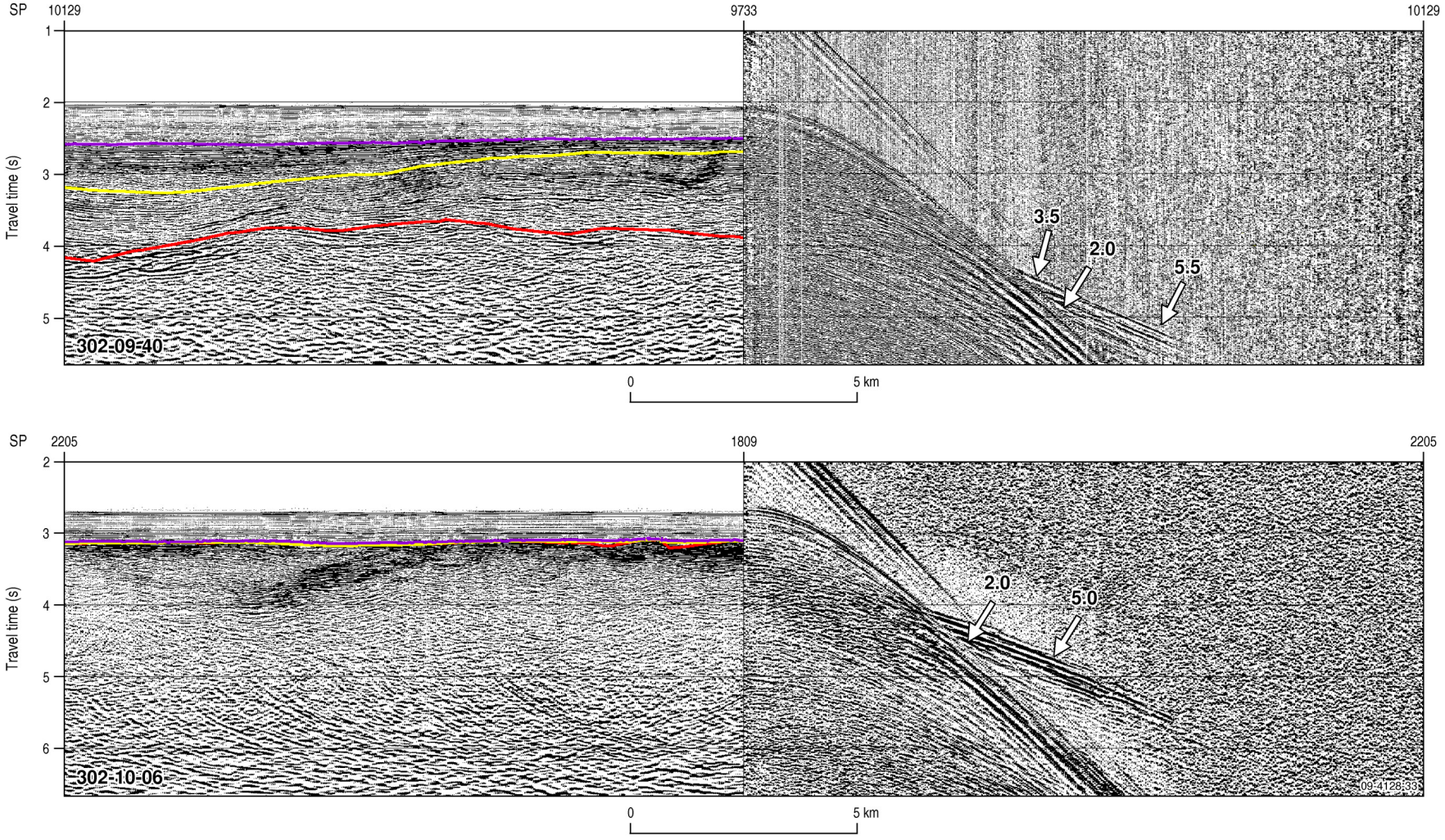
SP
10129
9733
10129
1
2
3
4
5
Travel time (s)
3.5
2.0
5.5
302-09-40
0
5 km
SP
2205
1809
2205
2
3
4
5
6
Travel time (s)
2.0
5.0
302-10-06
0
5 km

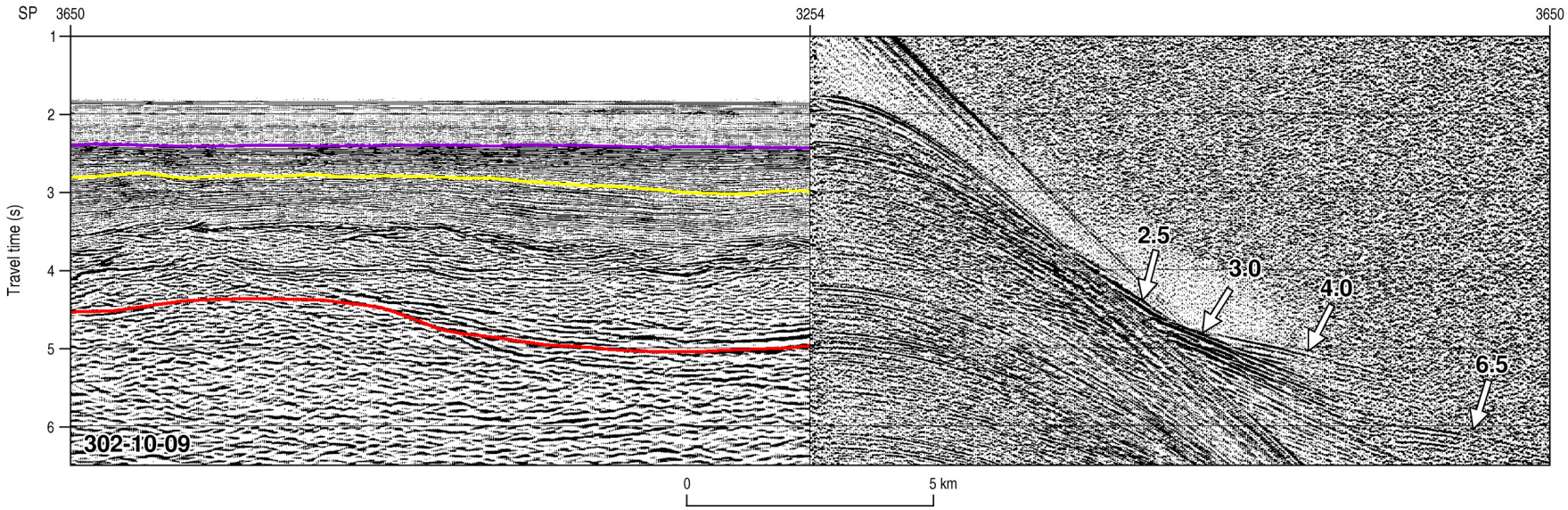
SP
3650
3254
3650
Travel time (s)
1
2
3
4
5
6
2.5
3.0
4.0
6.5
302-10-09
0
5 km

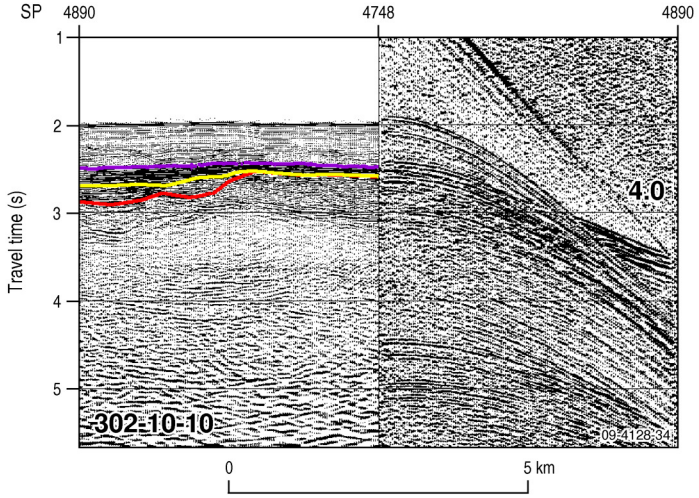
SP
4890
4748
4890
Travel time (s)
1
2
3
4
5
4.0
302-10-10
0
5 km

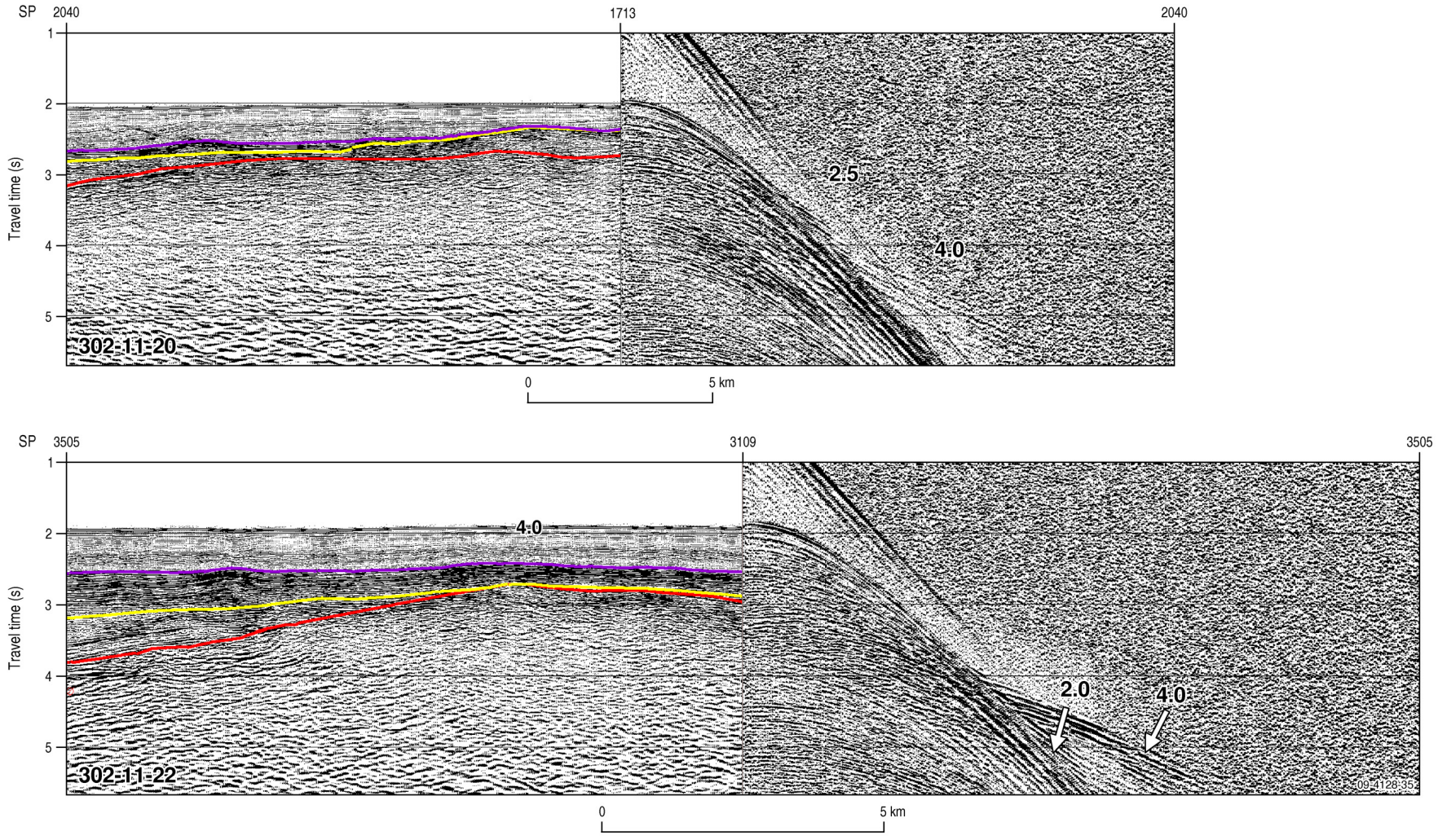
SP
2040
1713
2040
1
2
3
4
5
Travel time (s)
2.5
4.0
302-11-20
0
5 km
SP
3505
3109
3505
4.0
2.0
4.0
302-11-22
0
5 km

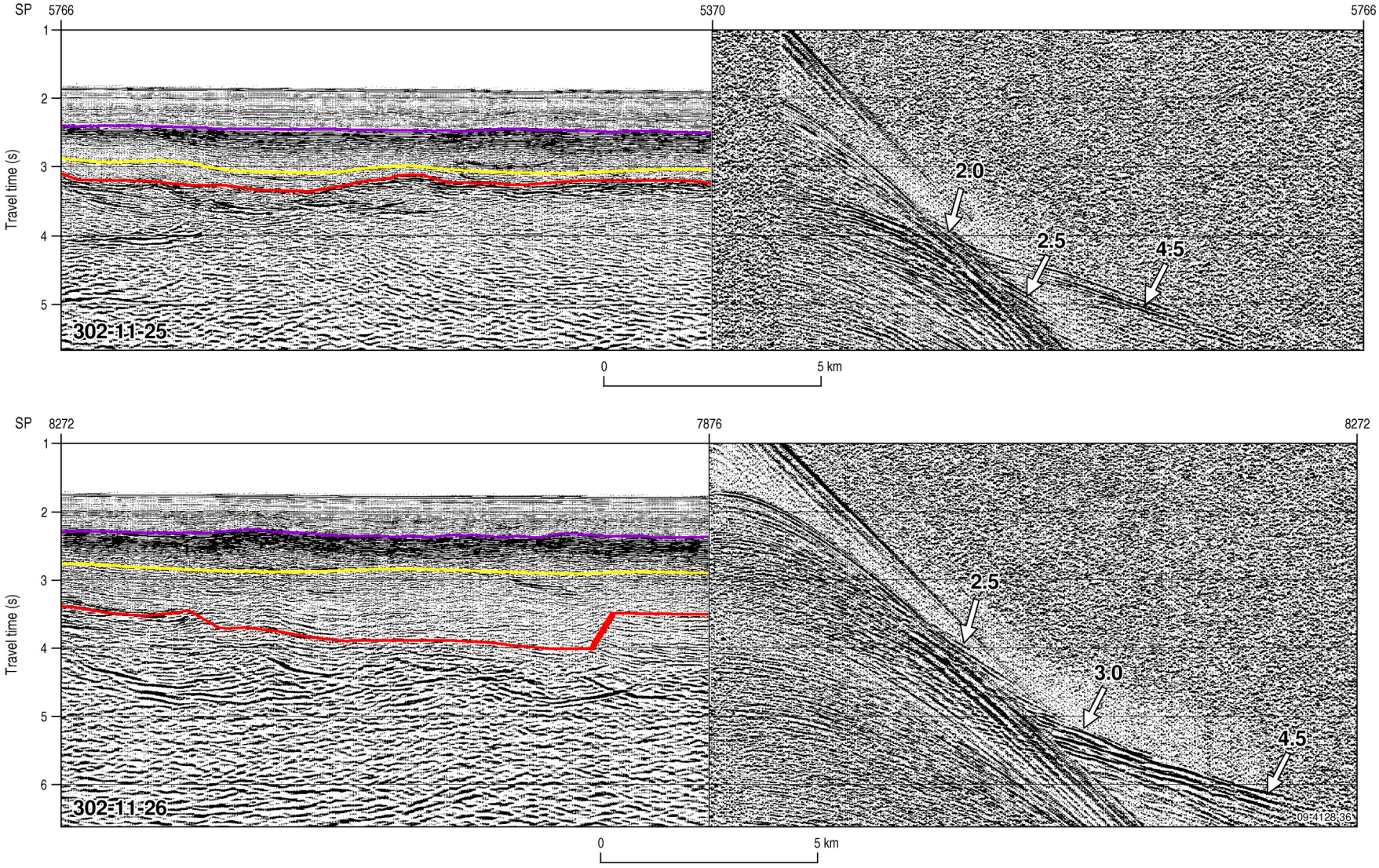
SP
5766
5370
5766
1
2
3
4
5
Travel time (s)
2.0
2.5
4.5
302-11-25
0
5 km
SP
8272
7876
8272
1
2
3
4
5
6
Travel time (s)
2.5
3.0
4.5
302-11-26
09-4128-36
0
5 km

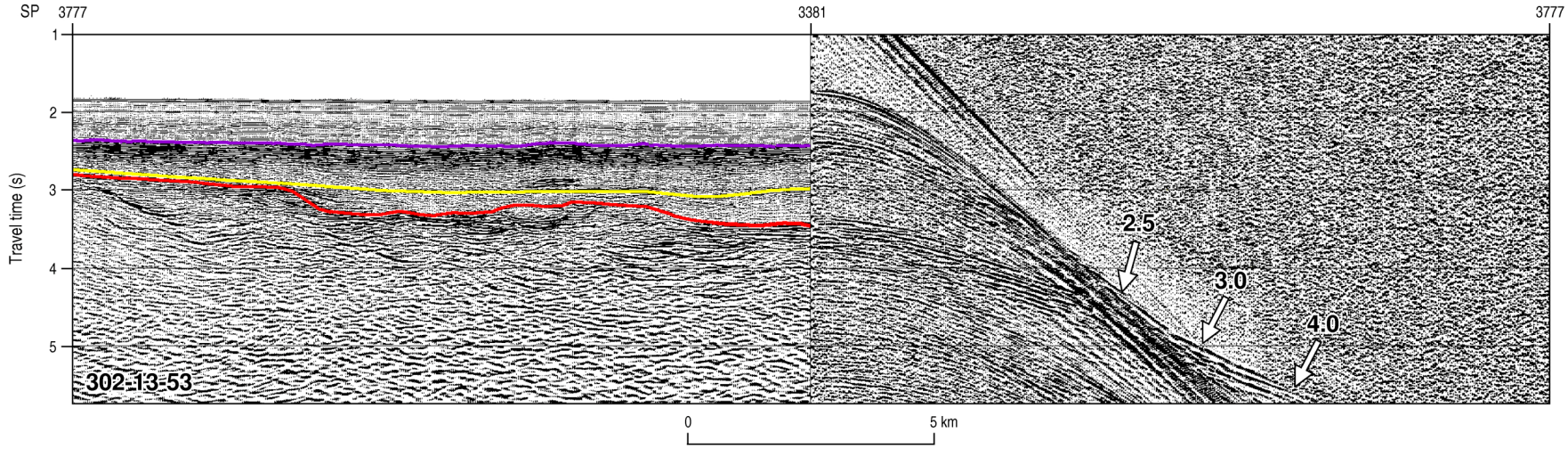
SP
3777
3381
3777
1
2
3
4
5
Travel time (s)
2.5
3.0
4.0
302-13-53
0
5 km

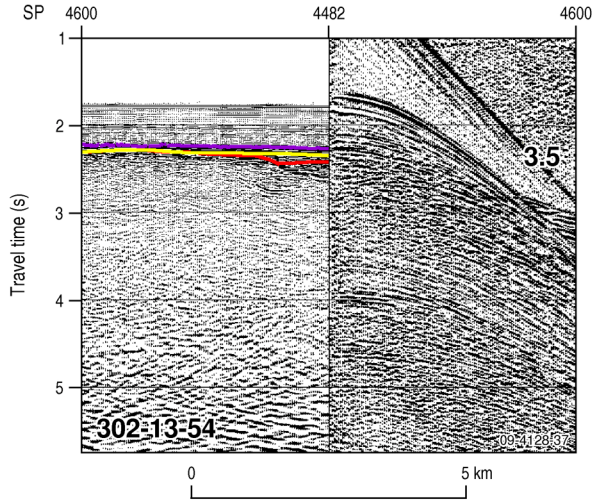
SP
4600
4482
4600
1
2
3
4
5
Travel time (s)
3.5
302-13-54
0
5 km

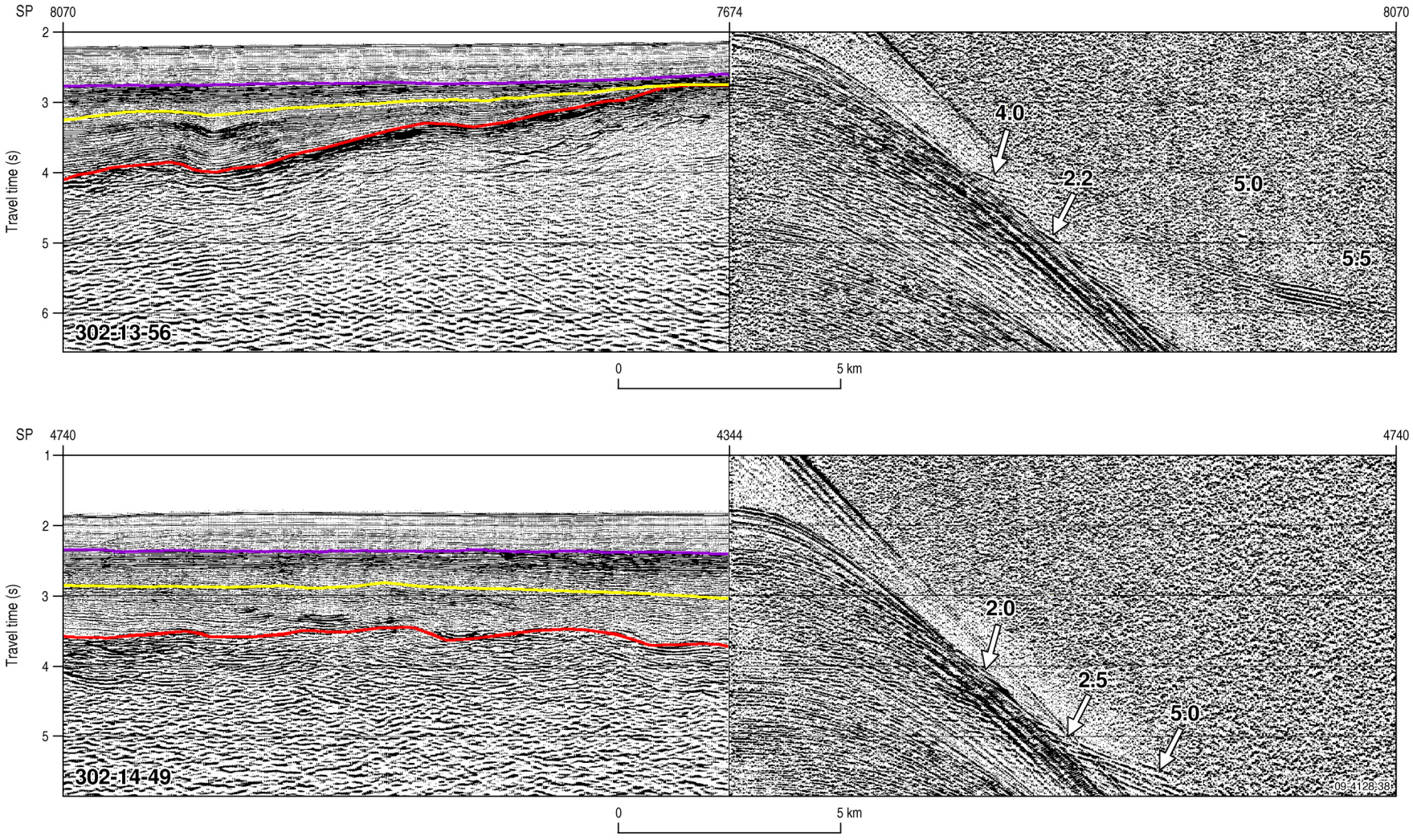
SP
8070
7674
8070
2
3
4
5
6
Travel time (s)
4.0
2.2
5.0
5.5
302-13-56
0
5 km
SP
4740
4344
4740
1
2
3
4
5
Travel time (s)
2.0
2.5
5.0
302-14-49
0
5 km

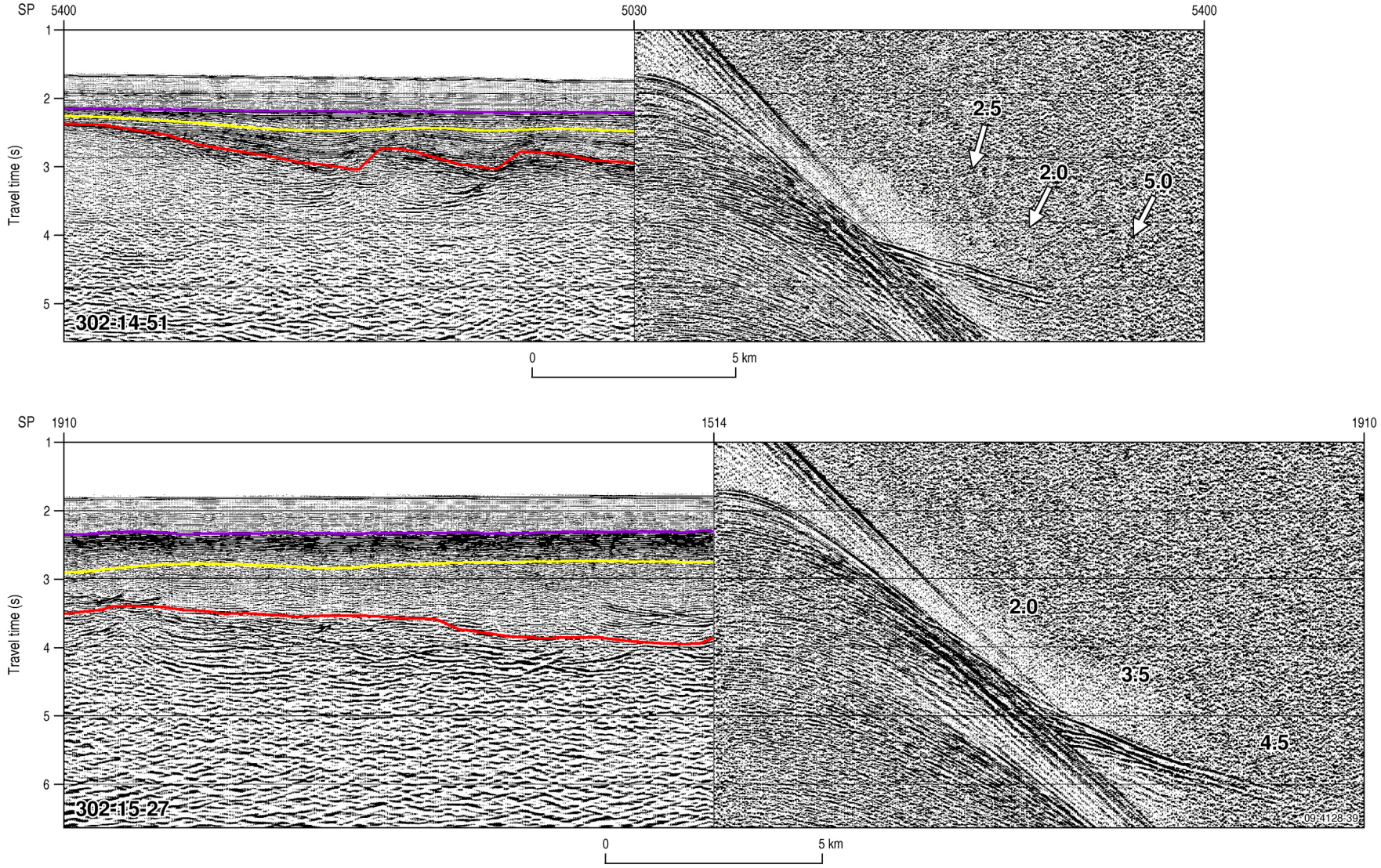
SP
5400
5030
5400
1
2
3
4
5
Travel time (s)
2.5
2.0
5.0
302-14-51
0
5 km
SP
1910
1514
1910
1
2
3
4
5
6
Travel time (s)
2.0
3.5
4.5
302-15-27
09-4128-39
0
5 km

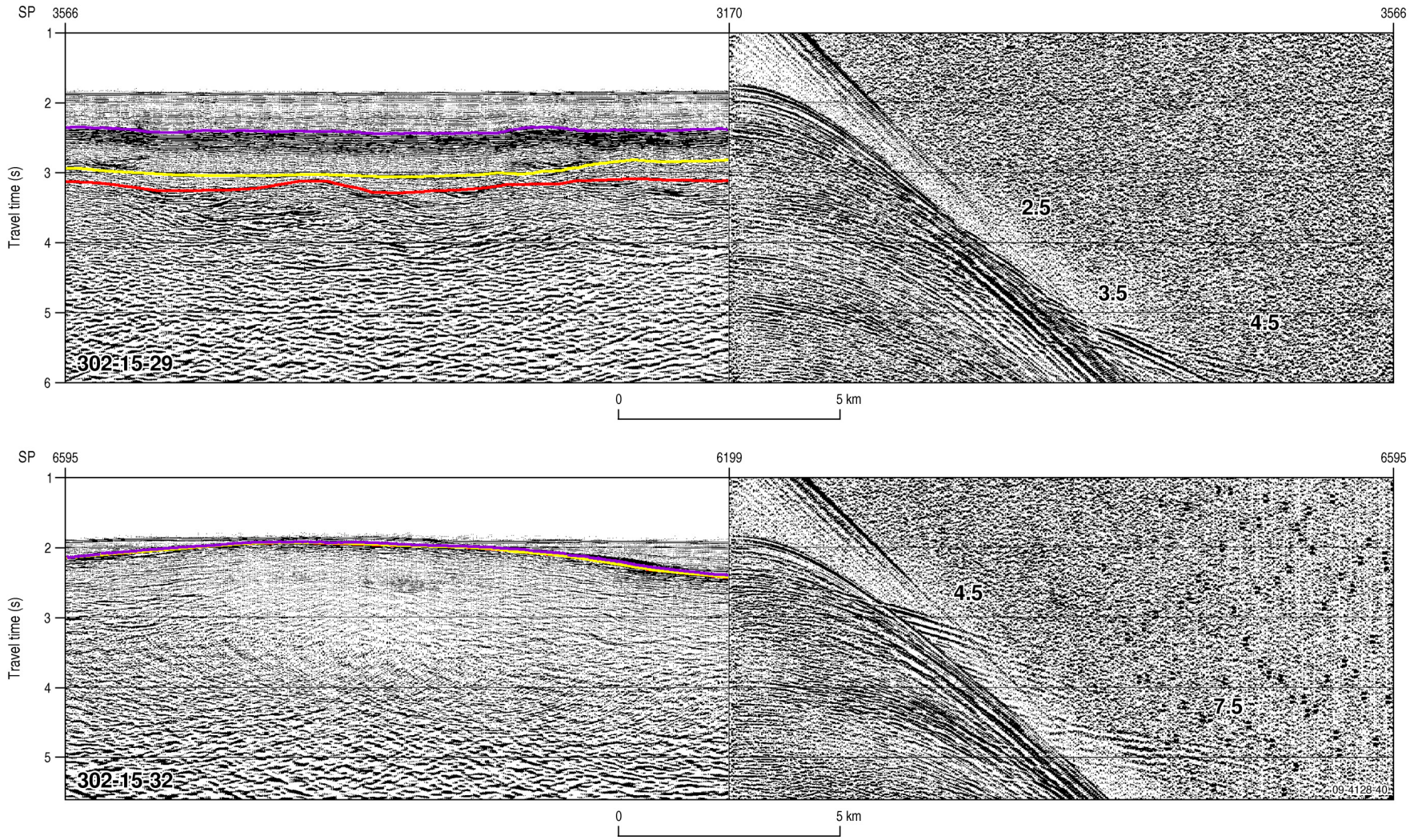
SP
3566
3170
3566
1
2
3
4
5
6
Travel time (s)
2.5
3.5
4.5
302-15-29
0
5 km
SP
6595
6199
6595
1
2
3
4
5
Travel time (s)
4.5
7.5
302-15-32
09-4128-40
0
5 km

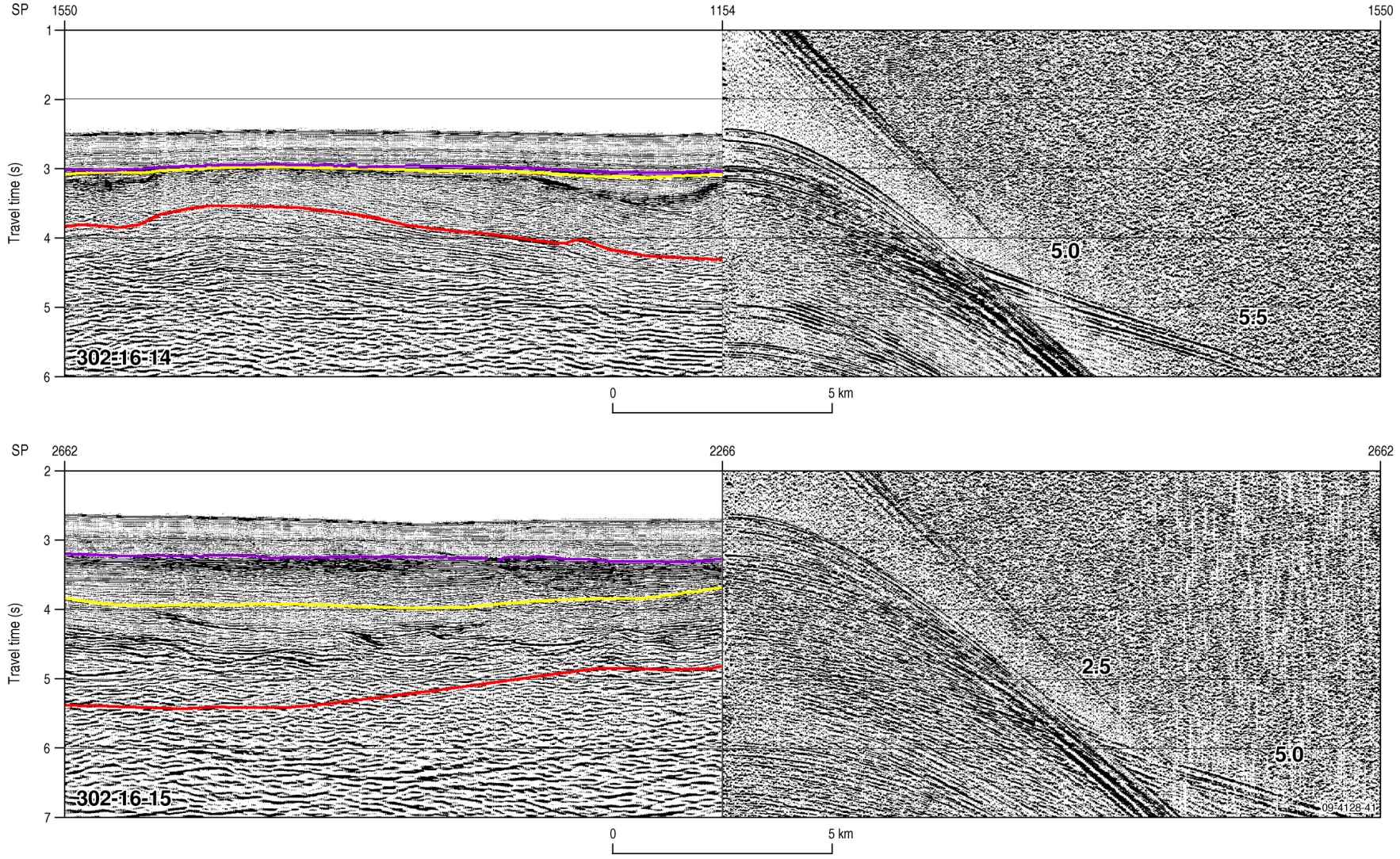
SP
1550
1154
1550
Travel time (s)
1
2
3
4
5
6
302-16-14
5.0
5.5
0
5 km
SP
2662
2266
2662
Travel time (s)
2
3
4
5
6
7
302-16-15
2.5
5.0
09-4128-41
0
5 km

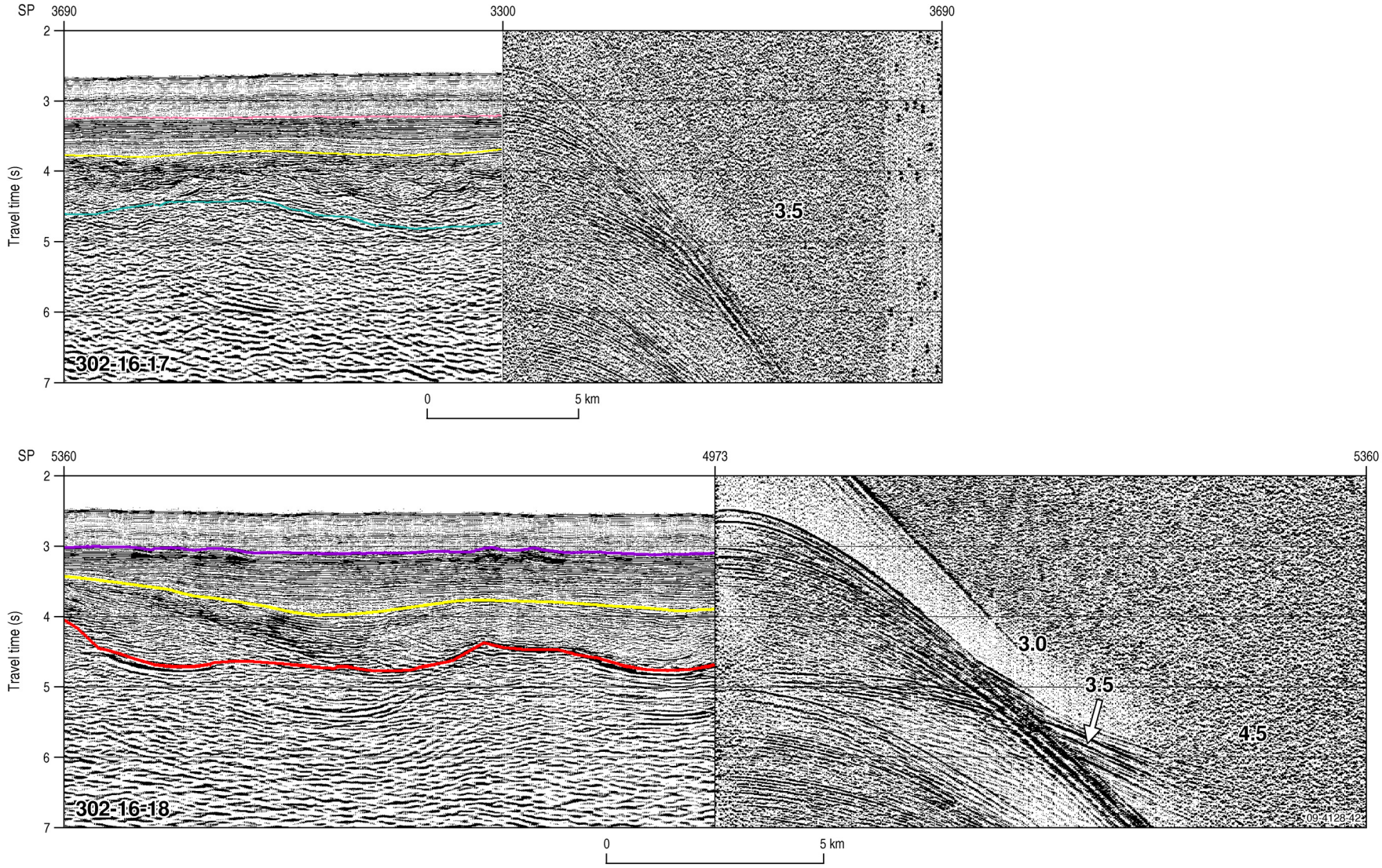
SP
3690
3300
3690
2
3
4
5
6
7
Travel time (s)
3.5
302-16-17
0
5 km
SP
5360
4973
5360
2
3
4
5
6
7
Travel time (s)
3.0
3.5
4.5
302-16-18
0
5 km

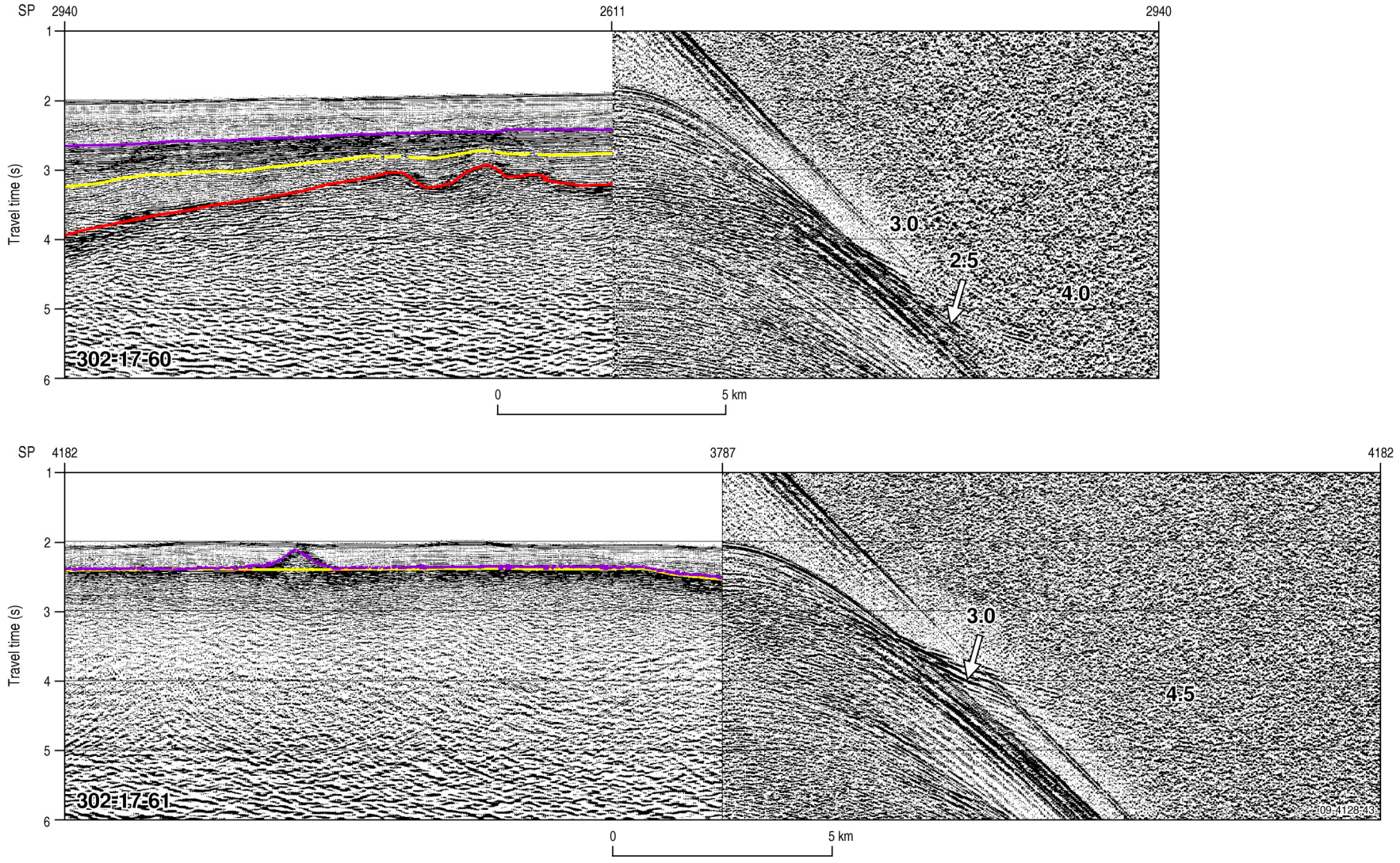
SP
2940
2611
2940
1
2
3
4
5
6
Travel time (s)
3.0
2.5
4.0
302-17-60
0
5 km
SP
4182
3787
4182
1
2
3
4
5
6
Travel time (s)
3.0
4.5
302-17-61
09-4128-43
0
5 km

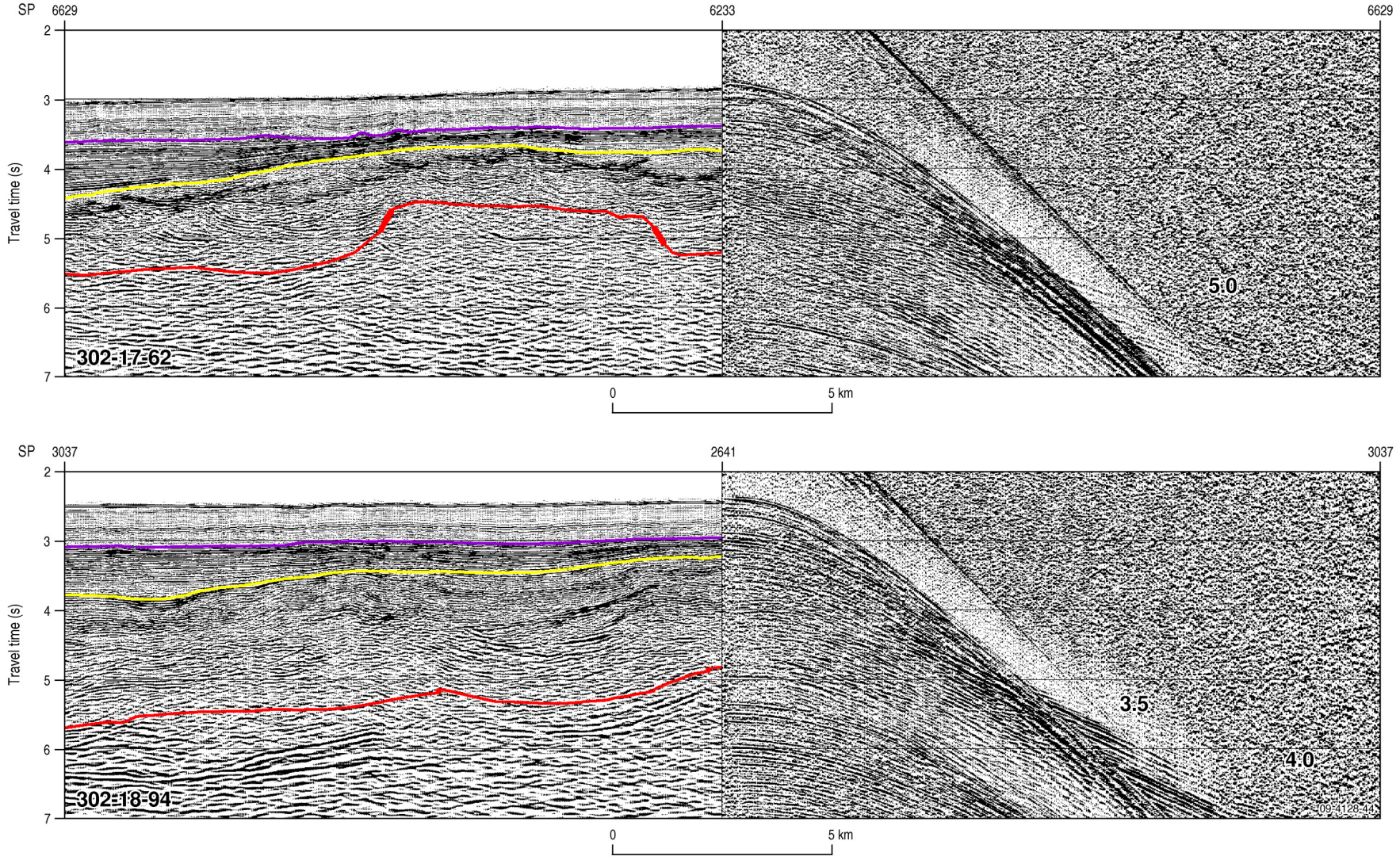
SP
6629
6233
6629
2
3
4
5
6
7
Travel time (s)
302-17-62
5.0
0
5 km
SP
3037
2641
3037
2
3
4
5
6
7
Travel time (s)
302-18-94
3.5
4.0
0
5 km
09-4128-44

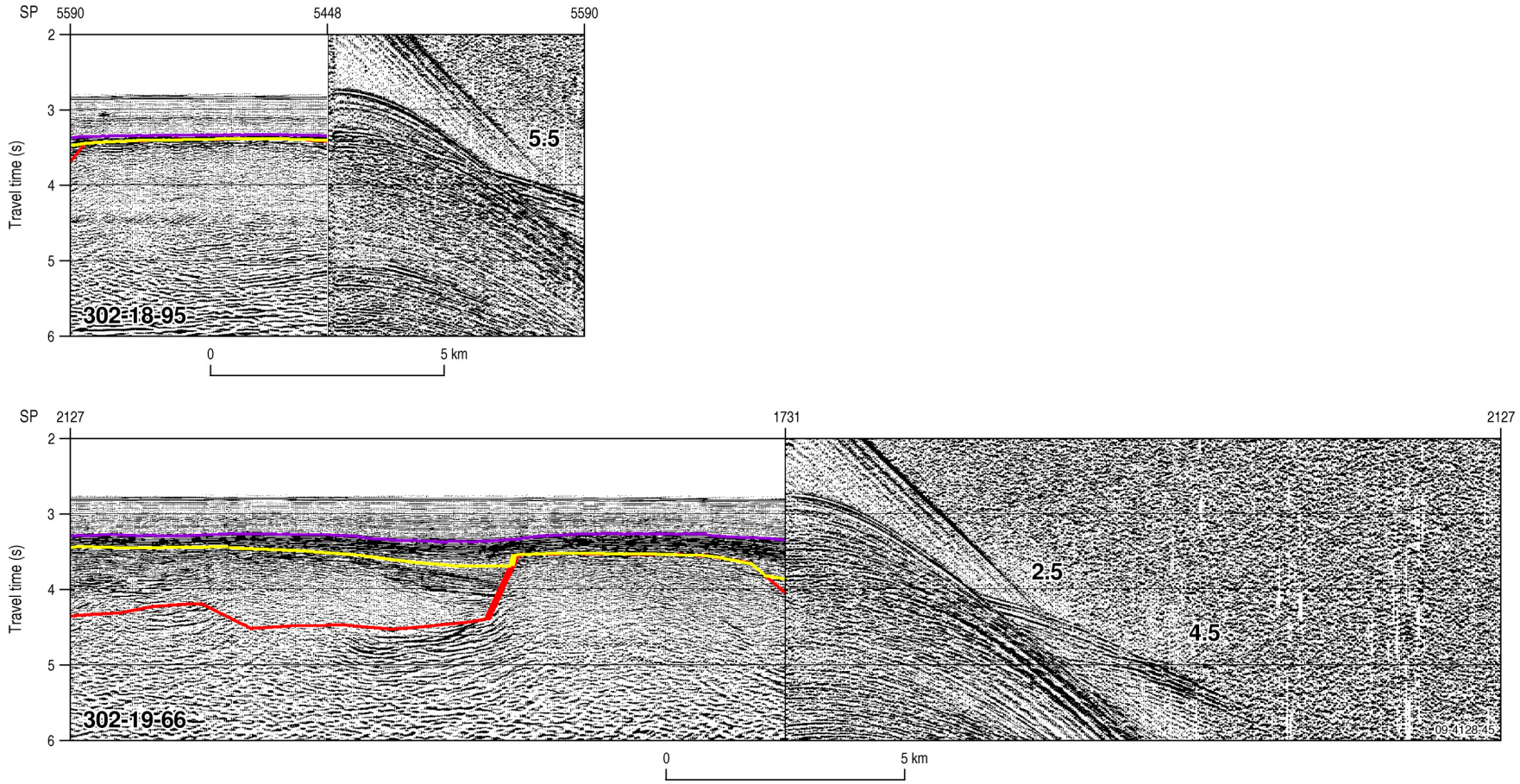
SP
5590
5448
5590
2
3
4
5
6
Travel time (s)
5.5
302-18-95
0
5 km
SP
2127
1731
2127
2
3
4
5
6
Travel time (s)
2.5
4.5
302-19-66
0
5 km

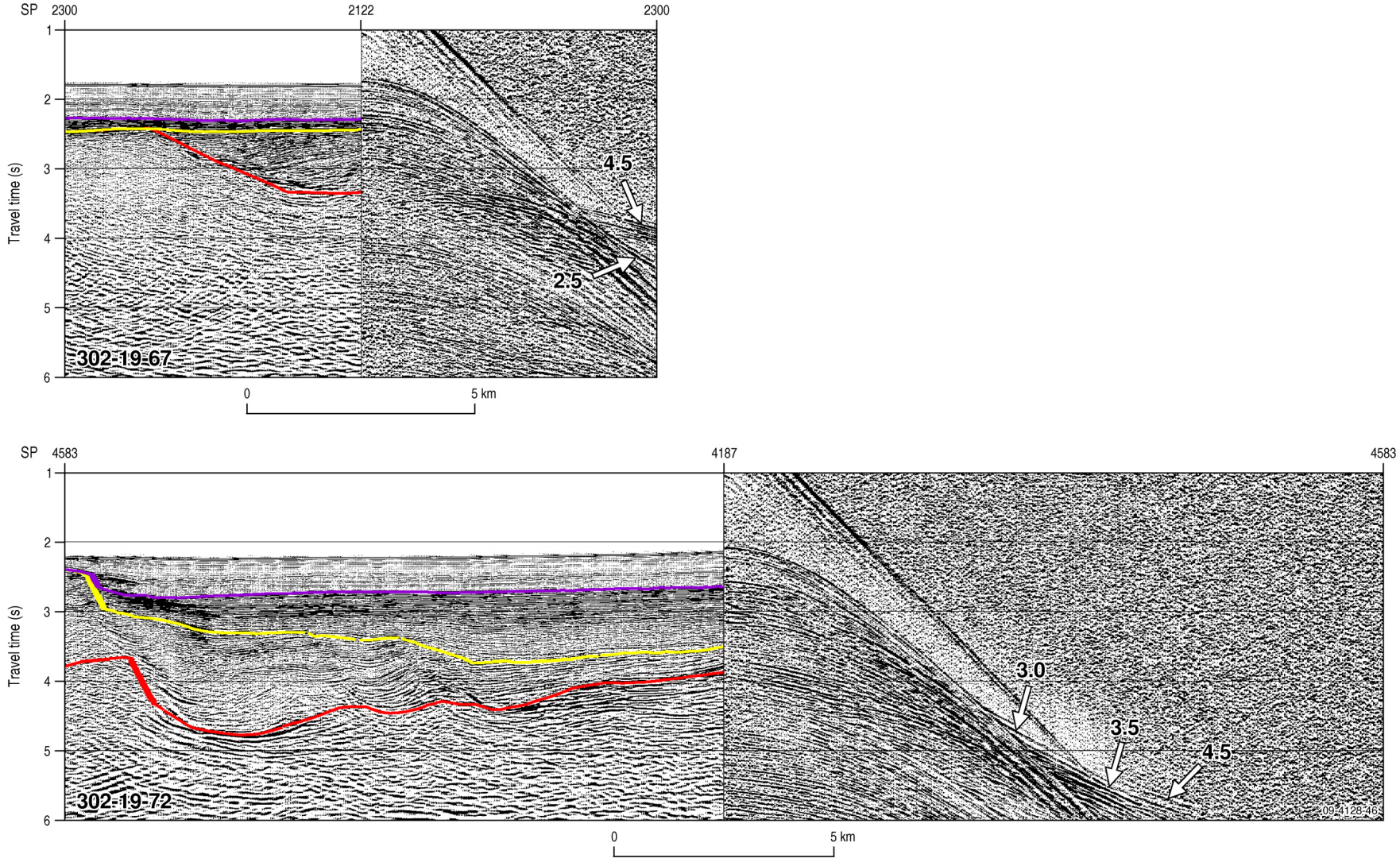
SP 2300
2122
2300
1
2
3
4
5
6
Travel time (s)
4.5
2.5
302-19-67
0
5 km
SP 4583
4187
4583
3.0
3.5
4.5
302-19-72
09_4128-46
0
5 km

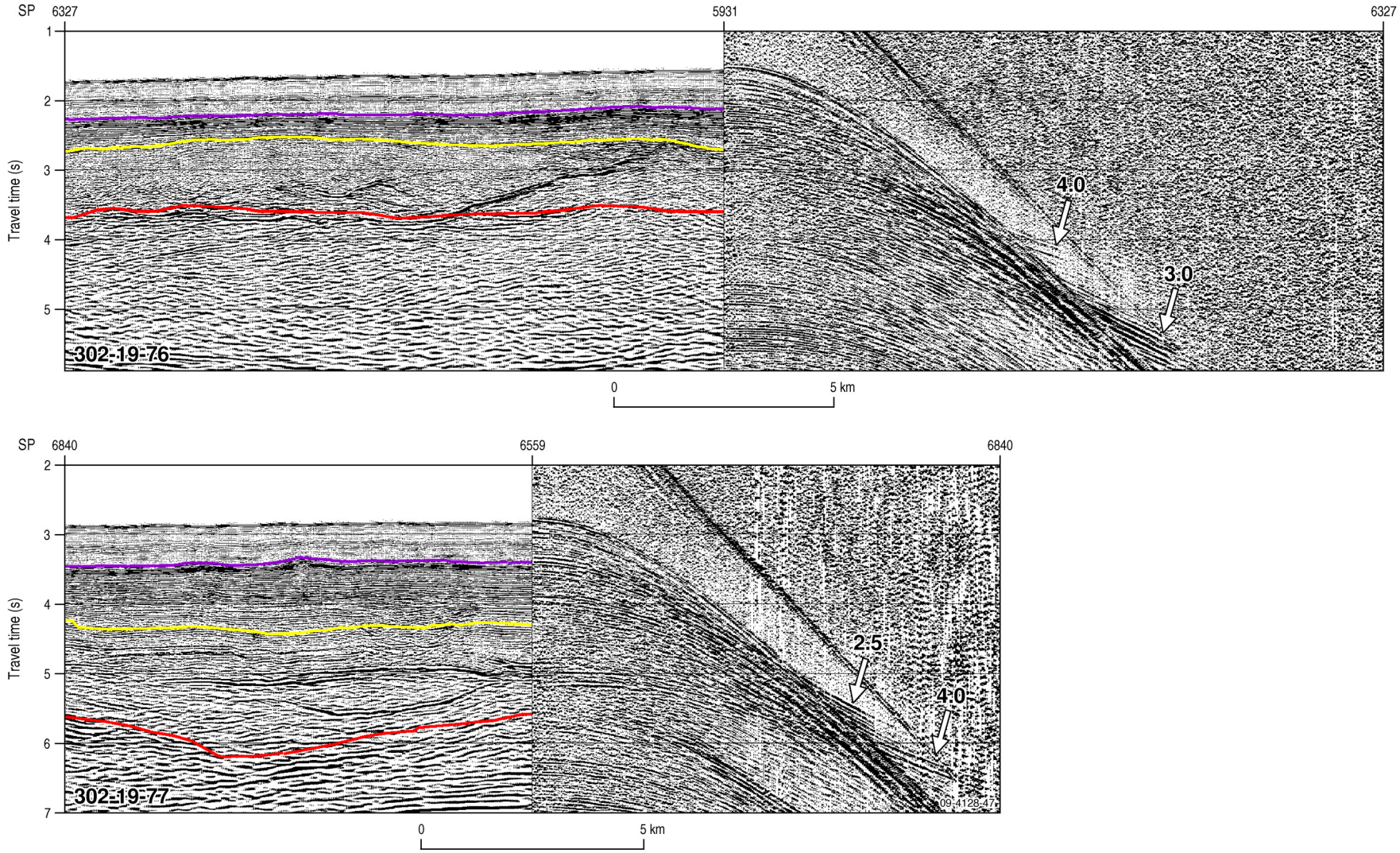
SP
6327
5931
6327
1
2
3
4
5
Travel time (s)
4.0
3.0
302-19-76
0
5 km
SP
6840
6559
6840
2
3
4
5
6
7
Travel time (s)
2.5
4.0
302-19-77
09-4128-47
0
5 km

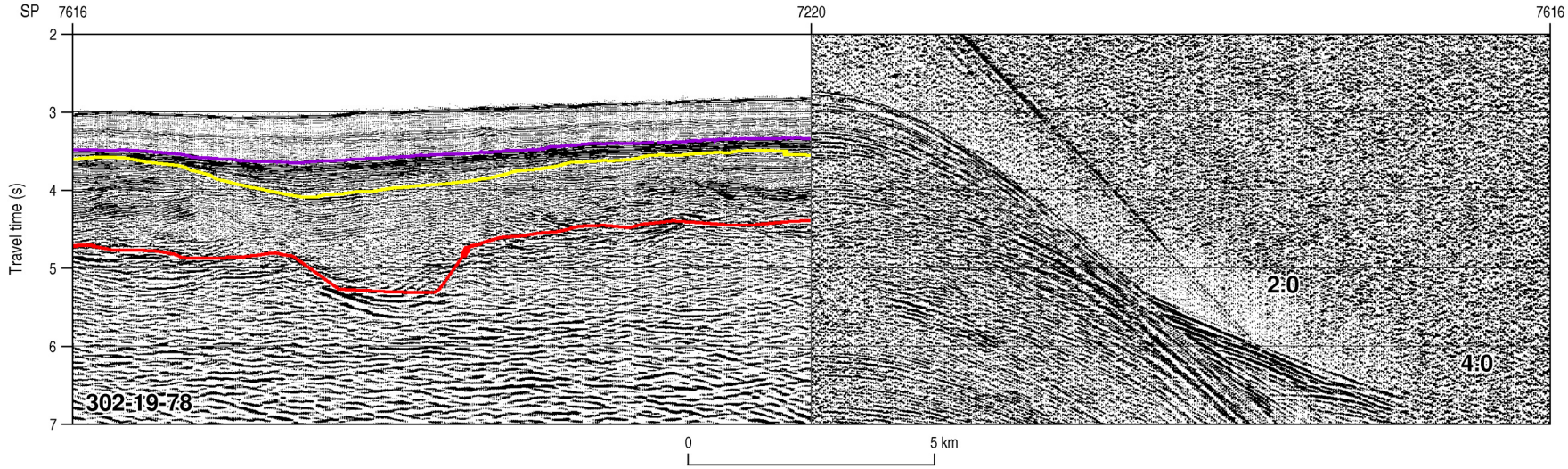
SP
7616
7220
7616
2
3
4
5
6
7
Travel time (s)
302-19-78
2:0
4:0
0
5 km

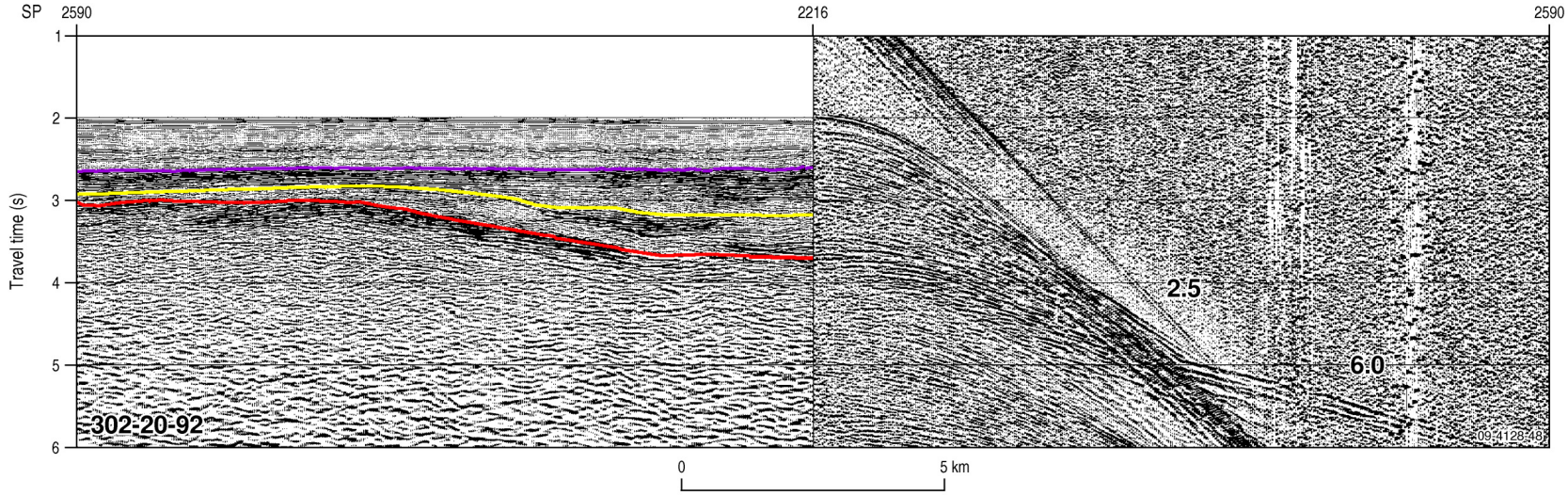
SP
2590
2216
2590
1
2
3
4
5
6
Travel time (s)
302-20-92
2:5
6:0
0
5 km

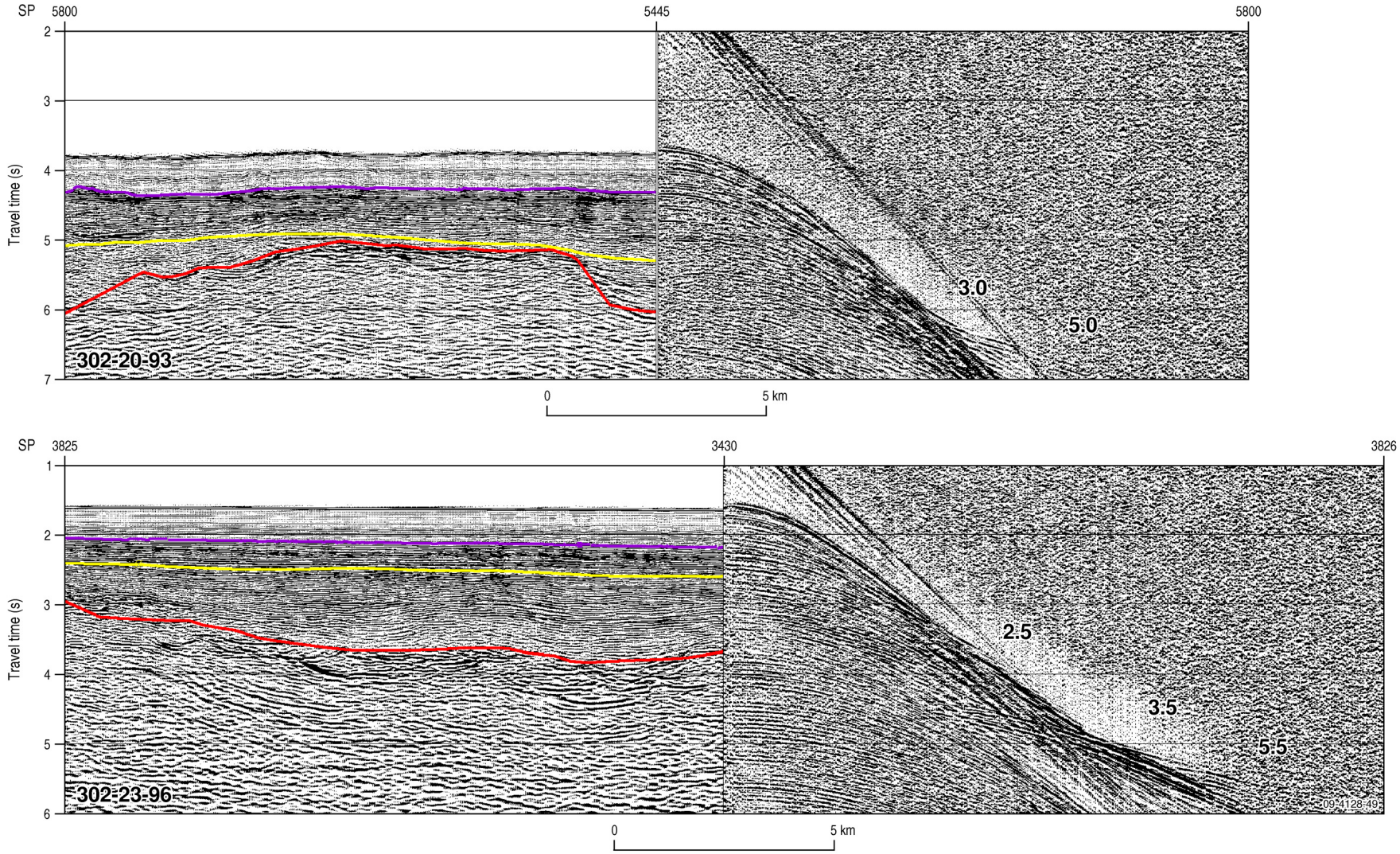
SP
5800
5445
5800
2
3
4
5
6
7
Travel time (s)
302-20-93
3.0
5.0
0
5 km
SP
3825
3430
3826
1
2
3
4
5
6
Travel time (s)
302-23-96
2.5
3.5
5.5
0
5 km
09-4128-49

Appendix 2 – Forward ray-traced 2D velocity models

The 2D models developed by forward ray-tracing are shown in this appendix. In each figure, the upper half is the vertical section, with depth and horizontal axes in kilometres, containing the velocity model boundaries. The shallowest layer is water with a velocity of 1.5 km/s. The curved paths are the synthetic rays computed on the basis of the velocity distribution, indicated approximately by the labels. The lower half of each figure shows the observed (dots) and computed (thin lines) travel times of interpreted refraction events. It has a vertical axis of travel time with a reduction of D/6, where D is distence from energy source in kilometres. Therefore, events with a velocity of 6 km/s will appear horizontal in the lower half of the diagram. Parts of each diagram not traversed by rays should be considered unreliable. The 1D models given numerically in Appendix 3 are vertical slices from the 2D models at positions of maximum ray coverage.

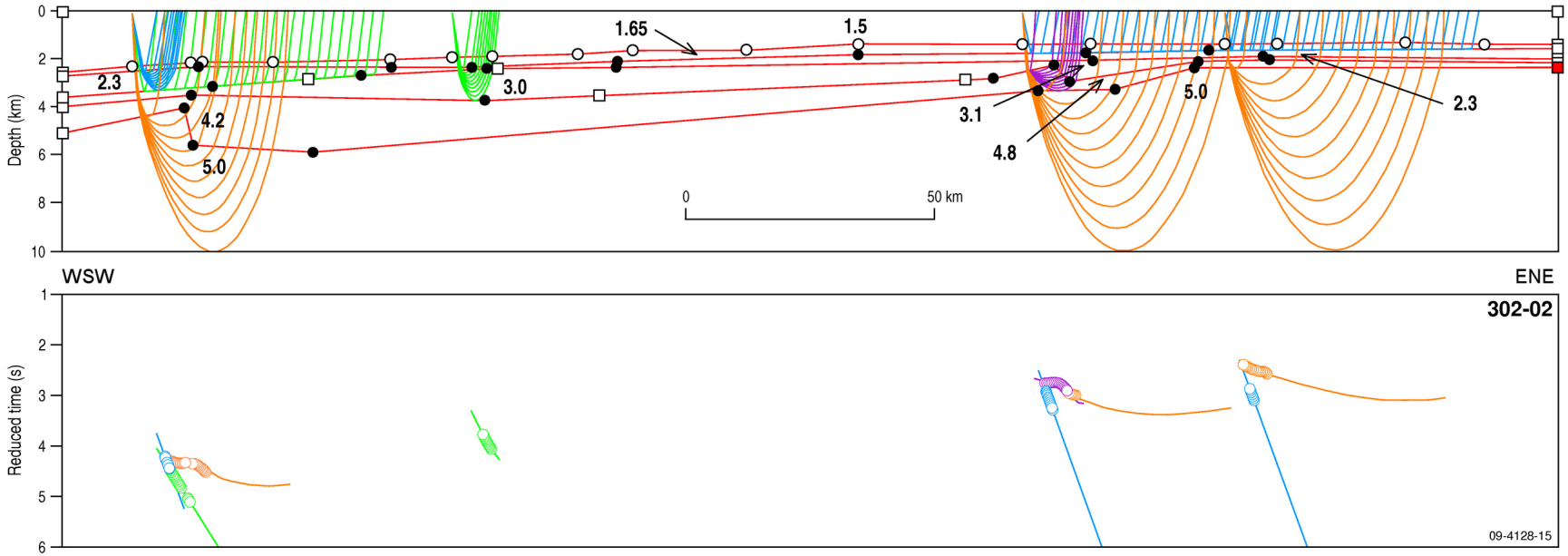

Figure 15. *Ray paths for velocity model 302-02. The travel time scale has had reducing velocity of 6km/s applied. Sonobuoys left to right: 42, 43, 46, 47. Velocities are km/s; horizontal scale is km.*

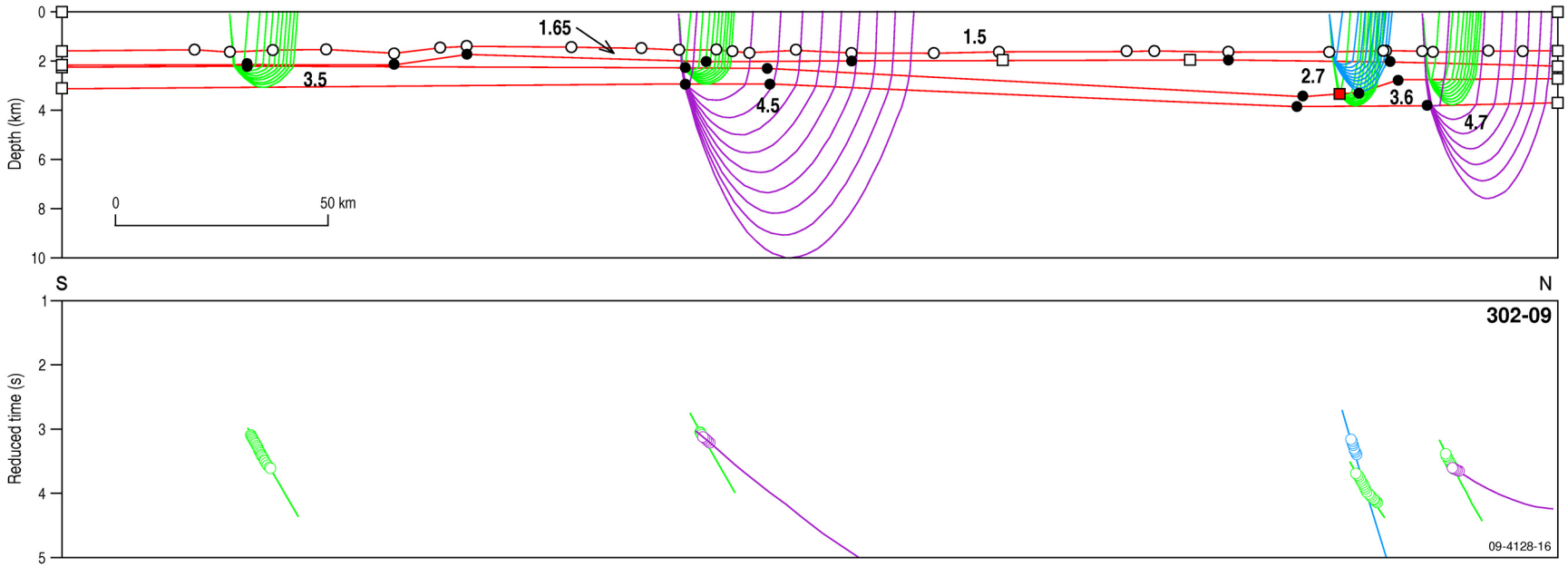

Figure 16. *Ray paths for velocity model 302-09. The travel time scale has had reducing velocity of 6km/s applied. Sonobuoys left to right: 34, 36, 39, 40. Velocities are km/s; horizonal scale is km.*

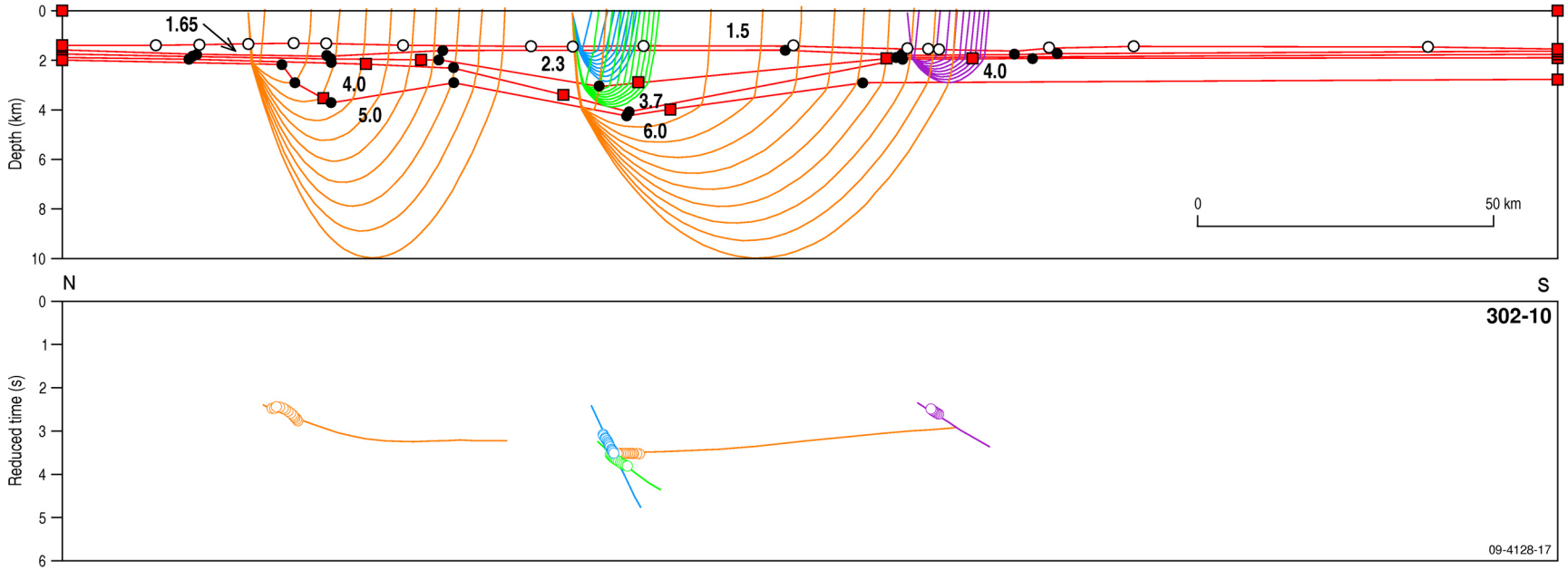

Figure 17. *Ray paths for velocity model 302-10. The travel time scale has had reducing velocity of 6km/s applied. Sonobuoys left to right: 06, 09, 10. Velocities are km/s; horizonal scale is km.*

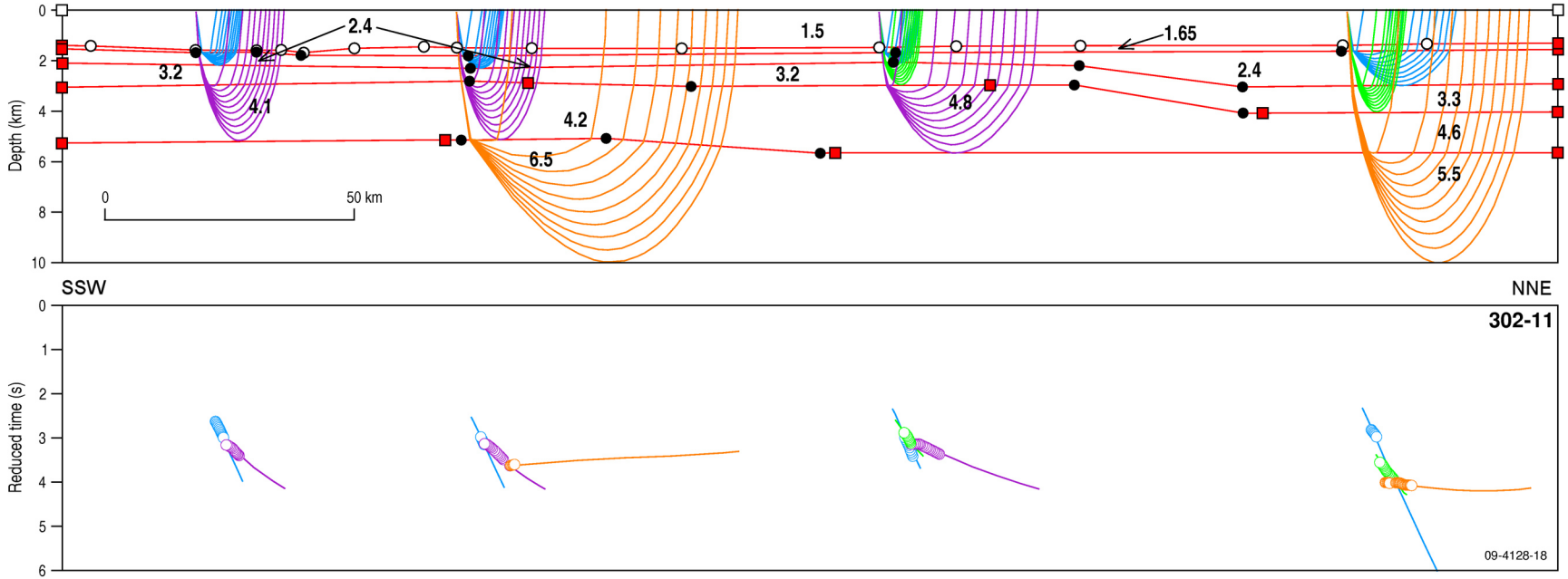

Figure 18. *Ray paths for velocity model 302-11. The travel time scale has had reducing velocity of 6km/s applied. Sonobuoys left to right: 20, 22, 25, 26. Velocities are km/s; horizonal scale is km.*

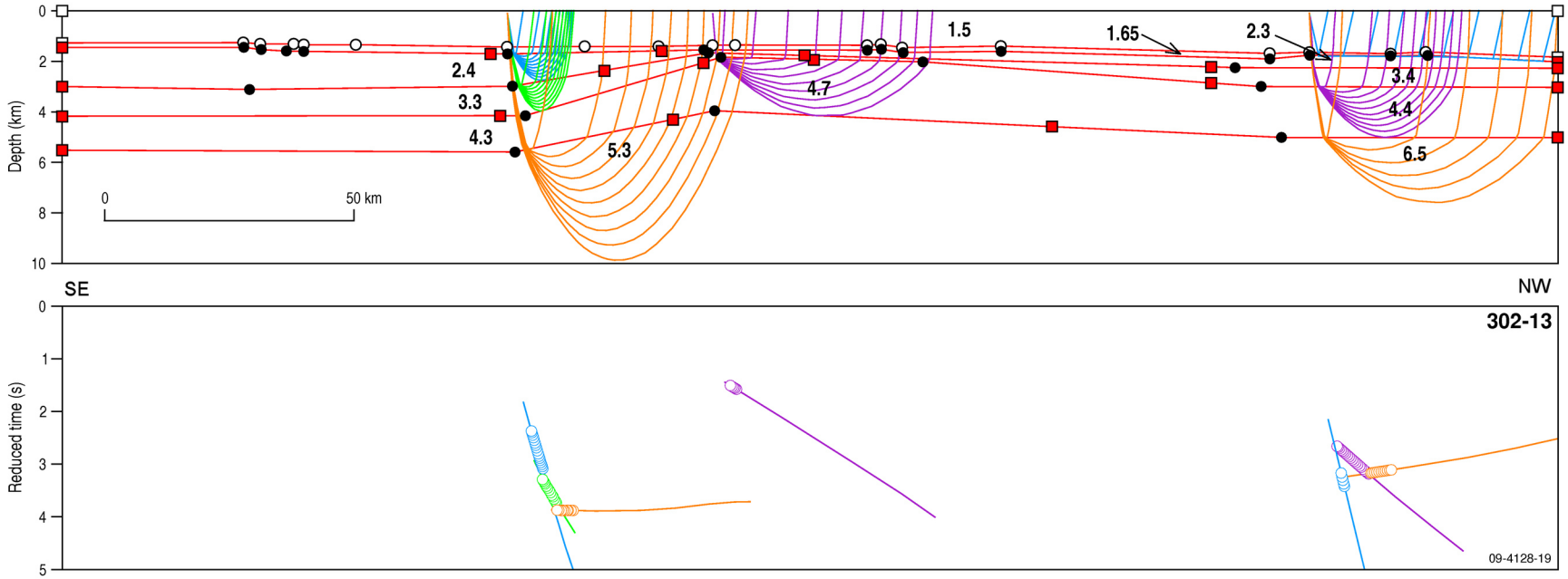

Figure 19. *Ray paths for velocity model 302-13. The travel time scale has had reducing velocity of 6km/s applied. Sonobuoys left to right: 53, 54, 56. Velocities are km/s; horizonal scale is km.*

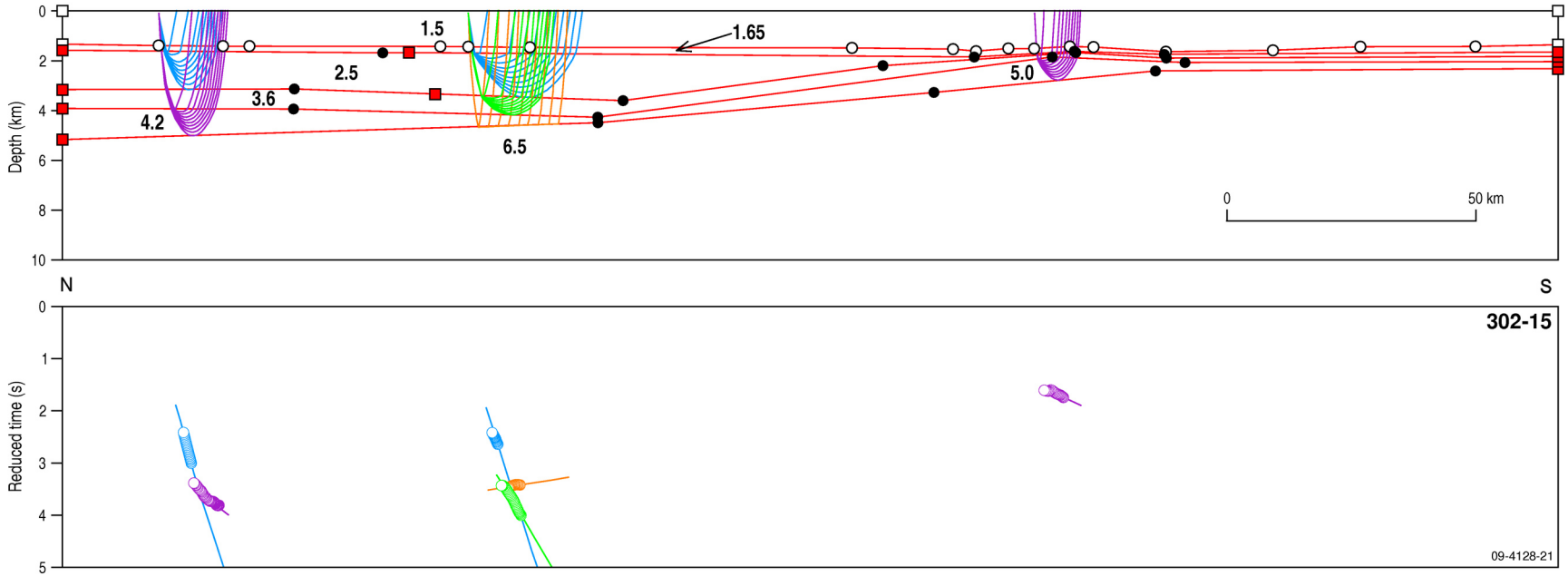

Figure 20. *Ray paths for velocity model 302-14. The travel time scale has had reducing velocity of 6km/s applied. Sonobuoys left to right 49, 51. Velocities are km/s; horizonal scale is km.*

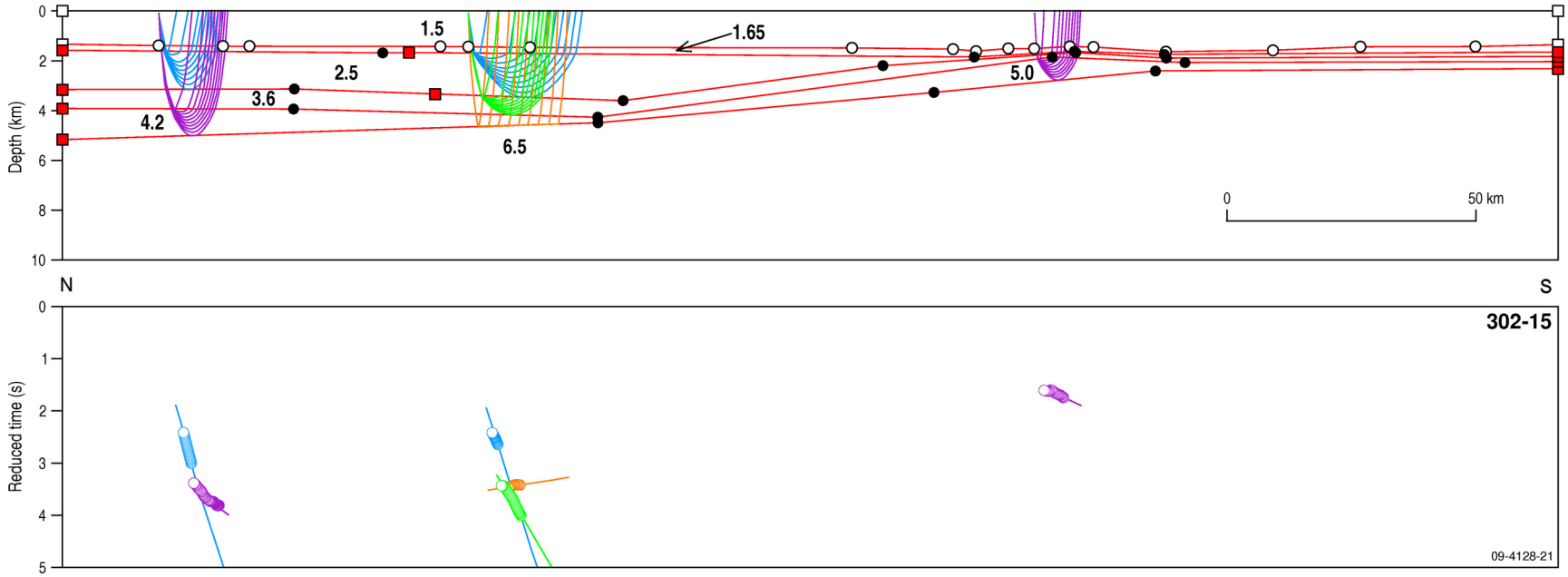

Figure 21. *Ray paths for velocity model 302-15. The travel time scale has had reducing velocity of 6 km/s applied. Sonobuoys left to right 27, 29, 32. The refractor of apparent velocity 7.5 km/s identified on sonobuoy 32 data was not modelled here, as it appears to be an intrabasement event not imaged in the reflection seismic section. Velocities are km/s; horizonal scale is km.*

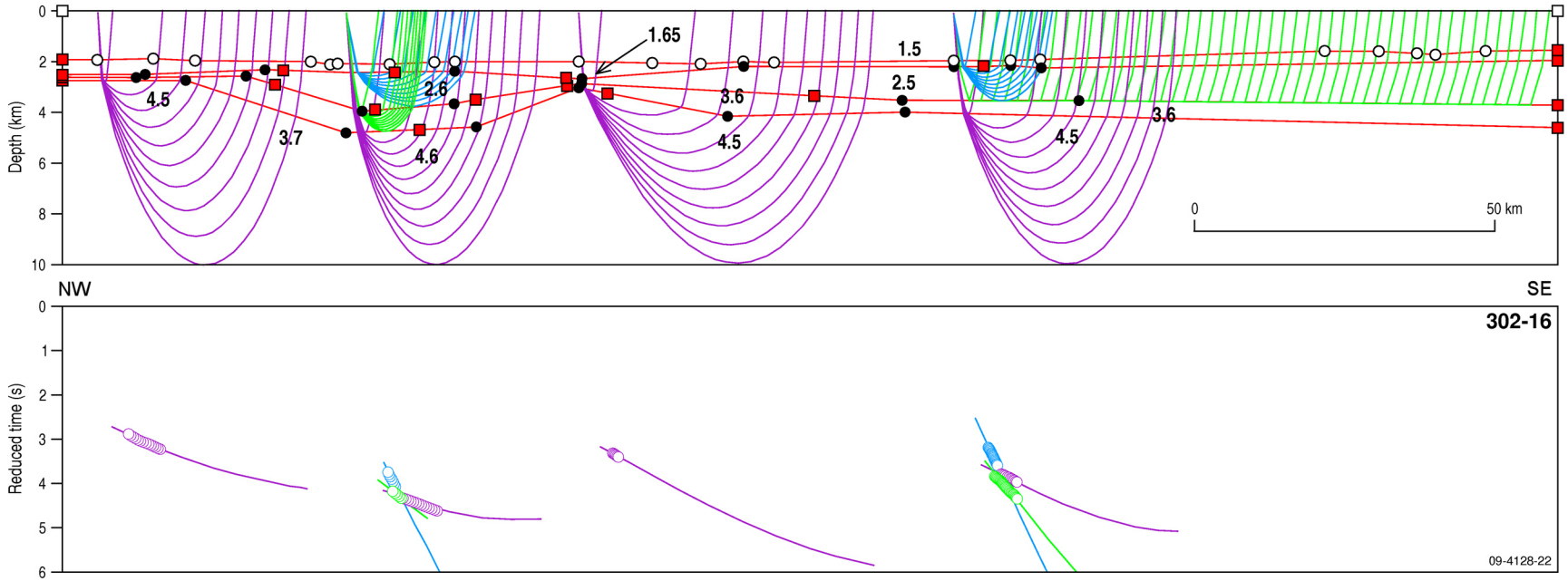

Figure 22. *Ray paths for velocity model 302-16. The travel time scale has had reducing velocity of 6km/s applied. Sonobuoys left to right 14, 15, 17, 18. Velocities are km/s; horizonal scale is km.*

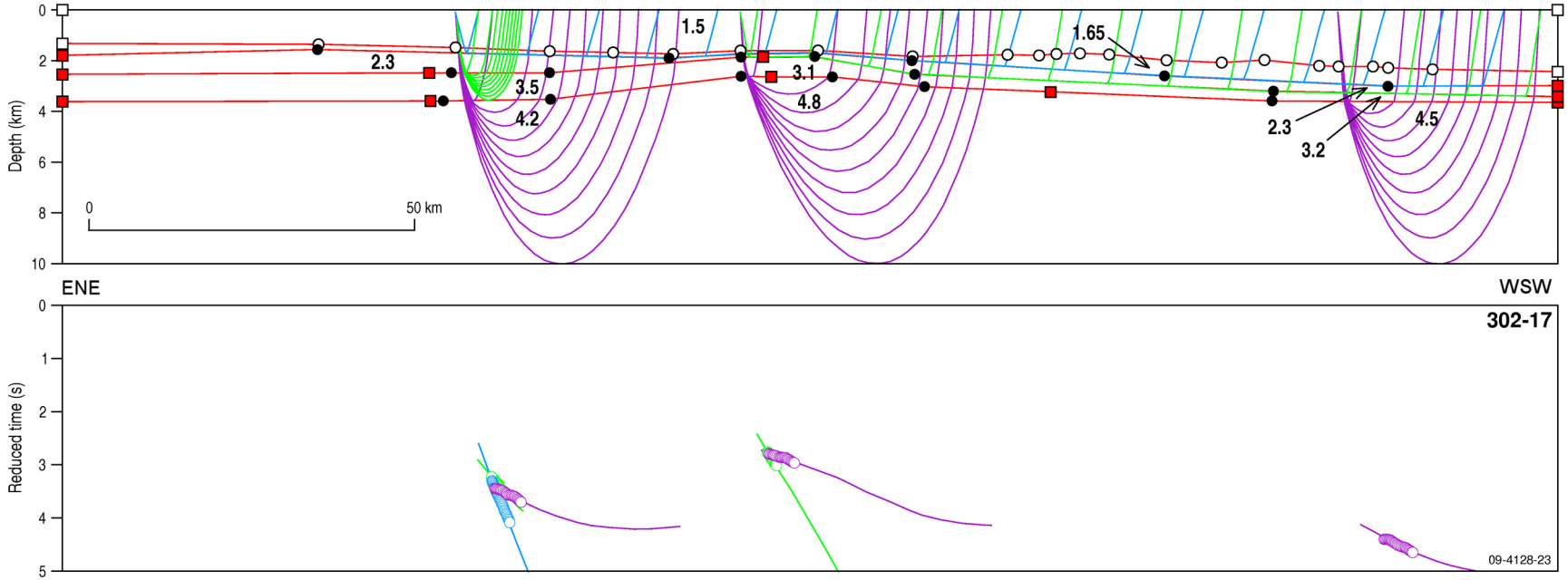

Figure 23. *Ray paths for velocity model 302-17. The travel time scale has had reducing velocity of 6km/s applied. Sonobuoys left to right: 60, 61, 62. Velocities are km/s; horizonal scale is km.*

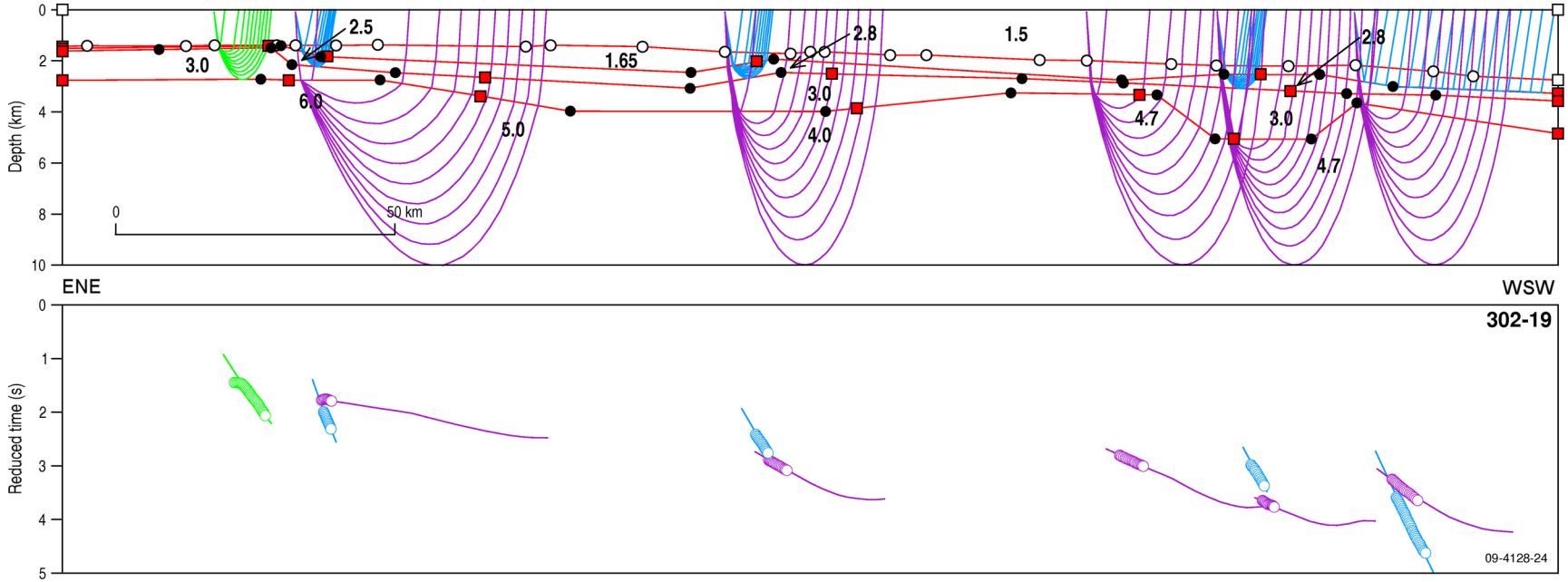

Figure 24. *Ray paths for velocity model 302-19. The travel time scale has had reducing velocity of 6km/s applied. Sonobuoys left to right: 66, 67, 72, 76, 77, 78. Velocities are km/s; horizonal scale is km.Appendix 3 – 1D velocity slices from 2D ray-traced models*

Appendix 3 – Velocity slices from 2D ray-traced models

The following lists the results of ray-trace forward modelling of the sonobuoy data for survey GA-302. Each '#' delimited header record is followed by the velocity function extracted in the vicinity of the sonobuoy close to the location of maximum ray coverage. The contents of the header record are as follows:

Sonobuoy identifier # line name and distance of 1D velocity model from start of line # latitude (°) # longitude (°) # water depth (m)

The first row following each header are depths (km) and the second row are corresponding interval velocities (km/s).

The 1D models were extracted from the Sigma software model file using program '*sigmax.pl*' developed by the author and transposed into the format below using program '*transpose.pl*'.

```
--------------------------------------------------------------------------------
302-02-42#GA 302-02 at 22 km, spn1590#-27.44030#160.35252#-2161#
  0.000   2.161   2.161   2.407   2.407   3.264   3.264   3.574   3.574   4.161   4.161   4.700
  1.500   1.510   1.600   1.700   2.207   2.493   3.000   3.500   4.000   4.500   5.000   5.139
302-02-43#GA 302-02 at 83 km, spn3215#-27.19312#160.90279#-1911#
  0.000   1.911   1.911   2.363   2.363   2.432   2.432   2.800
  1.500   1.510   1.600   1.700   2.228   2.472   2.645   2.889
302-02-46#GA 302-02 at 198 km, spn6280#-26.72131#161.93436#-1374#
  0.000   1.374   1.374   1.771   1.771   2.078   2.078   2.298   2.298   3.323   3.323   3.600
  1.500   1.510   1.600   1.700   2.266   2.434   2.808   3.344   4.700   4.900   5.000   5.062
302-02-47#GA 302-02 at 238 km, spn7350#-26.55514#162.29143#-1363#
  0.000   1.363   1.363   1.641   1.641   1.912   1.912   2.057   2.057   2.394   2.394   2.800
  1.500   1.510   1.600   1.700   2.279   2.421   2.883   3.287   4.700   4.900   5.000   5.080
302-09-34#GA 302-09 at 51 km, spn2360#-28.49491#161.70576#-1528#
  0.000   1.528   1.528   2.114   2.114   2.204   2.204   2.600
  1.500   1.510   1.600   1.700   2.000   2.800   3.517   3.564
302-09-36#GA 302-09 at 158 km, spn5215#-27.54506#161.50980#-1578#
  0.000   1.578   1.578   2.008   2.008   2.274   2.274   2.930   2.930   3.300
  1.500   1.510   1.600   1.700   2.000   2.800   3.551   3.651   4.500   4.542
302-09-39#GA 302-09 at 318 km, spn9480#-26.12404#161.22443#-1555#
  0.000   1.555   1.555   2.026   2.026   2.965   2.965   3.700
  1.500   1.510   1.600   1.700   2.600   2.800   3.522   3.658
302-09-40#GA 302-09 at 333 km, spn9880#-25.99069#161.19800#-1554#
  0.000   1.554   1.554   2.086   2.086   2.748   2.748   3.788   3.788   4.200
  1.500   1.510   1.600   1.700   2.600   2.800   3.407   3.652   4.851   4.931
302-10-06#GA 302-10 spn1990 at 37 km#-26.39839#161.67863#-1306#
  0.000   1.306   1.306   1.803   1.803   1.893   1.893   2.046   2.046   2.299   2.299   3.600
  1.500   1.510   1.600   1.700   2.100   2.500   3.000   3.200   3.900   4.000   5.000   5.253
302-10-09#GA 302-10 spn3455 at 92 km#-26.89440#161.68936#-1401#
  0.000   1.401   1.401   1.585   1.585   3.008   3.008   3.904   3.904   4.127   4.127   4.700
  1.500   1.510   1.600   1.700   2.100   2.500   3.530   3.730   3.900   4.188   5.834   5.899
302-10-10#GA 302-10 spn4870 at 145 km#-27.37288#161.69992#-1522#
```

```
  0.000   1.522   1.522   1.780   1.780   1.874   1.874   1.920   1.920   2.300
  1.500   1.510   1.600   1.700   2.100   2.500   3.000   3.100   3.900   3.983
302-11-20#GA 302-11  spn1880 at 33 km#-28.44677#161.91180#-1554#
  0.000   1.554   1.554   1.660   1.660   2.159   2.159   2.973   2.973   3.300
  1.500   1.510   1.600   1.700   2.400   2.500   3.000   3.500   3.700   3.817
302-11-22#GA 302-11 spn3320 at 87 km#-27.96928#162.02095#-1474#
  0.000   1.474   1.474   1.792   1.792   2.278   2.278   2.852   2.852   5.123   5.123   5.400
  1.500   1.510   1.600   1.700   2.400   2.500   3.000   3.500   3.700   4.500   6.369   6.381
302-11-25#GA 302-11 spn5590 at 172 km#-27.21705#162.19086#-1426#
  0.000   1.426   1.426   1.677   1.677   2.104   2.104   2.980   2.980   3.200
  1.500   1.510   1.600   1.700   2.400   2.500   3.000   3.500   4.547   4.578
302-11-26#GA 302-11 spn8095 at 266 km#-26.38521#162.37689#-1348#
  0.000   1.348   1.348   1.607   1.607   2.989   2.989   4.061   4.061   5.647   5.647   6.000
  1.500   1.510   1.600   1.700   2.400   2.500   3.000   3.500   4.500   4.700   5.500   5.581
302-13-53#Capel-Faust Basins 302-13 spn3270 at 85 km#-27.19304#162.45561#-1420#
  0.000   1.420   1.420   1.701   1.701   3.005   3.005   4.191   4.191   5.625   5.625   6.000
  1.500   1.510   1.600   1.700   2.297   2.500   3.100   3.500   4.000   4.500   5.300   5.360
302-13-54#Capel-Faust Basins 302-13 spn4680 at 138 km#-26.94617#161.99751#-1356#
  0.000   1.356   1.356   1.563   1.563   1.727   1.727   1.874   1.874   2.300
  1.500   1.510   1.600   1.700   2.270   2.500   3.318   3.500   4.700   4.720
302-13-56#GA 302-13 spn7880 at 258 km#-26.38227#160.96837#-1657#
  0.000   1.657   1.657   1.789   1.789   2.280   2.280   3.023   3.023   5.058   5.058   5.400
  1.500   1.510   1.600   1.700   2.070   2.500   3.400   3.500   4.300   4.500   6.410   6.437
302-14-49#GA 302-14 spn4550 at 133 km#-26.89114#162.45636#-1395#
  0.000   1.395   1.395   1.889   1.889   2.085   2.085   4.703   4.703   4.900
  1.500   1.510   1.600   1.700   2.109   2.500   3.000   4.000   4.700   4.858
302-14-51#GA 302-14 spn5215 at 158 km#-27.05866#162.62543#-1329#
  0.000   1.329   1.329   1.501   1.501   2.603   2.603   3.464   3.464   3.734   3.734   4.000
  1.500   1.510   1.600   1.700   2.129   2.500   3.000   4.000   4.681   5.000   5.500   5.542
302-15-27#GA 302-15 spn1695 at 26 km# -26.61401#162.44322#-1367#
  0.000   1.367   1.367   1.618   1.618   3.148   3.148   3.931   3.931   4.200
  1.500   1.510   1.600   1.700   2.187   2.600   3.530   3.630   4.087   4.213
302-15-29#GA 302-15 spn3400 at 90 km#-27.18804#162.37462#-1421#
  0.000   1.421   1.421   1.701   1.701   3.446   3.446   4.169   4.169   4.598   4.598   4.800
  1.500   1.510   1.600   1.700   2.456   2.600   3.400   3.500   4.300   4.800   6.500   6.504
302-15-32#GA 302-15 spn6415 at 203 km#-28.20222#162.25301#-1414#
  0.000   1.414   1.414   1.620   1.620   1.681   1.681   1.876   1.876   2.100
  1.500   1.510   1.600   1.700   2.210   2.600   3.400   3.500   4.677   4.811
302-16-14#GA 302-16 spn1350 at 13 km#-26.62708#160.18697#-1867#
  0.000   1.867   1.867   2.500   2.500   2.618   2.618   2.733   2.733   3.300
  1.500   1.510   1.600   1.700   2.000   2.400   3.183   3.483   4.544   4.696
302-16-15#GA 302-16 spn2575 at 59 km#-26.96843#160.45027#-2024#
  0.000   2.024   2.024   2.405   2.405   3.700
  1.500   1.510   1.600   1.700   2.563   2.669
302-16-17#GA 302-16 spn3455 at 92 km#-27.21305#160.64032#-2001#
  0.000   2.001   2.001   2.585   2.585   2.926   2.926   3.290   3.290   4.400
  1.500   1.510   1.600   1.700   2.311   2.511   3.056   3.393   4.500   4.584
302-16-18#GA 302-16 spn5215 at 158 km#-27.70188#161.02164#-1936#
  0.000   1.936   1.936   2.162   2.162   3.532   3.532   4.076   4.076   4.300
  1.500   1.510   1.600   1.700   2.400   2.600   3.300   3.800   4.500   4.543
```

```
302-17-60#GA 302-17 spn2790 at 67 km#-26.43860#161.38458#-1505#
  0.000   1.505   1.505   1.740   1.740   2.456   2.456   3.544   3.544   3.800
  1.500   1.510   1.600   1.700   2.100   2.500   3.097   3.659   4.319   4.401
302-17-61#GA 302-17 spn3935 at 110 km#-26.60301#160.99358#-1537#
  0.000   1.537   1.537   1.696   1.696   1.845   1.845   2.610   2.610   2.900
  1.500   1.510   1.600   1.700   2.100   2.500   2.706   3.500   4.783   4.831
302-17-62#GA 302-17 spn6470 at 205 km#-26.96155#160.12599#-2273#
  0.000   2.273   2.273   2.999   2.999   3.287   3.287   3.597   3.597   4.100
  1.500   1.510   1.600   1.700   2.100   2.500   2.939   3.500   4.340   4.509
302-19-66#GA 302-19 spn1830 at 31km#-26.80225#162.25691#-1372#
  0.000   1.372   1.372   1.442   1.442   1.509   1.509   1.800
  1.500   1.510   1.600   1.700   2.000   2.100   3.000   3.119
302-19-67#GA 302-19 spn2200 at 45km#-26.85538#162.12920#-1372#
  0.000   1.372   1.372   1.743   1.743   2.208   2.208   2.738   2.738   2.900
  1.500   1.510   1.600   1.700   2.301   2.476   3.000   3.500   5.880   5.893
302-19-72#GA 302-19 spn4360 at 126km#-27.16038#161.38751#-1697#
  0.000   1.697   1.697   2.016   2.016   2.594   2.594   3.982   3.982   4.300
  1.500   1.510   1.600   1.700   2.700   2.900   3.000   3.500   4.256   4.374
302-19-76#GA 302-19 spn6070 at 190km#-27.39845#160.79840#-2017#
  0.000   2.017   2.017   2.725   2.725   2.856   2.856   3.311   3.311   3.800
  1.500   1.510   1.600   1.700   2.700   2.900   3.000   3.500   4.639   4.775
302-19-77#GA 302-19 spn6710 at 214km#-27.48706#160.57692#-2170#
  0.000   2.170   2.170   2.540   2.540   3.104   3.104   5.060   5.060   5.300
  1.500   1.510   1.600   1.700   2.700   2.900   3.000   3.500   4.665   4.754
302-19-78#GA 302-19 spn7400 at 240km#-27.58250#160.33661#-2248#
  0.000   2.248   2.248   2.988   2.988   3.321   3.321   3.851   3.851   4.200
  1.500   1.510   1.600   1.700   2.700   2.900   3.000   3.500   4.310   4.434
```

Appendix 4 – Sonobuoy SEG-Y format data

These data are on the CD that forms part of this document. The filename nomenclature uses the identifier as described for Table 3.

File	Size (bytes)
302-01-03.sgy	9093600
302-01-05.sgy	10984320
302-02-42.sgy	10135920
302-02-43.sgy	5433360
302-02-46.sgy	10475280
302-02-47.sgy	8972400
302-03-79.sgy	10426800
302-04-83.sgy	4948560
302-04-84.sgy	8439120
302-05-85.sgy	4997040
302-06-88.sgy	8293680
302-07-11.sgy	10693440
302-08-58.sgy	2936640
302-09-34.sgy	10111680
302-09-36.sgy	10038960
302-09-39.sgy	8852660
302-09-40.sgy	10380032
302-10-06.sgy	9748080
302-10-09.sgy	11323680
302-10-10.sgy	3469920
302-11-20.sgy	7954320
302-11-22.sgy	9748080
302-11-25.sgy	9966240
302-11-26.sgy	10329840
302-13-53.sgy	10426800
302-13-54.sgy	2888160
302-13-56.sgy	11566080
302-14-49.sgy	9626880
302-14-51.sgy	8996640
302-15-27.sgy	9626880
302-15-29.sgy	10451040
302-15-32.sgy	10960080
302-16-14.sgy	10596480
302-16-15.sgy	11760000
302-16-17.sgy	9481440
302-16-18.sgy	9408720
302-17-60.sgy	8002800
302-17-61.sgy	9966240
302-17-62.sgy	9651120
302-18-94.sgy	9942000
302-18-95.sgy	3469920
302-19-66.sgy	10572240
302-19-67.sgy	4342560
302-19-72.sgy	11250960
302-19-76.sgy	9942000
302-19-77.sgy	6839280
302-19-78.sgy	10693440
302-20-92.sgy	9093600
302-20-93.sgy	8633040
302-22-91.sgy	3615360
302-23-96.sgy	9966240